This is to certify that the
thesis entitled

A NEW SYSTEM DEVELOPED TO CHARACTERIZE THERMOELECTRIC DEVICES FOR POWER GENERATION APPLICATIONS

presented by

JARROD L. SHORT

has been accepted towards fulfillment
of the requirements for the

Master of Science	degree in	Electrical and Computer Engineering

Major Professor's Signature

4-28-05

Date

A NEW SYSTEM DEVELOPED TO CHARACTERIZE THERMOELECTRIC DEVICES FOR POWER GENERATION APPLICATIONS

By

Jarrod L. Short

A THESIS

Submitted to
Michigan State University
in partial fulfillment of the requirements
for the degree of

MASTER OF SCIENCE

Department of Electrical and Computer Engineering

2005

ABSTRACT

A NEW SYSTEM DEVELOPED TO CHARACTERIZE THERMOELECTRIC DEVICES FOR POWER GENERATION APPLICATIONS

By

Jarrod L. Short

This document describes work accomplished in the Pulsed Laser Deposition and Transport Characterization Laboratory of Michigan State University (MSU) where a new measurement system has been developed for testing thermoelectric power generation devices based on new materials. Previous work done at MSU has focused on the search, synthesis, and characterization of new thermoelectric materials. This work extends that effort with a focus on developing the materials into working devices. Device fabrication can be as challenging and important as finding more efficient thermoelectric materials; so, present and future work is weighted more heavily on the fabrication and testing of thermoelectric devices made from the previously synthesized materials, namely the Pb-Sb-Ag-Te based "LAST" material [10, 41]. Thermoelectric devices have their own unique properties apart from the materials that make them, and the measurement systems currently used at MSU to investigate the raw materials lack the abilities to test fabricated devices. Therefore, a new measurement system was developed at MSU to investigate the properties of thermoelectric devices used for power generation applications. This thesis presents an introduction to thermoelectrics, as well as the process of developing the new device measurement system, its abilities and limitations, and results from the system.

ACKNOWLEDGEMENTS

For God's graces, my families love, support and motivation, advisor's patience and guidance, Hogan Hero's, and friend's confidence whom have all inspired me to accomplish more than I ever thought possible~ thank you.

TABLE OF CONTENTS

LIST OF TABLES

LIST OF FIGURES

1 Introduction to Thermoelectrics

Fossil fuels are predicted to be nearly extinct by the late twenty-first century, so present day consumer technologies are frequently designed to operate electronically at low power. Electrical energy sources are more environmentally friendly and are often created from abundant sources of sunlight, heat, water, or air. Several technologies exist using electrical energy as an alternative to fossil fuels, and thermoelectrics are one type that converts energy between forms of heat and electricity.

1.1 How Thermoelectric Technology Works

Solar powered calculators, cars, houses, and satellites are just a handful of examples demonstrating alternative energy sources born from semiconductor technology. Solar powered devices work by using semiconductor materials to convert light energy into electricity, while thermoelectric devices use semiconductor materials to convert energy between heat flow and electricity. Thermoelectric devices are typically made of two pieces of semiconductor material connected electrically in series and thermally in parallel. A common configuration of a device shown in figure 1 utilizes a metallic conductor at the junction between N and P-type semiconductor elements that are sandwiched between two electrically insulating, thermal conducting plates.

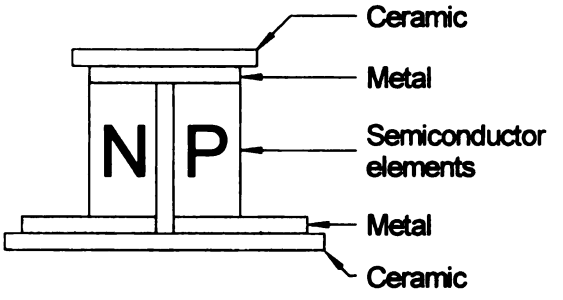

Figure 1: Thermoelectric device materials.

In figures 2A-C, electrical current flows into the bottom of one thermoelectric material, through a top electrically conducting material, down through another thermoelectric material, and back to the voltage source or sink. As shown in figure 2A, if a DC source is applied to a thermoelectric device, Peltier heating and cooling at the ohmic metal-semiconductor junction results in one side becoming hot, and the other cold. If the direction of the applied current is reversed, the heat flows in the opposite direction (figure 2B). As true heat pumps, thermoelectric devices are reversible and can also convert the flow of heat into electricity. If a temperature gradient is applied to a thermoelectric material, *forcing* heat to flow, then this energy is converted to electricity (figure 2C).

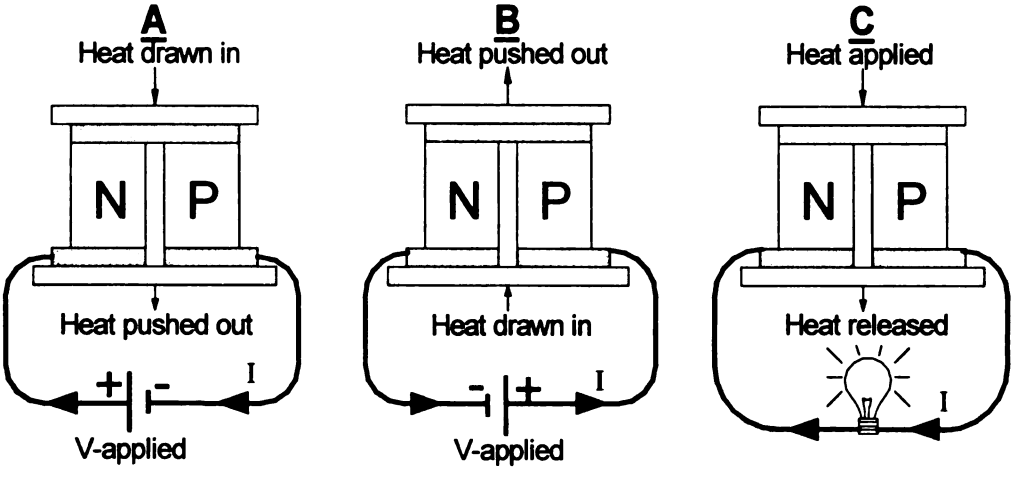

Figure 2A-C: Thermoelectric devices in three different operating modes.

Thermoelectrics are majority carrier devices usually made of extrinsic semiconductors where the free charge carrier density is adjusted to best convert energy between forms of heat and electricity. The majority carrier is responsible for the electrical and a portion of the thermal currents. If a temperature gradient is applied across a device, a thermal current forms consisting of phonons and free charge carriers. The charge carriers at the hot side have a higher thermal energy than those at the cold side, so they preferentially diffuse to the cold side of the device thus contributing to charge and thermal currents. Under open circuit conditions, the carriers accumulate at the cold side forming a potential that produces an electric field. This electric field continues to increase until an equilibrium condition is reached and the net charge flow goes to zero [1].

To best utilize the majority carrier effects, thermoelectric devices are made of repeated patterns of P and N type semiconductor materials placed electrically in series and thermally in parallel. The simplest device is made from one piece of each type of material, and is known as a thermoelectric couple (figure 3).

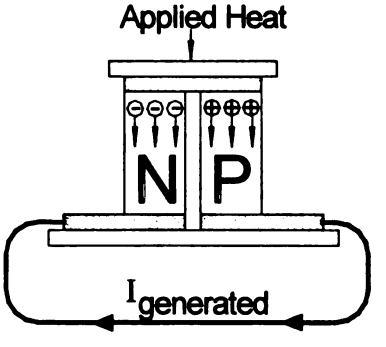

Figure 3: Thermoelectric couple as a majority carrier device.

The amount of heat that a device can pump is proportional to the size of the device. For a fixed length of the N and P legs of the device, an increase in the thermal cross-sectional area of the legs will cause the device to generate more electricity, or pump larger quantities of heat. If the cross-sectional area is increased by cascading couples electrically in series and thermally in parallel, then there is an increase in the voltage across the device. If the cross-sectional area is increased by increasing the dimensions of each of the two legs, there is an increase in the current through the device. A thermoelectric device made from a single couple would produce voltages too small for most present day applications. In order to make a device that sources a practical voltage, the leg cross-sectional areas are kept small and several couples are cascaded electrically in series and thermally in parallel.

1.2 *Thermoelectric Applications*

There are many applications for thermoelectrics, from medical to automotive, and consumer electronics to space exploration. Depending on the application, cost, size, weight, efficiency, power out and reliability, all factor in to deciding how and when to apply thermoelectrics as a means of cooling or for power generation. Thermoelectric technology is not always an appropriate substitute for other technologies, but many times they can be. Some examples are provided here, and many others exist [4].

Chlorofluorocarbon (CFC) chillers are often used for cooling purposes in industry, and are often near twenty percent efficient [2]. However, chilling units can be mechanically complex and require routine expensive maintenance. For example, conventional chiller systems can be quite acoustically and electromagnetically noisy and cause interference with other people and equipment. Because thermoelectrics operate on DC and have no moving parts, they offer less electromagnetic interference, are cleaner for the environment, and require less routine maintenance. Most industry fabricated thermoelectrics for cooling are presently limited to efficiencies of five to ten percent, and therefore are less efficient than CFC chillers. Nevertheless, thermoelectric chillers are a popular alternative to overcoming many of the problems encountered with conventional CFC based chiller systems.

Within the auto industry, thermoelectric climate control is available [2]. Wasted heat energy to brakes, engine, and exhaust systems are potential places thermoelectrics could be utilized to harness waste heat and turn it into electricity. With automobiles becoming equipped with more electronics and converting traditional mechanical systems to electrical systems, such as in belt-less engines, thermoelectrics may be quite convenient in power recovery systems. Thermoelectrics are not presently suitable for use in the automotive industry as power recovery systems because the efficiency does not justify the expense. Should the efficiency improve and fabrication costs decrease, many more applications are expected.

Many space exploration missions involving nuclear powered satellites are able to use thermoelectrics to convert heat produced from radioactive energy into electricity. Because of the long half life on several radioactive materials, images and information can be acquired about our galaxy for several years or decades. In fact, thermoelectric generators have been used for decades by NASA, either using radioisotope or nuclear fission reactor fuels [3]. Solar power based systems are often limited as the means to energy supply when missions are distant from or in an indirect path with the sun, so thermoelectric based systems are often a reliable alternative.

1.3 Renewed Interest in Thermoelectrics, TFD's

Many other applications are available for thermoelectrics [4]. The need for thermoelectrics is not new, but their low conversion efficiencies have kept them out of many commercial markets and therefore out of the consumer eye. Theoretical predictions and experimentally verified improvements in conversion efficiency have spurred a renewed interest in recent years. Many new materials and manufacturing processes have been discovered, however much of the renewed interest in thermoelectric technology has grown from exploiting quantum effects to improve conversion efficiency [21]. Such quantum effects have been realized in thin film devices (TFD) and have shown efficiencies far superior to traditional bulk materials. As charge carriers are confined, the allowed energies for those carriers is reduced, and an increase in the density of states at the

remaining allowed energies results. There is an increasing sharpness of the density of states at discrete energies as the charge carriers are increasingly confined to two, one, or zero dimensions.

Due to rapid progress in TFD technologies, TFD research and development has attracted many efforts in the thermoelectric community since its first appearance in the late twentieth century. However, like traditional bulk grown materials, TFD's have their own set of new challenges to overcome whether used for power generation or cooling applications. Such challenges include the needs to improve the manufacturing cost and time, and increase the ability to have large temperature gradients across them. The power produced from a thermoelectric generator is directly proportional to the temperature gradient established, and higher gradients are required to yield more power out.

Efforts from quantum based TFD research have redirected some bulk material research to achieve properties similar to TFD's. This redirected focus may lead to bulk materials containing quantum structures that improve efficiencies without the need for complex manufacturing processes used for TFD's. There are a couple groups investigating the incorporation of nanodots into bulk materials, including MSU.

2 Fundamentals of Thermoelectric Technology

2.1 Seebeck Effect

The basics for how most thermoelectric technology works can be explained by the fundamental relations contributed by scientists Seebeck, Peltier and Thomson. In 1822, T. J. Seebeck discovered the first of three main thermoelectric effects, which is described with reference to figure 4 [5].

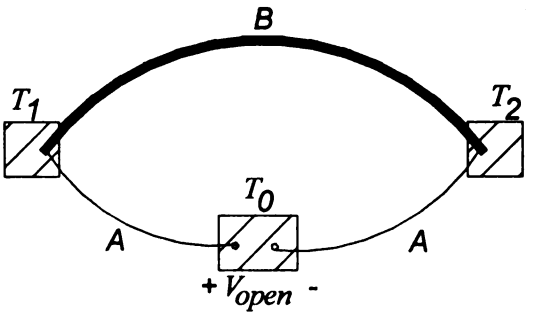

Figure 4: Seebeck effect, for polarity shown, $\alpha_A > \alpha_B$ for $T_2 = T_1 + \Delta T$.

Given two different materials, *A* and *B*, joined with their junctions maintained at temperatures T_1 and T_2, with a break at T_0, an open circuit voltage is created if $T_1 \neq T_2$. The details for the type of gradient between T_1 and T_2 do no reflect the open circuit voltage, V_{open}, for homogenous materials. The generated voltage is generally linear for small temperature gradients in homogenous materials, and is proportional to the temperature gradient through a temperature dependent Seebeck coefficient, $\alpha_{AB}(T')$, as,

$$V_{open} = \alpha_{AB}(T')(T_1 - T_2) \quad \text{(V)} \qquad (1)$$

The "Seebeck coefficient" refers to a junction of two dissimilar materials where each material contributes an absolute Seebeck coefficient "thermopower", $\alpha_x(T')$, to yield the net Seebeck coefficient. More generally in terms of the thermopower of material A, $\alpha_A(T')$, and material B, $\alpha_B(T')$:

$$V_{open} = \int_{T'=T_1}^{T'=T_2} (\alpha_A(T') - \alpha_B(T'))dT' = \int_{T'=T_1}^{T'=T_2} \alpha_{AB}(T')dT' \quad \text{(V)} \qquad (2)$$

In addition to the Seebeck coefficient being temperature dependent, the type of materials forming the junction will dictate whether the Seebeck coefficient is a positive or negative value.

2.2 *Peltier Effect*

The Peltier effect was discovered in 1834 by J. C. A. Peltier and can be demonstrated by passing a current through the junction of two different materials [5]. Peltier observed that under these conditions, heat, P_Q, is absorbed or liberated at the junction. For an applied current through two materials where $\alpha_A > \alpha_B$, heat is liberated at the right junction and absorbed at the left.

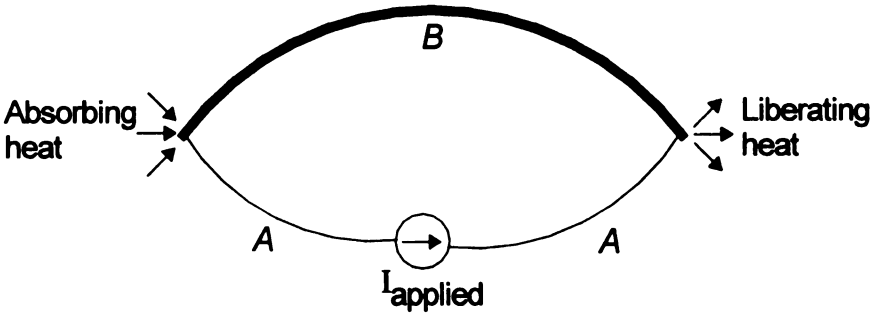

Figure 5: Peltier effect, $\alpha_A > \alpha_B$.

Peltier discovered this effect to be reversible, in that if the direction of current is reversed, so is the direction of heat exchange at the boundaries of materials *A* and *B*. The Peltier heat, P_Q, is related to the current, I, by the Peltier coefficient as,

$$P_Q = \pi_{AB} I \quad \text{(W)} \tag{3}$$

The Peltier coefficient relates to the Seebeck effect through Kelvin relations as,

$$\pi_{AB} = T\alpha_{AB} \quad \text{(V/K)} \tag{4}$$

2.3 *Thomson Effect*

The third and final thermoelectric effect discussed is the Thomson effect, discovered in 1854 [5]. Essentially, when an electrical current passes through a homogeneous material subjected to a temperature gradient, a Thomson heat is generated, T_Q. The direction of heat flow (absorbed or emitted) is related to the type of material, the temperature dependence of the thermopower, and the direction of current flow relative to the temperature gradient. For a metal wire shown in figure 6, heat is liberated when the current flows toward regions of colder temperature [6].

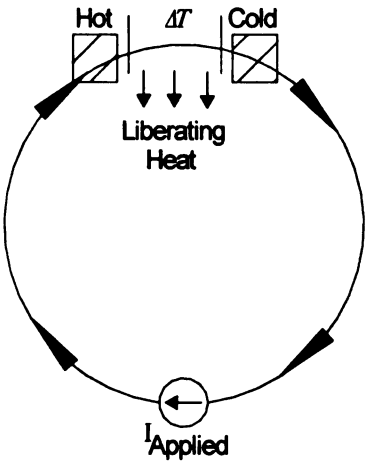

Figure 6: Thomson effect on single homogeneous material.

The Thomson coefficient, τ, relates the Thomson heat and electrical current through,

$$T_Q = -\tau I \Delta T \quad \text{(W)} \tag{5}$$

where $T_Q > 0$ implies heat is liberated, and can be readily related through Kelvin relations with the Seebeck effect as,

$$\tau = T\frac{d\alpha}{dT} \quad \text{(V/K)} \tag{6}$$

or

$$\alpha(T) = \int_{T'=0}^{T'=T} \frac{\tau(T')}{T'} dT' \quad \text{(V/K)} \tag{7}$$

2.4 *Thermocouples*

With the fundamentals of thermoelectrics established, it is possible to better understand how thermoelectric devices operate through a brief explanation of

how thermocouples work. A thermocouple is a device that produces a voltage proportional to the difference in temperature along its length by use of the Seebeck effect. There exist eight NIST standardized thermocouple types which have been well characterized, but a thermocouple can essentially be made of any two dissimilar electrical conductors [7]. To form a single-ended thermocouple, the ends of each conductor are joined at a single point to ensure good electrical and thermal connection between the conductors. Figure 7 will be used with the following calculations in determining temperature, where T_1 is the temperature to be determined, V_{TC} is the measured thermocouple voltage, and T_0 is a reference temperature for the thermocouple not equal to T_1.

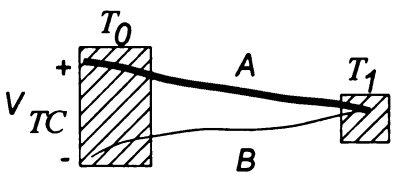

Figure 7: Single-ended thermocouple.

Using Kirchoff's voltage law, it's possible to sum up contributions from each material's generated thermoelectric voltage when a temperature gradient exists across the materials from T_0 to T_1.

$$V_{TC} = \int_{T'=T_0}^{T'=T_1} \alpha_A(T')dT' + \int_{T'=T_1}^{T'=T_0} \alpha_B(T')dT' = \int_{T'=T_0}^{T'=T_1} \alpha_A(T')dT' - \int_{T'=T_0}^{T'=T_1} \alpha_B(T')dT'$$

$$= \int_{T'=T_0}^{T'=T_1} [\alpha_A(T') - \alpha_B(T')]dT' = \int_{T'=T_0}^{T'=T_1} \alpha_{AB}(T')dT' \quad (8)$$

The above voltage depends on the temperature, T_0, of the meter measuring the voltage. The Seebeck coefficient data, $\alpha_{AB}(T')$, for standard thermocouples is typically given relative to a reference junction maintained at 0°C; however equation 9 allows a thermocouple to be referenced to any temperature [8].

$$V_{Measured} = \int_{T'=0°C}^{T'=Tref} \alpha_{AB}(T')dT' + \int_{T'=0°C}^{T'=Tjunction} \alpha_{AB}(T')dT' \quad (9)$$

Each of the integrals in equation 9 can be solved separately using a standard thermocouple look up table or a curve fit to the standard data [7].

A common question is why there is no Seebeck voltage contribution due to extension wires from the measurement instruments to reference junction.

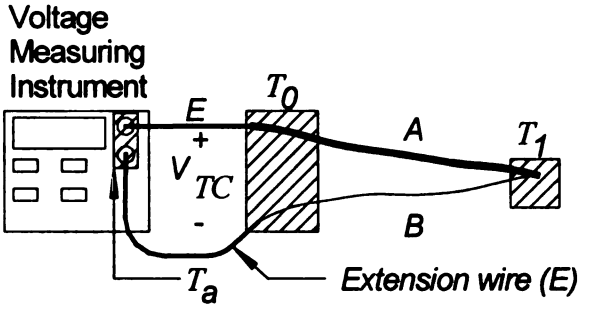

Figure 8: Thermocouple measurement.

Previous calculations assume the extension wires are made of the same material and that the temperature gradient along the wires from measurement instrument to the reference junction are equal allowing Seebeck contributions to cancel. Adding the measurement wires into the derivation yields,

$$V_{TC} = \int_{T'=T_a}^{T'=T_0} \alpha_E(T')dT' + \int_{T'=T_0}^{T'=T_1} \alpha_A(T')dT' + \int_{T'=T_1}^{T'=T_0} \alpha_B(T')dT' + \int_{T'=T_0}^{T'=T_a} \alpha_E(T')dT'$$

$$= \int_{T'=T_a}^{T'=T_0} \alpha_E(T')dT' + \int_{T'=T_0}^{T'=T_1} \alpha_A(T')dT' + \int_{T'=T_1}^{T'=T_0} \alpha_B(T')dT' - \int_{T'=T_a}^{T'=T_0} \alpha_E(T')dT'$$

$$= \int_{T'=T_0}^{T'=T_1} \alpha_A(T')dT' + \int_{T'=T_1}^{T'=T_0} \alpha_B(T')dT' = \int_{T'=T_0}^{T'=T_1} \alpha_A(T')dT' - \int_{T'=T_0}^{T'=T_1} \alpha_B(T')dT'$$

$$= \int_{T'=T_0}^{T'=T_1} \alpha_{AB}(T')dT' \qquad (10)$$

This is the same result as found previously without the extension wiring contributions. If the thermocouple material changes from sample to instrument, the temperature at the point of material change must be known. This point of material change is often referred to as the reference junction, and requires use of another temperature sensor such as a well calibrated diode or platinum resistor.

The single-ended thermocouples of figures 7 and 8 are used if an absolute temperature is to be measured. If a temperature gradient is to be measured with single-ended thermocouples, two are needed, and this results in four measurement wires. However, a differential thermocouple can also be used to obtain the temperature gradient, and only uses two wires. Figure 9 shows an example of a differential thermocouple, made of materials A and B surrounded by shaded isothermal regions T_0, T_1, and T_2 where $T_0 \neq T_1 \neq T_2$.

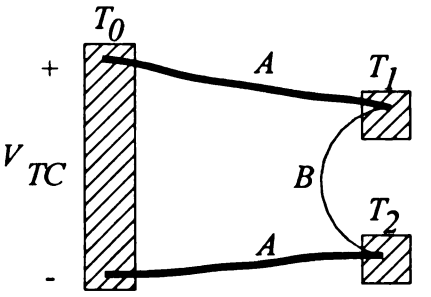

Figure 9: Differential thermocouple.

Following the same procedures as for the single-ended thermocouple, the temperature gradient can be obtained by integrating the Seebeck coefficient for the thermocouple over the range of temperature defined.

$$V_{TC} = \int_{T'=T_0}^{T'=T_1} \alpha_A(T')dT' + \int_{T'=T_1}^{T'=T_2} \alpha_B(T')dT' + \int_{T'=T_2}^{T'=T_0} \alpha_A(T')dT'$$

$$= \int_{T'=T_2}^{T'=T_1} \alpha_A(T')dT' + \int_{T'=T_1}^{T'=T_2} \alpha_B(T')dT'$$

$$= \int_{T'=T_2}^{T'=T_1} \alpha_A(T')dT' - \int_{T'=T_2}^{T'=T_1} \alpha_B(T')dT'$$

$$= \int_{T'=T_2}^{T'=T_1} [\alpha_A(T') - \alpha_B(T')]dT' = \int_{T'=T_2}^{T'=T_1} \alpha_{AB}(T')dT' \qquad (11)$$

For small temperature gradients, the last integration can be linearly approximated so that $\lim_{dT \to 0} \Rightarrow \alpha_{AB}\left(\frac{T_1 + T_2}{2}\right) \cong \alpha_{AB}(T_{Average}) \cong \alpha_{AB}(T_1) \cong \alpha_{AB}(T_2)$. Here, $\alpha_{AB}(T_1)$ and $\alpha_{AB}(T_2)$ indicate α_{AB} as a function of temperature. This approximation yields a simple result for obtaining the temperature gradient that is independent of the reference temperature.

$$T_1 - T_2 = \frac{V_{TC}}{\alpha_{AB}(T_{Average})} \tag{12}$$

As with the single-ended thermocouple, a reference temperature must be measured by another sensor in a region local to the gradient in order to identify $\alpha_{AB}(T_{Average})$.

For measuring large temperature gradients with a differential thermocouple, if either the average, hot or cold side temperatures is known, the other temperatures may be found from a fitting technique. For example, figure 10 shows how it may be possible to use the type K thermocouple with a linear approximation, but a type E thermocouple may require a polynomial fit [9].

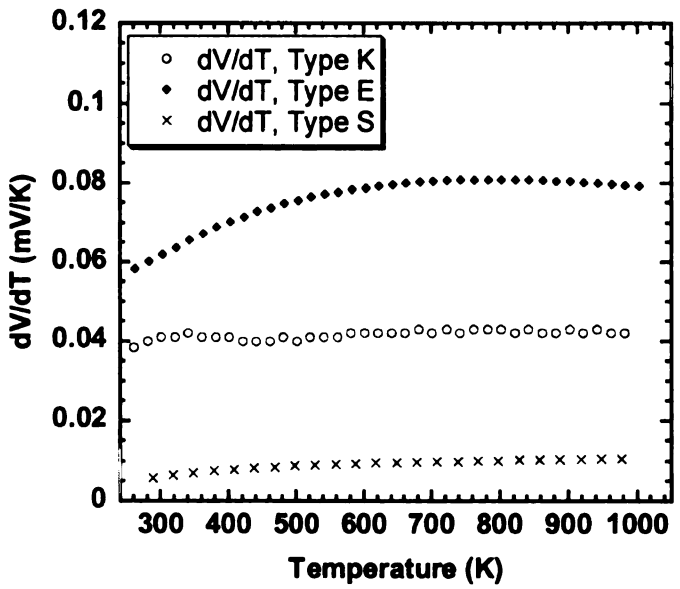

Figure 10: dV/dT for type K, E, and S thermocouples.

Once the range of temperature measurements is known, it is possible to choose one thermocouple over another depending on the temperatures measured, sensitivity of the thermocouple, cost, and susceptibility to oxidation. For

example, figure 11 shows how it may be useful to use a type E thermocouple over a type K or S for its increased sensitivity.

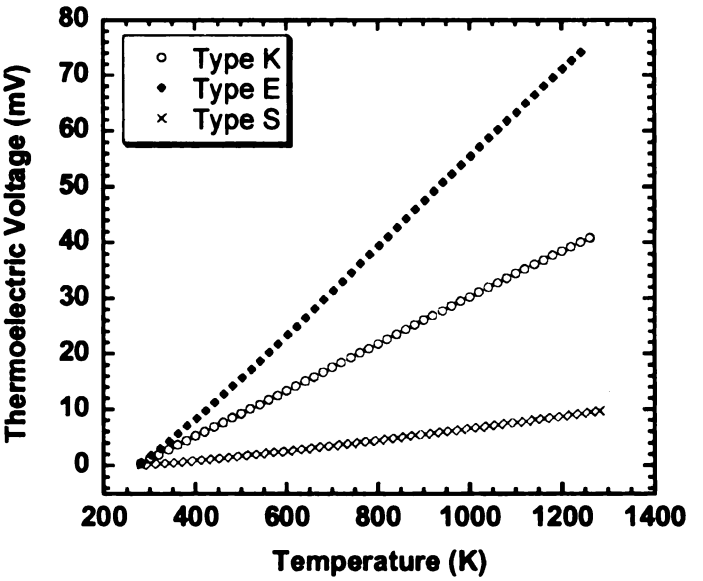

Figure 11: Comparing type E, K, and S thermocouples.

2.5 Thermocouples and Thermoelectric Devices

A single couple thermoelectric device functions as a thermocouple, such that if a temperature gradient is applied across its two dissimilar materials, a Seebeck voltage is generated that is proportional to the gradient. Consider the following example of a thermoelectric device made from several cascaded thermocouples thermally in parallel and electrically in series, also known as a "thermopile", in figure 12, where materials A and B alternate. The shaded regions are isothermal.

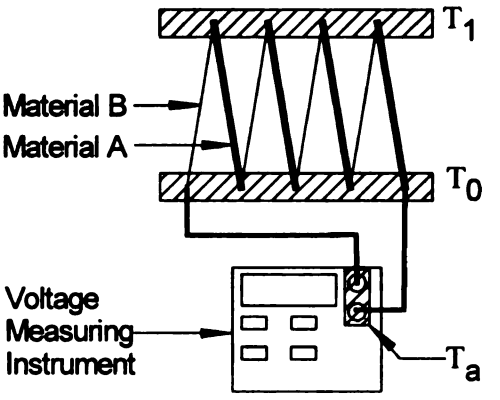

Figure 12: Thermocouple based thermoelectric device.

The thermocouples are identical and each produce equivalent voltages, and the extension wires between T_0 and instrument have canceling Seebeck voltages. Therefore, the measured voltage is just one thermocouple voltage repeated four times.

$$V_{Measured} = (4)\int_{T'=T_0}^{T'=T_1} \alpha_{AB}(T')dT' \qquad (13)$$

So for a thermoelectric device of *X*-couples, the voltage produced scales proportionally with the Seebeck coefficient *X*-times. The electrical power out increases for the device with increased number of couples, but so must the power in to establish the same temperature gradient across them. Therefore, the efficiency as the ratio of power out to power in remains constant for devices made of a single couple, as well as for *X*-couples. Thermocouples are made of metals which have low thermoelectric efficiencies. Therefore, other materials are used which have much better thermoelectric performance. Reasons for why some materials have better performance than others are discussed further.

3 Thermoelectric Materials

3.1 Ideal Material Properties

The efficiency of a thermoelectric material is proportional to a property known as the figure of merit, *Z*. For power generation applications, the efficiency ideally relates to the figure of merit as follows [10].

$$\eta_{ideal} = \frac{\left(\frac{T_{Hot} - T_{Cold}}{T_{Hot}}\right)}{\left[2 - \frac{1}{2}\left(\frac{T_{Hot} - T_{Cold}}{T_{Hot}}\right) + \frac{4}{ZT_{Hot}}\right]} \tag{14}$$

The figure of merit is further related to the material properties: Seebeck voltage, $\alpha(T)$, electrical conductivity, $\sigma(T)$, and thermal conductivity, $\kappa(T)$, which are all functions of temperature (T) [11].

$$Z = \frac{\sigma(T)\alpha(T)^2}{\kappa(T)} \tag{15}$$

Since the material properties change as a function of temperature, so must the efficiency. Each known thermoelectric material has a range of temperatures it performs most efficiently in. Different materials are suited for different temperature applications, and to date there is no single material suited for all applications.

The figure of merit shows that an ideal thermoelectric material should be a thermally insulating electrical conductor. Unfortunately for thermoelectrics, nature's elements are found as conductors, non-conductors or semiconductors for which electrical and thermal properties are directly coupled. Hence, good

electrical conductors are poor thermal insulators and good thermal insulators are poor electrical conductors. This limitation makes thermoelectric materials unique, so nature's materials need to be engineered to possess the ideal thermoelectric properties.

3.2 Engineering Thermoelectric Materials

Engineering thermoelectric materials for increased efficiency often requires a lowering of the thermal conductivity or increasing the electrical conductivity. One approach to developing a good thermoelectric material involves starting with a good electrical conductor, such as a metal, and engineering the material to decrease its thermal conductivity. A second approach is to start with a low thermally conductive material, such as an oxide, and increase its electrical conductivity. However, analytical and experimental research shows that the most efficient thermoelectric materials occur as semiconductors and semimetals [12,13]. As shown in figure 13, semiconductors and semimetals tend to yield the highest figure of merit. One important characteristic of materials with high thermoelectric figures of merit is that they share a common free charge carrier density on the order of 10^{18} - 10^{21} cm^{-3} [6].

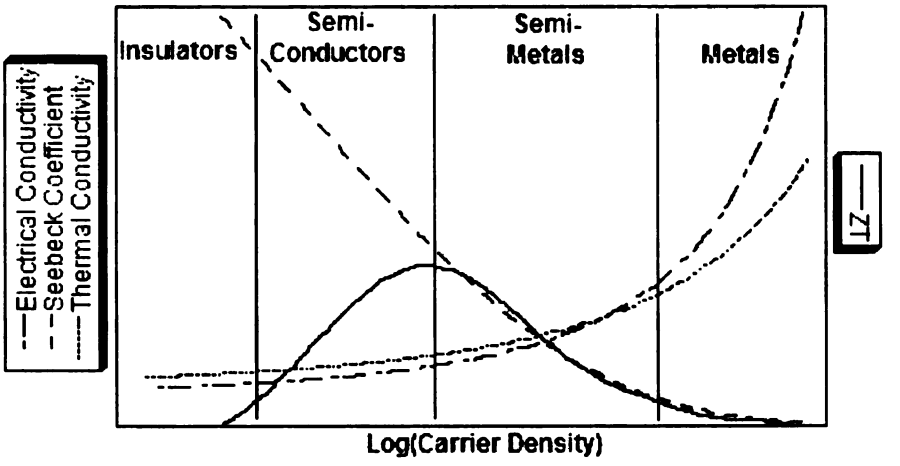

Figure 13: Ideal thermoelectric materials.

As shown in figure 13, increasing the thermoelectric power causes a reduction in electrical conductivity. An increase in electrical conductivity leads to an increase in the electronic contribution in thermal conductivity. It is a challenge to find efficient thermoelectric materials because the parameters are dependent on the free charge carrier density, and while one parameter is optimized with a low carrier density, another requires a high density. There are several ways to enhance material properties to satisfy one parameter while having little or no affect on the other, and some of these techniques are described further. Such techniques include new approaches to material synthesis, as well as a variety of fabrication methods.

3.2.1 Improving Efficiency, Lowering Thermal Conductivity

Since the efficiency of thermoelectric materials requires a low thermal conductivity, an understanding of how to achieve this is discussed. Thermal

conductivity is the ability for a material to conduct heat. Both the phonons and the charge carriers can conduct heat through the material, therefore

$$\kappa_{Total} = \kappa_{Electronic} + \kappa_{Lattice} \tag{16}$$

At very low temperatures, the atoms vibrate very slowly, so the lattice thermal conductivity can be very small or negligible compared to the electronic contribution. At sufficiently high temperatures the lattice vibrates much more, so the lattice thermal conductivity becomes dominant. Between these extremes, both mechanisms contribute to the thermal conductivity of a material. When engineering a thermoelectric material for low thermal conductivity, it is often possible to reduce one component of the thermal conductivity without appreciably affecting the other material parameters.

When manipulating characteristics of thermoelectric materials to reduce the thermal conductivity, it is useful to recall the Wiedemann-Franz Law. This law is usually applied to metals, and states that the electrical conductivity and thermal conductivity are often proportional to temperature through a constant [57]. Hence, if the materials electrical conductivity is increased, the electronic thermal conductivity will increase proportionally with temperature. This constant of proportionality applies for temperatures above the Debye temperature, θ_D, and is generally referred to as the Lorentz number, *L*, for the material [14].

$$L = \frac{\kappa}{\sigma} = (s+2)\left(\frac{k_B}{e}\right)^2 T \text{ for } T > \theta_D \tag{17}$$

Here, s, k_B and q are the scattering parameter, Boltzmann constant as $k_B = 8.616 \times 10^{-5}$ eV/K, and electron charge as $q = 1.6x10^{-19}C$ respectively. The scattering parameter indicates the type of dominant scattering: $s = 0$ for pure phonon, $s = 1$ for mixed and $s = 2$ for ionized impurity scattering [15]. For metals, the Lorentz number is 2.45x10^{-8} W-Ω/deg^2 [57], or it can be calculated directly as shown below [16].

$$L = \left(\frac{k_B}{q}\right)^2 \left[\left(\frac{(s+3)}{(s+1)}\right)\left(\frac{F_{s+2}}{F_s}\right) - \left(\frac{(s+2)^2 {F_{s+1}}^2}{(s+1)^2 {F_s}^2}\right)\right] \tag{18}$$

The Fermi integrals, F_i, are found with respect to the reduced chemical potential, ζ, and referenced from the conduction band edge as,

$$F_i = \int_0^\infty \frac{x^i}{e^{(x-\zeta)}+1} dx \tag{19}$$

The reduced chemical potential is found directly from the thermopower, and for an N-type material is given by,

$$\zeta = \left[\alpha \frac{q}{k_B} + \left(\frac{(s+2)}{(s+1)} \frac{F_{s+1}}{F_s}\right)\right] \tag{20}$$

For the LAST materials at some arbitrary temperature, 400K, with mixed scattering, the Lorentz number can be calculated as $2.28x10^{-8} \frac{W\Omega}{K^2}$ [17]. From this, the lattice and electronic contributions may be decoupled to give the electronic contribution from Wiedemann-Franz as $\kappa_{Electronic} = L\sigma T$. Using literature data for the LAST material with a measured overall thermal conductivity

of $2.1\frac{W}{mK}$, this results in $\kappa_{Electronic} = 0.684\frac{W}{mK}$ and

$\kappa_{Lattice} = \kappa_{Total} - \kappa_{Electronic} = 2.1 - 0.684 = 1.416\frac{W}{mK}$. This result agrees well with the optimal figure of merit requirement on thermal conductivity where higher values of ZT have been observed when $\frac{\kappa_{Electronic}}{\kappa_{Lattice}} \sim 0.5$ [27].

The thermal conductivity can be adjusted by limiting or altering the dominant scattering mechanism, but the type of scattering must be known. Most metals and semimetals have an increasing lattice contribution and decreasing electronic contribution with increasing temperature; so for high temperatures, the goal is usually to reduce the dominant lattice contribution. Many times in thermoelectric material engineering, the goal is to reduce either the thermal or electronic contribution without inversely affecting the other. Due to the Wiedemann-Franz Law, it is not always best to reduce the electronic component of the thermal conductivity for high charge carrier density materials since it will adversely affect the electrical conductivity and have little or no affect on the figure of merit. Therefore, much effort is placed on reducing the thermal conductivity of a material through the lattice component, and this can be achieved through tuning of the scattering mechanisms.

3.2.1.1 Lattice Thermal Conductivity Reduction, Atom Substitution

One way to reduce the lattice thermal conductivity involves substitution of one of atom with another. The mass fluctuation increases the scattering of phonons and thus decreases the lattice thermal conductivity. For example, Skutterudites are minerals of $(Co,Ni)As_{3-X}$ composition that exhibit good thermoelectric properties [18]. They have high thermopower and electrical conductivity, but also have a high thermal conductivity. Therefore the lattice thermal conductivity of Skutterudites is commonly reduced by substituting particular lattice site atoms, adding atoms into the unit cell voids, or both.

3.2.1.2 Lattice Thermal Conductivity Reduction, Grain Boundaries

A second way to reduce the lattice thermal conductivity involves phonon scattering at grain boundaries. Phonon scattering is increased at the grain boundaries, thus decreasing the lattice thermal conductivity. However, grain boundaries also scatter charge carriers causing a lowering of the electrical conductivity. This trade-off effect in the conductivities can sometimes be partially decoupled through different fabrication methods with cold or hot pressing [19]. Such fabrication methods involve grinding the raw elements down to a particular particle size, and then pressing the ground material into a desired shape. The material now has an increase in grain boundaries, where a grain of the material is a region of continuous crystal growth without any defects. Perfect crystalline materials would have no grain boundaries, and would allow an ideal path for

charge carriers, as well as phonons. Polycrystalline materials are a collection of crystalline regions that are touching, but discontinuous; and discontinuous implies that the atomic lattice contains one or more defects. The material grain size can be adjusted to scatter the phonons but promote charge carrier travel. By sintering the pressed material, grains begin to grow together. The growth can be controlled by the initial particle size, pressing force, and sintering conditions of time, temperature, and atmosphere [20].

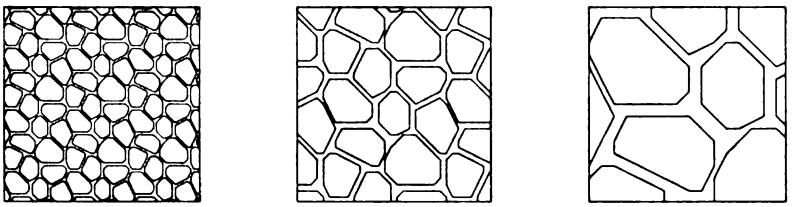

Figure 14: Sintering affects on grain size., least sintering (*left*), most (*right*).

3.2.1.3 Lattice Thermal Conductivity Reduction using QSL's

A third way to achieve reduced lattice thermal conductivity is through phonon scattering with least affect on the charge carriers. Calculations have been predicted and experimentally verified to show this is possible through reduction of the dimensionality of the material to that of 2-D, 1-D, 0-D quantum confined structures [21]. 2-D quantum superlattice structures (QSL) can be made in a variety of ways [22,23], and one popular approach is through molecular beam epitaxial growth (MBE). MBE is a process by which layers of atoms are grown in precise layers, and this allows tuning of the thermoelectric properties through quantum confinement. This tuning allows for higher in-plane charge carrier mobilities leading to reduced scattering effects, and thus a reduced lattice

thermal conductivity [24]. The high mobility desired in thermoelectric materials is across plane, but mobility is taken as inversely proportional to a weighted average of the scattering effects [25]. The mobility and thermal conductivity can be indirectly related to ZT through the *B*-factor, $ZT \sim B$ where $B \sim \frac{\mu}{\kappa_{lattice}}$ [21]. A second approach to reducing the dimensionality involves growing 1-D nanowires that are smaller in diameter than the mean phonon wavelengths. Such nanowires inhibit phonon travel while promoting charge carrier movement, leading to low thermal conductivities with high electrical conductivity, and higher figure of merits. For example, superlattice (SL) P-type Bi_2Te_3 based materials have shown substantial improvements in the figure of merit, ZT = 2.4, compared to the respective bulk value of 1.14 [26]. Although QSL devices have potential to offer higher efficiencies than bulk materials, the technology is relatively new compared to bulk made devices, so they bring forth many new challenges and opportunities for future research. One such challenge is that QSL devices are usually so thin that the overall thermal conductance of the device can be large, so it is difficult to establish a high temperature gradient. QSL also faces challenges of reducing fabrication costs and time, as they are presently more involved processes than required for bulk material processing. QSL technology opens many new doors of exciting research for thermoelectric applications, and such obstacles must be addressed if they are ever to dominate bulk material fabricated devices in the marketplace.

3.2.1.4 Lattice Thermal Conductivity Reduction, Bandgap Engineering

A fourth way to reduce the lattice thermal conductivity is to synthesize materials with small band gaps, since small band gap materials usually have low lattice thermal conductivities [27]. However, thermoelectrics are majority carrier devices, and materials with small band gaps may have problems of keeping a high thermopower before minority carrier generation occurs. A relationship of optimal band gap to maximum thermopower, which occurs at some maximum temperature, can be approximated by the following [28].

$$E_{gap} = 2qT_{\max}\alpha_{\max} \tag{21}$$

Here, q, is the electron charge of 1.6x10^{-19} C, E_{gap} is the band gap, $\alpha_{\max}$ is the maximum thermopower, and $T_{\max}$ is the temperature at which the thermopower peaks before minority carriers play a significant role.

3.2.2 Improving Efficiency, Increasing Electrical Conductivity

Good thermoelectric materials should have a high electrical conductivity. It is possible to increase the conductivity of semiconductors with impurities, but the choice and concentration of impurities is critical for good material properties. The reasons for this are similar to discussion earlier for ideal thermoelectric materials, and the relationship can be derived further with respect to the free charge carrier density. The electrical conductivity, considering a single carrier, gives

$$\sigma = q\mu_x n = \frac{q\mu_x}{2\pi^2}\left(\frac{2k_B T}{\hbar^2}\right)^{3/2}\left(m_n^*\right)^{3/2} F_{1/2} \tag{22}$$

where μ_x is the mobility in the *x* direction, m_n^* is the density of states effective mass, k_B is Boltzmann's constant (8.616×10^{-5} eV/K), T is temperature, $\hbar$, is Plank's reduced constant, q is the electronic charge (1.602×10^{-19} C), and $F_{1/2}$ is the Fermi-Dirac function of order one half as defined in section 3.2.1. As mentioned, the choice and concentration of impurities is critical for improving thermoelectric performance. For example, the impurity should be a shallow donor so as not to act as a mid-band hopping site for valence band carriers into the conduction band, and vice-versa. As heat is provided to a semiconductor, this energy can cause an electron to change energy levels. If the appropriate amount of heat is provided for good thermoelectric performance, the charges will scatter in the band, but not from band to band. Carriers generated from band to band are undesirable because they generally oppose the net flow of electrical current.

3.3 Measurements of Bulk Materials

Measurement of electrical and thermal conductivities, and Seebeck coefficient obtained in the Pulsed Laser Deposition and Transport Characterization Laboratory at MSU are discussed. Results of system measurement accuracy have been verified and are readily available elsewhere, so only the processes are briefly described here [17, 45, 50].

3.3.1 Electrical Conductivity Measurements of Bulk Materials

Electrical conductivity is taken using a four point probe technique [29]. This technique is usually used when measuring highly conductive materials, such as those used for thermoelectrics, since a two point probe would contribute dominating lead and contact resistances. The general technique involves applying current to a sample, and measuring the ohmic voltage produced. The sample conductivity is found from the measured dimensions, voltage and known current supplied.

$$\sigma = \frac{Il}{VA} \quad (\Omega^{-1}\mathrm{m}^{-1}) \tag{23}$$

Here, $\sigma, \mathrm{I}, \mathrm{V}, \mathrm{l}$, and A are the conductivity, current supplied, voltage measured, length and cross-sectional area of the sample, respectively.

Although thermoelectric materials are good electrical conductors, the ends of the sample under test are often nickel electroplated to ensure an even current distribution throughout the sample.

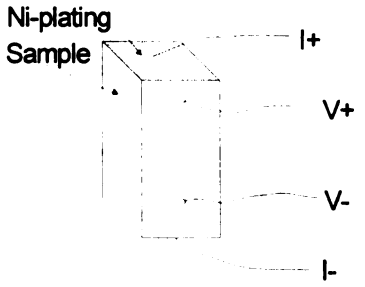

Figure 15: Electrical conductivity test.

Measurements made at low temperatures are often made using wires of 1-3 mil copper that are adhered with indium solder or conductive paint. For high temperature measurements, the technique is the same, but lead wires are often made of 1 mil constantan, chromel, or platinum, and adhered with the silver paint. Copper leads are rarely used for high temperature measurements due to its reactivity and oxidation effects. The supplied current produces an ohmic voltage drop across the material, and thermoelectric materials produce an additional voltage due to the Seebeck effect. The Seebeck effect is due to DC electron flow, and the ohmic voltage can be isolated by applying an AC current to inhibit temperature gradients. However as commonly used is this lab, a Keithley model 2400 sourcemeter and 2182 nanovoltmeter have been configured to reverse the polarity of a DC current fast enough to show comparable results to AC testing utilizing a lock-in amplifier [45].

3.3.2 Thermopower Measurements on Bulk Materials

The thermopower of a material is generally determined by measuring the temperature gradient and voltage simultaneously by use of single ended thermocouples.

$$\alpha = \frac{dV}{dT} \quad \text{(V/K)} \tag{24}$$

For low temperatures, 80-400K, type T thermocouples of 1 or 3 mil diameter wire are used to measure the temperature gradient. Both single-ended and differential thermocouples have been used, however single-ended styles are

more accurate for measuring thermopower of a sample since the location of temperature gradient and electric potential are monitored in the exact same location [46]. For high temperature applications, type E, K and S thermocouples of 1 and 3 mil diameter wire are commonly used to measure the temperature gradient.

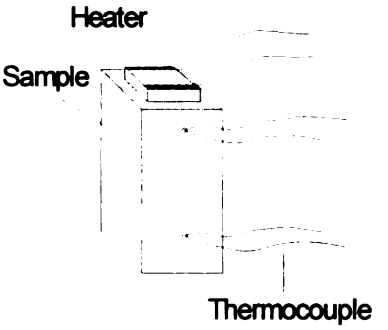

Figure 16: Thermopower and thermal conductivity measurements.

To establish the temperature gradient, a small surface mount resistor or platinum sense resistor is prepared adhered to one side of the sample with a metallic paint or solder, as shown in figure 16 above.

The Maldonado technique is commonly used for rapid measurement of thermopower and thermal conductivity on bulk materials [30, 45, 50]. This technique provides a pulsing heat as opposed to the traditional steady-state approach and offers several advantages. First, this method does not require the long waiting time to approach steady-state. Second, the thermopower is taken as a linear fit of several measurements of dV/dT, not just a single steady-state value.

3.3.3 Thermal Conductivity Measurements of Bulk Materials

The thermal conductivity is also obtained through the Maldonado technique, simultaneously with thermopower. All that is required to obtain thermal conductivity in addition to the thermopower is the measurement of the heater power. Then, thermal conductivity is obtained as,

$$\kappa = \frac{P \cdot l}{dT \cdot A} \quad \left(\frac{W}{m \cdot K}\right) \tag{25}$$

where $\kappa, P, l, A,$ and dT are thermal conductivity, power delivered to the resistive heater, length of the sample along direction of heat flow, cross sectional area of the sample, and temperature gradient respectively. This measurement relies on all power generated in the heater to flow through the sample by means of conduction. However, the supplied heat also travels by means of convection, conduction to the measurement wiring and radiation to the cooler ambient environment, so accurate measurements must account for these. To minimize the losses, the samples are sealed under 10^{-6} Torr vacuum for testing to minimize convection losses, lead wires are kept long and small in cross sectional area to reduce conductive losses, and the sample stage housing is electroplated and polished to reduce radiation losses. Losses are not avoidable, but can be reduced so their affect on the measurement is secondary or negligible [45].

4 Thermoelectric Devices

4.1 Why investigate thermoelectric devices at MSU

New thermoelectric compounds are being developed at MSU for purposes of power generation, such as the LAST material, and are exhibiting excellent properties for temperature ranges of 500-700°K. In fact, the LAST material presently out performs many popular materials for power generation in this temperature region.

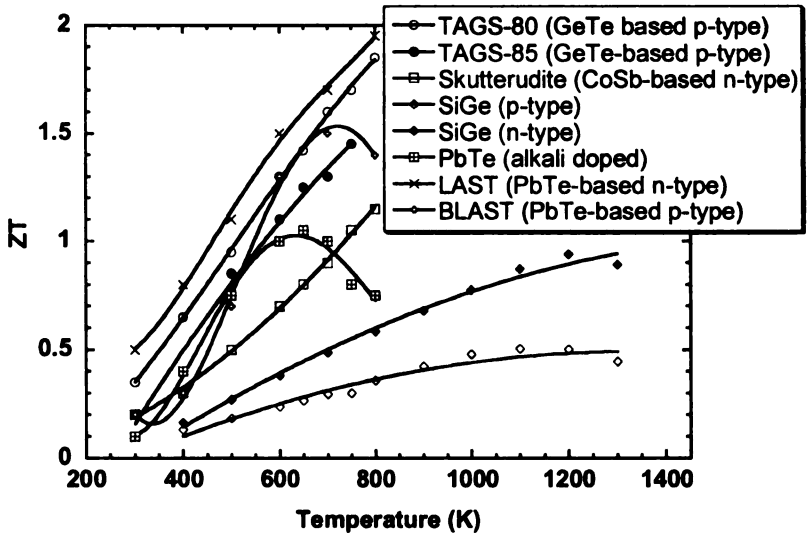

Figure 17: ZT comparisons with LAST.

The next steps for these materials involve developing them as a working device. As presented by others in the thermoelectric community, challenges in device fabrication and testing provide an entire new area in thermoelectrics. Initial research was exploratory synthesis to find a promising material with high ZT. The focus at MSU is now drawn toward improving fabrication methods and expedited testing on large quantities of devices. In order to begin testing, it is

important to know how devices operate, what properties does the thermoelectric community commonly use to characterize device performance, and how does one measure these properties.

4.2 Thermoelectric Efficiency and Carnot Cycles

Thermoelectric power generators ideally operate as Carnot cycles, and Carnot cycles are defined as reversible processes in which energy can be converted between work and heat. In a Carnot cycle for which a heat engine operates between a hot and cold reservoir, such as a thermoelectric device, some of the heat energy is converted to work through a chemical process and the other is rejected to the cold reservoir. This phenomenon comes from thermodynamic experiments, and the conversion of energy between work and heat for a given engine has never been shown to be 100%. As explained by Lord Kelvin, the ratio of heat transfer between the hot and cold reservoirs is proportional to the absolute temperatures of the reservoirs. Therefore, the conversion efficiency of a Carnot process, η_C, is limited by the heat transfer or absolute temperatures [5].

$$\eta_C = \frac{\Delta T}{T_{Hot}} \tag{26}$$

Thermoelectric generators operate ideally as Carnot engines, but further limitations arise from adverse effects of irreversible Joule and Thomson heating that prevents them from being fully reversible. Nevertheless, thermoelectric generating processes are commonly considered to be Carnot limited since this represents the upper limit to their efficiency when the adverse effects are

minimized. Thermoelectric device efficiencies are commonly referred to in literature in terms of their ideal performance, or "Carnot" efficiency. A more realistic value of thermoelectric device efficiency includes limitations from material properties, and is often referred to as the "reduced efficiency". The reduced efficiency is generally defined in terms of the Carnot efficiency.

4.3 Thermoelectric Device Efficiency

In addition to being Carnot limited, thermoelectric devices are also limited by the temperature dependent properties of the materials that make them. For power generation applications, efficiency is the ratio of power out to power in [31]. The power out is defined as the electricity given to some fixed load due to some power from an applied heat source.

$$\eta_{Ideal} = \frac{P_{ElectricalOut}}{Q_{SuppliedIn}} = \frac{I^2 R_{Load}}{\kappa(T)\Delta T + \alpha_{Hot}(T) T_{Hot} I - \frac{1}{2} I^2 R_{Module}} \qquad (27)$$

The heat flow given by the denominator of the previous equation can be defined separately in order to identify how the heat distributes throughout the device.

$\kappa(T)\Delta T$ → Thermal conduction

$\alpha_{Hot}(T) T_{Hot} I$ → Peltier effect

$\frac{1}{2} I^2 R$ → Joule heating

In describing heat flow through a thermoelectric device, it is usually convenient to know how much heat goes in, and how much passes through due to thermal

conduction, $\kappa(T)\Delta T$, that was not converted to electricity, $\alpha_{Hot}(T)T_{Hot}I$. When the device converts the heat to electricity and electrical current flows, the resistance causes Joule heating. For understanding the heat flow mathematically, the device can be split into two sections, the part that the heat flows in to, and the other half that the heat flows out of. Because the entire device experiences current flow and therefore Joule heating, half of the Joule heat can be considered to flow toward the hot side and half to the cold side. In this regard, the half Joule heating that flows to the hot side can be thought of as contributing to the total heat sourced into the device.

The efficiency can also be maximized by adjusting the thermoelement lengths and cross sectional areas. When this is done, the efficiency can be written as a function of the figure of merit and Carnot efficiency, where the Peltier and thermal conduction terms are disguised in the figure of merit, ZT_{Hot}.

$$\eta_{Ideal} = \frac{P_{Electrical\,Out}}{Q_{Supplied\,In}} = \eta_C \frac{\left(\frac{R_{Load}}{R_{Module}}\right)}{\frac{\left(\frac{R_{Load}}{R_{Module}}+1\right)^2}{ZT_{Hot}} + \left(\frac{R_{Load}}{R_{Module}}+1\right) - \left(\frac{\Delta T}{2T_{Hot}}\right)} \quad (28)$$

Thus, the device efficiency varies as a function of temperature gradient and load.

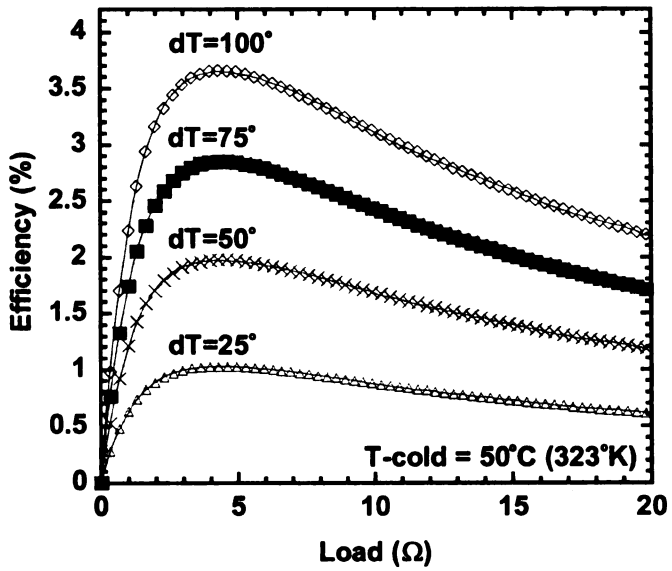

Figure 18: Efficiency versus gradient and load.

A more realistic device will include electrical contact resistances due to interfaces between the device materials and metal interconnects. This efficiency including contact resistance, η_{wcr}, can be found as,

$$\eta_{wcr} = \frac{P_{Electrical\,Out}}{Q_{Supplied\,In}} = \eta_C \frac{\left(\frac{R_{Load}}{R_{Module}}\right)}{\left[\frac{(\Gamma+1)^2}{ZT_{Hot}} + (\Gamma+1) - \left(1+2\left(\frac{R_{Chs}}{R_{Module}}\right)\right)\left(\frac{\Delta T}{2T_{Hot}}\right)\right]} \quad (29)$$

where R_{Chs} is the contact resistance of the hot side of the device and

$$\Gamma = \frac{R_{Load} + R_{Contact}}{R_{Module}} \quad (30)$$

Figure 19 shows an example of how contact resistance affects efficiency when the temperature gradient is held constant across some fictitious material.

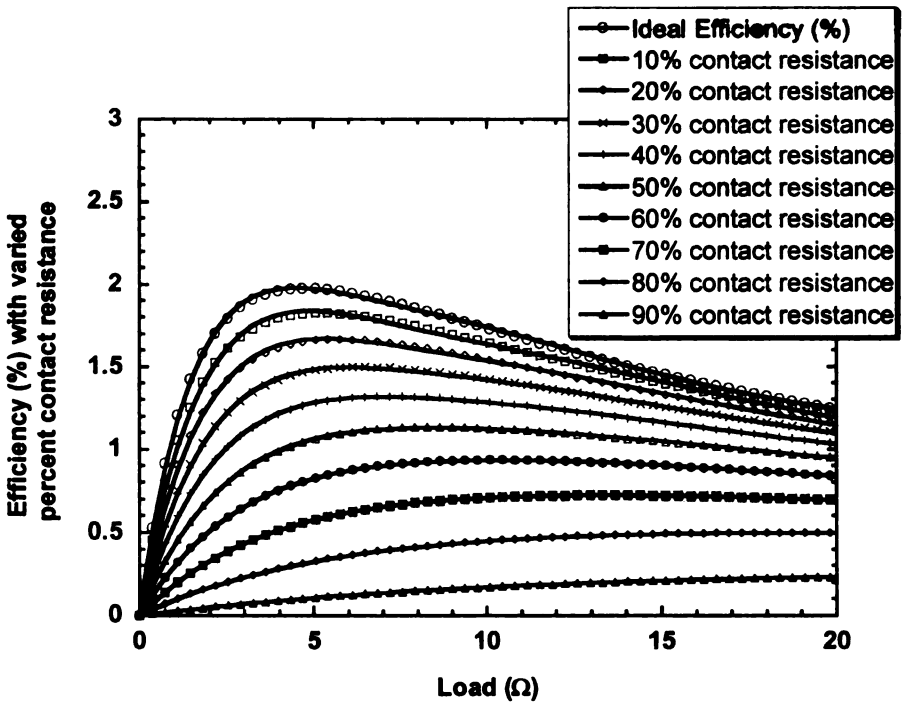

Figure 19: Efficiency with varied percent contact resistance.

The equations given previously apply for devices under small gradients, < 10°K. For devices operated under load conditions and larger temperature gradients, the total heat flow[1] is more accurately described with consideration of the Thomson heat, $Q_{Thomson} = \Theta \tau \Delta T I$.

$$Q_{Load} = \kappa(T)\Delta T + \alpha_{Hot}(T)T_{Hot}I - \frac{1}{2}I^2 R_{Module} - \Theta\tau\Delta T I \qquad (31)$$

where Θ is the ratio of Thomson heat that flows toward the cold side of the device [32]. This ratio ranges from 0 to 1 and depends on the homogeneity of the materials used and temperature difference applied, but is typically treated as

[1] Note, the notation used to describe heat flow through a device when operated under load conditions changes from $Q_{Supplied\ In} \rightarrow Q_{Load}$.

Joule heating where the heat is distributed evenly along the length of the material and half contributes to each of the hot and cold sides. τ is the Thomson coefficient, $\tau = T_{Ave}\frac{d\alpha}{dT}$. Rewriting for large temperature gradients,

$$Q_{Load} = \kappa(T)\Delta T + \alpha_{Ehot}(T)T_{Hot}I - \frac{1}{2}I^2R_{Module} \tag{32}$$

where $\alpha_{Ehot}(T)$ is the Seebeck and Thomson effect combined as,

$$\alpha_{Ehot}(T) = \alpha_{Hot}(T) - \frac{\tau\Delta T}{2T_{Hot}} \tag{33}$$

In similar form, the figure of merit changes to,

$$Z = \frac{\sigma(T)\alpha_{Ehot}(T)^2}{\kappa(T)} = \frac{\sigma(T)\left(\alpha_{Hot}(T) - \frac{\tau\Delta T}{2T_{Hot}}\right)^2}{\kappa(T)} \tag{34}$$

and the efficiency is as stated previously for η_{wcr}, but with Thomson effects disguised in the figure of merit.

4.4 Measurements of Devices using Z-Meters

As shown previously, thermoelectric device efficiency depends on the figure of merit, so a device's figure of merit is of primary interest. Measurement techniques and instruments have been designed and improved by the thermoelectric community to efficiently and accurately measure a device's figure of merit. A "Z-Meter" is an instrument that determines the figure of merit for a thermoelectric material or device, and several types exist [33]. One type

simultaneously measures electrical conductivity, thermal conductivity and Seebeck coefficient as a function of temperature, and determines the figure of merit by calculation of such measured parameters. A second type, designed by Harman, calculates the figure of merit from a ratio of two voltages [34]. Harman's method applies an AC current to a sample which causes an ohmic voltage, V_ρ, and then applies a DC current to measure the steady-state additive ohmic and Seebeck voltages. The Seebeck voltage, V_α, is extracted and used with the ohmic voltage to calculate the figure of merit, ZT.

$$ZT = \frac{V_\alpha}{V_\rho} = \frac{V_{DC} - V_{AC}}{V_{AC}} = \frac{V_{DC}}{V_{AC}} - 1 \tag{35}$$

or more commonly written as a ratio of measured resistances,

$$ZT = \frac{R_{DC}}{R_{AC}} - 1 \tag{36}$$

Harman's method has shown to give good results in comparison with the first type of Z-Meter when near adiabatic conditions are achieved. This method has shown promising results for bulk material and device measurements [35,36].

This thesis focuses on developing a new measurement system for characterizing devices made for power generation applications, so particular attention is given to systems previously designed for high temperature measurements. One particular type of Z-Meter was established to test bulk PbTe samples up to 973°K [33]. This Z-meter design along with several others from previous device measurement systems have lead to the development of a new system that can test devices under large gradients in addition to the single pellets and couples

that Z-Meters are commonly used for. The new system offers many features that enable it to be more flexible than prior designs built by others [37,38,39,40].

5 A New Thermoelectric Device Testing System (DTS)

5.1 DTS Objectives

Due to recent progress in discovering the LAST material, a new measurement system has been developed for use in the Pulsed Laser Deposition and Transport Characterization Laboratory at MSU to characterize thermoelectric devices used for power generation applications. A new system was needed because previous measurement systems in the lab were used for bulk material measurements and lacked the ability to fully characterize a device. The method chosen for characterizing such devices determined the objectives of system design.

The primary objective of this thesis was to build a system to test the efficiency of devices made from new thermoelectric materials synthesized at MSU, primarily from the LAST material [41]. Such testing must allow for optimized LAST performance, which requires 900°K to be established on the device hot side. Device characterization should also include to ability to test under varied temperature gradients and load conditions.

A secondary objective was to use an infrared (IR) camera to obtain the temperature profile across a device. The profile of a device is important because

it is useful for understanding if the heat distribution is linear, as most simplified 1-dimensional thermoelectric modeling and analysis assumes. The profile results may eventually lead to a more accurate thermoelectric model for simulating device operation. As with developments in Z-Meter designs, the IR camera was expected to provide an opportunity to test devices more efficiently through non-contact measurements.

A third objective was to design a system to be large enough to test devices of various sizes and types (single layer or stacked). Furthermore, the system chamber was to be large enough and adaptable to become a multi-testing system. In fact, two independent tests have been run at the same time in this system[1], and there exists much more room, electrical connections and unused ports to allow the system to adapt for even more testing.

With the above objectives set forth early on in the design process, a sketch was given, in the late summer of 2003, to indicate what the system might look like...

[1] Steady-state and AC methods on different modules.

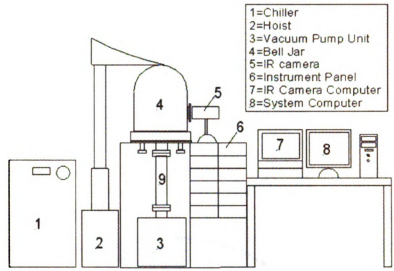

Figure 20: DTS System Concept.

A new system was progressing with part ordering, developing schematics, assembling, and testing. A year later, the system was ready to begin testing (figures 21 and 22).

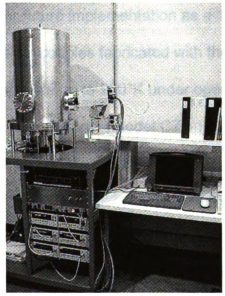

Figure 21: DTS with IR camera[1].

[1] IR camera from Indigo Systems, division of Flear International, model mid-infrared range Merlin

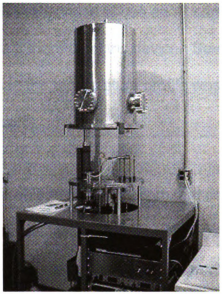

Figure 22: DTS open bell-jar.

5.2 DTS Capabilities

The primary objective for the system was to test thermoelectric devices made from the LAST material for future implementation as a 1kW thermoelectric generator (TEG). Several unicouples fabricated with the LAST material have been tested, some with hot side up to 900°K under open circuit conditions. A power generation device from Tellurex (model CZ1-1.0-127-1.27HT) has been tested under varying load and gradient conditions up to 448°K. Depending on device size and load conditions, the cold side temperature has been varied from 290-400°K. Larger size devices can also be tested, but the sample stage may need to be reconfigured for increased cooling capacity and supplied heater power. It may be useful to test larger size devices to identify how the efficiency of a 3-dimensional device scales according to typical 1-dimensional calculations.

A second objective for this system was to use an IR camera to obtain the temperature profile across a thermoelectric device. Several devices have been viewed with the camera and the temperature profile was obtained. Results are discussed further in section 6.

A third objective was to be able to build a system that could test devices of various sizes, and to be a multi-testing system. The system has tested unicouples and commercial devices. Due to the large chamber size, the system has tested two devices at one time, one with a steady-state technique and the other with an AC method [42]. The second measurements performed using the AC method were taken using two separate lock-in amplifiers and a different computer. In addition to testing two modules at once, the system is configurable for testing individual bulk material samples as well. A separate sample stage could be designed for use in this system to test materials at higher temperatures, and this is left for future work.

5.3 DTS Hardware

The design of the device testing system is made up of several main components: vacuum chamber, data acquisition equipment, cold plate, chiller, cold and hot side heaters, temperature sensors, sample stage, cart, vacuum system, hoist, infrared camera, and 400 MHz PC. The choice of components and their implementation into the system design is discussed in further detail.

5.3.1 DTS Chamber Bell-jar and Baseplate

The system chamber is made of an 18 inch ID, 0.25 inch thick stainless steel bell-jar and 22 inch OD baseplate, both custom made and assembled onto a custom rack by the Kurt J. Lesker company (KJL) in Pennsylvania. The rack has (2) 22 inch instrument bays and houses everything except the computer, infrared camera, rough pump and chiller. The large bell-jar has a #8 polished interior and brushed exterior finishes, is 30 inches high, and was selected to allow devices of various size arrays and heights to be measured. The bell-jar has two 6 inch conflat ports, one contains a 6 inch (2 inch viewable) sapphire window for infrared imaging, and the other is unused. The sapphire window was chosen specifically for mid-range IR transmission, the range defined by an IR camera purchased for co-use in this research. Sapphire transmits greater than 80% of wavelengths in the range of 1-5μm, while a typical quartz window only transmits a fraction of this[1]. The camera was chosen to detect wavelengths in the mid-IR range because the temperatures of the devices tested produce wavelengths in the middle of the infrared spectrum, near 3-5μm. The bell-jar self-aligns to the baseplate with four plastic tipped steel angle iron legs to align itself when being closed to the baseplate. The bell-jar seals to the baseplate with a Buna type O-ring. The bell-jar is attached to a standard duty electric hoist[2] for easy sample loading and unloading.

---

[1] Per information requested with the sapphire viewport purchased from the Kurt J. Lesker Company

[2] Kurt J. Lesker Company Part number: HSTST

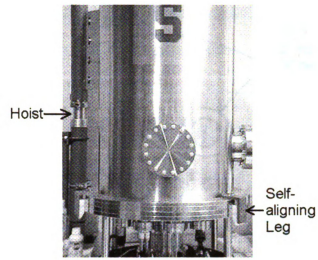

Figure 23: Bell-jar to Baseplate Self-aligning leg.

The custom baseplate has several various sized conflat style vacuum flange ports, and uses are specified in table 1.

Table 1: Baseplate conflat style feedthrough ports.

Size (inches)	Use
2.75	32-pin military electrical feedthrough
2.75	Power feedthrough, (4) 0.25 inch solid copper rods
2.75	Water feedthrough, (2) 0.25 inch O.D. stainless steel tubes
2.75	Thermocouple vacuum gauge
2.75	Bayard-Alpert (BA) ion gauge
2.75	Unused
6	Turbo vacuum pump
4	Unused

Figure 24 shows a sketch of the baseplate with all various sized feedthroughs.

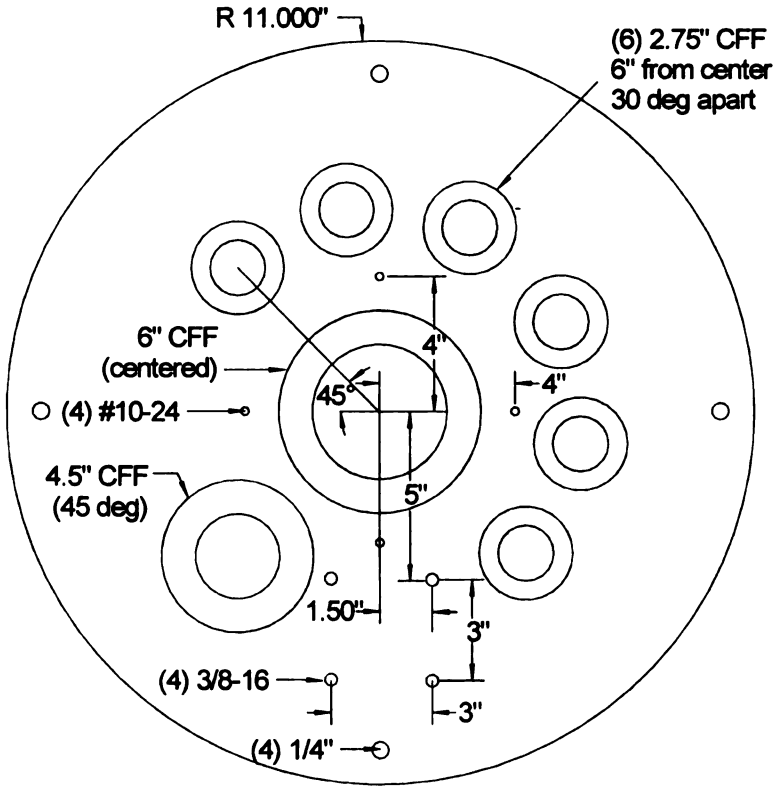

Figure 24: Device testing system baseplate (Bottom view).

Conflat flanges were chosen to give the best vacuum for large chamber size in a reasonable period of time. The system has a BOC Edwards dry scroll pump[1] to achieve sub 10^{-2} Torr vacuum pressures for this system chamber, and connects to a EXT255 series turbo molecular pump with a QF-25 flange and 48 inch long braided hydro-form bellow. The scroll pump has an adjustable bypass switch setting which is used to pump large humid chambers with less wear on the pump, and then is switched to pump the chamber further at full speed. The turbo pump is air cooled, has a feedback controller, connects directly to the chamber

[1] BOC Edwards Part Number: XDS-C Dry Pump.

baseplate through a 6 inch conflat flange, and is directly attached onto the baseplate's centered 6 inch conflat flange to reduce vacuum conductive losses. A dry system pumps to mid 10^{-6} Torr in just a couple of hours, and after many uses of testing, still achieves this in just a few hours. Depending on sample under test, the system pumps to upper 10^{-7} Torr range over a period of a few days. The analysis used for determining device efficiency assumes zero convection heat losses, so a testing environment providing UHV conditions considerably simplifies the analysis for device measurements.

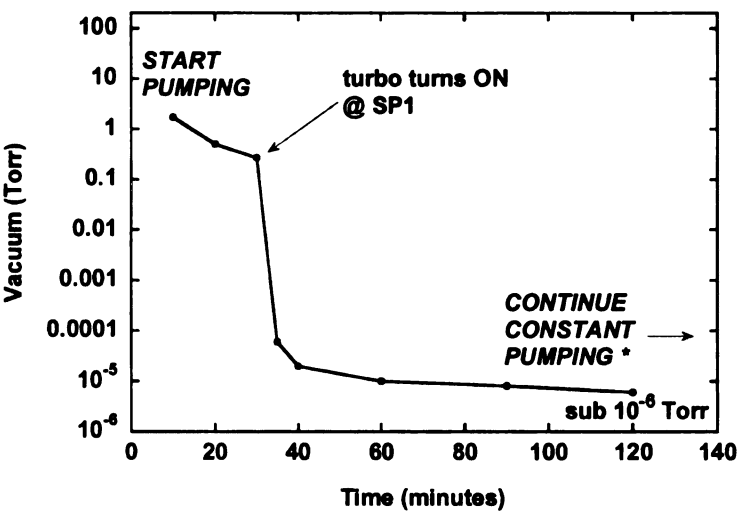

Figure 25: Device testing system pump-down time.

Vacuum pressures are monitored with a thermocouple gauge, BA hot filament ion gauge, and standard gauge controller[1]. The controller has two DB-9 connecters, one for gauge feedback, and the other for computer control; however, the system is currently not setup to computer control the vacuum

[1] KJL Vacuum controller part number: KJL4400

assembly. The controller also has a feature of taking an action at two user specified set points (SP1 and SP2) of vacuum pressure. The EXT255 Turbo is recommended for turn ON at vacuum pressures of 7 Torr or lower, so SP1 is set to 10^{-1} Torr to turn on the turbo pump[1]. SP2 is available to reduce the turbo pump speed or power in half when vacuum pressures become lower than desired, but is not presently used.

5.3.2 Measurement and Supply Equipment

In order to determine what measuring equipment was needed for this system, it was first appropriate to decide what transport properties of devices and samples would be measured. The desired measurements were determined from tests performed in the MSU Pulsed Laser Deposition and Transport Characterization Laboratory on thermoelectric compounds, as well as described in the previous section of this paper [31, 43]. Raw data collection is fully automated with a PC and National Instruments LabView ® software, version 7.0. This allows for obtaining large amounts of data in relatively short periods of time. Several Keithley brand instruments were chosen for their high accuracy and reliability, and are conveniently interchangeable with other lab equipment. Furthermore, many of the lab instruments are GPIB controlled by a computer[2], and already had several communication programs written in LabView® that were readily adapted for use in this system. One of the power supplies on this system is older

[1] EXT Compound Molecular pump instruction manual, page 21

[2] National Instruments PCI-GPIB card part number: 778032-01

and analog controllable only, so a digital to analog converter with USB interface is used to control the power supply[1].

Table 2: Measurement Instruments used.

Quantity	Mfg, model #	Description
1	Keithley, 2400	Current source meter
4	Keithley, 2182	Nanovoltmeter
1	Keithley, 2002	Multi-meter
1	Sorenson, DCS60-18E	1kW power supply
1	Sorenson, EMSII	250W power supply
1	Measurement Computing, PMD-1208LS	Digital-to-Analog converter, USB
1	National Instruments, GPIB card	GPIB interface card
1	Indigo Systems, Merlin	Infrared camera
1	Gateway, PC	Personal computer

Table 3: Device measurement and required instrumentation.

Parameter	Measurements	Meters Required
Efficiency	Power Out {V-OUT} Power IN {I-IN, V-IN}	2182#1: measures V-OUT 2002: measures I-IN & V-IN DCS#1: provides power IN
ZT	dT-open {V-TC} dT-closed {V-TC}	2182#2 for differential: measures V-TC *or* 2182#2 & 3 for single-ended: measures V-TC *or* Indigo Infrared Camera
Seebeck	Voltage dT	2182#1: measures V-OUT 2182's: same as for ZT
Resistance	Voltage Current	2400front: supplies I-IN 2182#1: measures V-OUT

[1] Measurement Computing part number: PMD-1208LS

The thermal conductance of the device is a calculated parameter found from the gradient and power supplied, or can be determined through ZT and device resistance for some average temperature. All leads from instrument to baseplate feedthrough[1] mate with a 32-pin military style connector[2].

5.3.3 Power Out, Electrical Loads

The baseplate contains a 2.75 inch power feedthrough[3] which has four copper rods, each rod of 0.25 inch diameter, see figure 26. This style feedthrough was chosen to given the least resistance between device and load. Many of the devices tested will be single couples, also known as unicouples, on order of milliohms, so any contact resistance between device and load may greatly influence the power out across the load, and thus efficiency calculations. The rods have been silver plated[4] for even less resistance and oxidation. The wiring from sample stage to feedthrough copper rod is braided 12 AWG, soldered at one end to a spade terminal and screwed onto the copper rods, and each screw is vented for quicker vacuum. The connection from load to atmospheric side of the feedthrough is made with a screwed on banana jack for convenient load switching during testing. Each load then has a male banana, and the contact resistance seen at the banana to banana is less than 10mΩ. This may be significant for unicouples of small dimensions whose overall resistance may be comparable.

---

[1] Kurt J. Lesker 32-pin feedthrough part number: IFDRG327013

[2] Newark 32-pin military connector part number: 93F9354

[3] Kurt J. Lesker power feedthrough part number: EFT1243253

[4] Cool-Amp silver plating part number: 1233-500 1/4

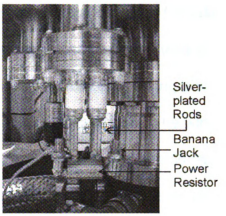

Figure 26: DTS load resistor.

A resistor switch box was originally going to be fabricated for autonomous operation in load switching, but one could not be readily located giving less than a 10-20mΩ switching contact resistance. This contact resistance may be considerable when testing unicouples with 10-20mΩ resistances, for which it is assumed all power from module transfers to the load under load testing conditions. There exist IC's with switching loads, but these are generally for RF use and have resistances much higher than that of a thermoelectric device whose resistances are generally several orders of magnitude smaller.

The load resistors are 25W ceramic, axial style power resistors[1] with standard aluminum housing. Power resistors are chosen because of their low resistances with 1% tolerances. Also, since these are designed to dissipate a large amount of power but are only typically dissipating milliwatts, their resistance does not change much when flowing small currents through them at room temperature; so, only the voltage needs to be measured. To confirm this, a few tests have been

[1] Huntington Electric Inc. axial style, 25W, power resistors, some standard order through Digi-key Corp.

performed monitoring current and voltage compared to just voltage, and both agree. It should be noted that each load has been tested using a four-point method, as well as the overall resistance of the wiring and connections to the device, for more accurate efficiency calculations. The wiring resistance contributes 65mΩ of resistance to the load, and should be reduced for efficiency testing of unicouples by increasing the lead wire diameter above the presently used 12 AWG copper.

5.3.4 Device Cold Side Temperature Stage Design

The cold side of the device is cooled with a CFC based chiller[1] of set point 20°C with adjustable pressure, and thus flow rate. The chiller is supplied with a special coolant to inhibit bacterial growth over time, and thus require less maintenance[2]. The chiller induces some vibration along the supply line to the baseplate, and the temperature can fluctuate due to tolerances of the chiller. Therefore, a vibration and thermal oscillation damper was placed inline between chiller and chamber connection. The damper was made by placing 25 feet of 0.375 inch OD coiled copper tubing in a 5-gallon bucket submerged in 80lbs. of concrete. Although this reduced the flow rate, it also reduced the vibration substantially and decreased the temperature fluctuation from 0.5° to 0.1° with sufficient heat pumping capacity for testing done so far to date.

---

[1] Kurt J. Lesker Company chiller part number: ATCKTR6001

[2] Kurt J. Lesker Company chiller coolant: Hexafluid

The chiller connects to a 2.75 inch conflat water feedthrough[1] made with 0.25 inch OD stainless steel tubing atmospheric side, and 0.25 inch VCO fittings on vacuum side. VCO style fittings were chosen to be sufficient for this UHV system, so VCR fittings were not required. The first cold plate was custom made by the MSU Physics Machine Shop, figure 27. It is made of 0.5 inch thick OFHC and 0.25 inch OD copper tubing, and all is nickel plated[2]. The cold plate connects with two VCO female fittings made of a nut and gland[3], which mate to two 4.75 inch compressed, flexible, convoluted tubes with 0.25 inch male VCO connectors[4].

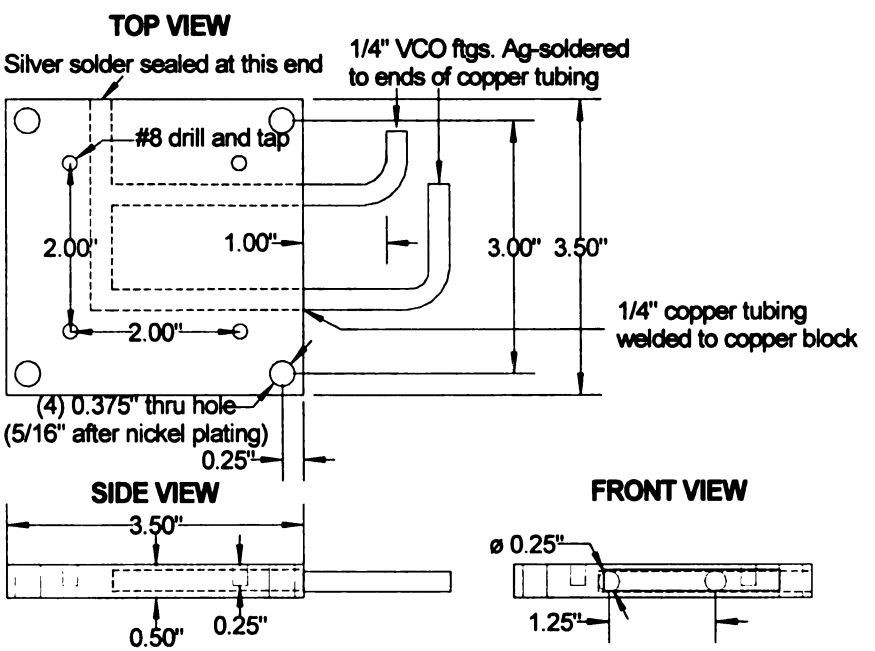

Figure 27: DTS custom cold plate.

---

[1] Kurt J. Lesker Company water feedthrough part number: LFT322MCTE

[2] Nickel plating done by Adams Plating, located in Lansing, MI

[3] Kurt J. Lesker Company VCO nut and gland part numbers: SS-4-VCO-4, SS-4-VCO-3

[4] H.E. Lennon convoluted tubing part number: 321-4-X-6FMO

The cold plate sits atop four vented standoffs that fix to the baseplate, and made to allow the cold plate to be raised and lowered. The height adjustment was implemented for direct view line with the bell-jar sapphire viewport used for infrared imaging with varied device heights.

A second cold plate was made to accommodate larger sized devices. This second cold plate is made of 0.5 x 3.5 x 6 inch aluminum with 0.375 inch OD stainless steel tubing[1], and has two silver soldered VCO female fittings attached by the MSU Physics Machine Shop. The cold plate was drilled for attaching the sample mounting stage and for standoffs to a baseplate support plate, figure 28.

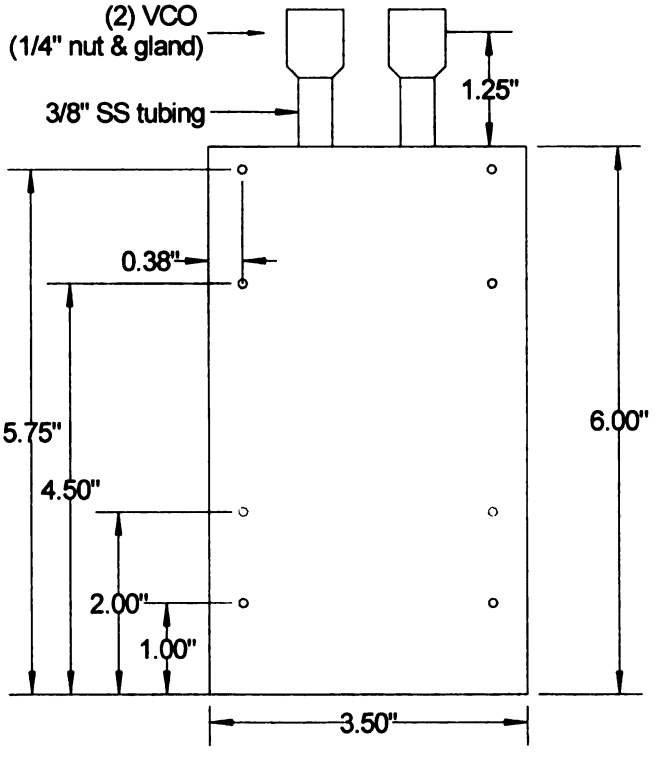

Figure 28: DTS large cold plate.

[1] McMaster Carr cold plate part number: 35035K36

Because it is not convenient to disconnect the cold plate each time to remove a sample, a sample stage was designed that screws to the cold plate for easy sample changing. The cold plate and sample stage were made thick to avoid warping, and ground and polished when fabricated to ensure good thermal contact. Although polished flat, a thin layer of Apeizon H thermal grease is used between cold plate and stage to ensure a better thermal contact. The stage consists of a 0.125 inch thick aluminum, and custom printed circuit board (PCB) to attach electrical leads from device to instrument feedthrough. Aluminum was chosen for the stage because of its high thermal conductivity, availability and ease of machining.

5.3.5 DTS Cold Side Stage Electrical Connections, PCB

The single-sided PCB has 15 electrical traces made from 0.03125 inch thick copper clad board. Two extra wide traces are also shown available for soldering the device leads to the baseplate feedthrough wiring, to the load for reduced contact resistance, figure 29.

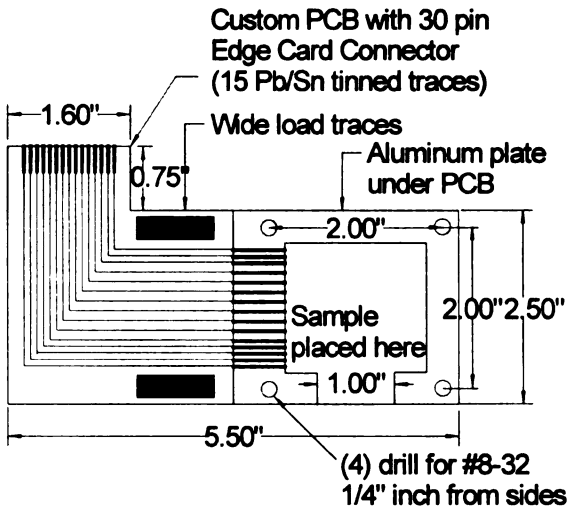

Figure 29: Custom PCB and small sample stage.

The PCB was designed using Layout software from Cadence, and then fabricated by the MSU ECE shop staff and T-tech prototyping machine. The PCB is made for a 30-pin edge card connector[1], but only half of the pins are used for the single-sided PCB. Other PCB's were made using ferric chloride etchant and permanent marker. Also, photoresist boards were experimented with and worked well, but the processing chemicals and developing time made this an inconvenient choice as well compared to the ECE shop router. The PCB was then GE varnished® to a 0.125 inch thick aluminum stock, ground and polished, for good mechanical bond and thermal contact for the thermocouple reference junctions. The aluminum plate was used to allow the device and PCB to be one piece, as opposed to mounting the device under test directly onto the cold plate. This design limits the cold side of device testing to the melting point of the varnish and PCB, but most device testing is generally done at

[1] Sullins Electronic Corp. edge card connector part number: EZC15DRXH

temperatures below such melting points. However, another design could easily be adapted for testing at higher temperatures, as may be required for bulk material measurements. The final PCB stage assembly, shown in figure 29, gets spring loaded with the device and screwed onto the small custom cold plate, and is good for testing devices up to 1.5 x 1.5 inches.

5.3.6 Cold Plate Stage Assembly

The final assembled design is made of the PCB based stage assembly and cold plate. The PCB aluminum stage has a Pt-103 sensor placed inside it to monitor the cold side temperature and provide a thermocouple reference temperature. The Pt-103 was initially placed next to the device under test, and adhered to the stage with silver paint, however, it was later determined that best results were obtained with the sensor placed inside the stage just below the device under test, experiencing the same heat flow with the device. To achieve this, a section of the aluminum was milled out, and only 1mm thick of aluminum remains between the device under test and sensor tip. The sensor and its lead wires were placed in the milled out region and then covered with an alumina epoxy[1] to ensure good heat flow from device to cold plate figure 30.

[1] Aremco ceramabond 668

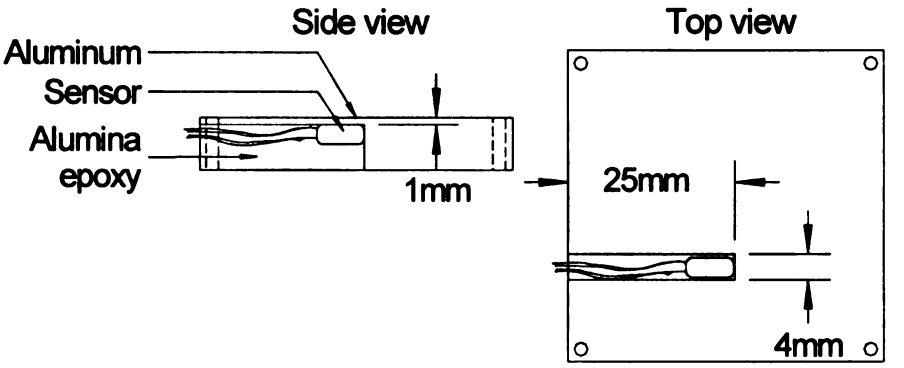

Figure 30: Sample stage with embedded temperature sensor.

The local temperature of the device cold side is desired, and the sensor would ideally be placed in direct contact with the device; however, a 1mm region of aluminum is in between the sensor and device. Due to its high thermal conductance[1], the temperature drop across the 1mm thick region of aluminum is considered negligible compared to the gradient across the device under test. The epoxy has a thermal conductivity rated 85% of alumina[2] when prepared properly[3], near 17 W/m·K. The temperature drop across the alumina epoxy is considered negligible since it is not directly between device and sensor. Between the device cold side surface and temperature sensor is a thin layer of Apeizon-H thermal grease to adhere the device to aluminum stage plate. The thermal grease has a thermal conductivity near 0.2 W/m·K (0.002W/cm·K), is recommended for use to 240°C (513°K), does not melt but becomes harder as temperature increases [44]. The grease has excellent stiction properties, cleans easily with acetone, and sometimes is preferred over metallic paints which can

[1] Aluminum thermal conductivity from Goodfellow, as 237 W/m·K (0-100°C)

[2] Alumina thermal conductivity from Goodfellow, as 20-25 W/m·K (0-100°C)

[3] As stated 85% of alumina by Aremco engineer through a phone conversation

lose their bond due to coefficient of thermal expansion differences. It is important not to apply too much thermal grease or an undesirable temperature gradient could occur between the cold side temperature sensor and device surface. For example, a device of size 1.44 in^2 (9.29 cm^2) covered with the grease, applied of just 100μm (0.01cm) thickness, it is possible to have a appreciable temperature drop,

$$\Delta T = Q / \mathrm{K} = \frac{10.0W}{(0.002W / cm * K)\left(9.290cm^2 / 0.010cm\right)} \cong 5.000°.$$

The cold plate assembly is shown below in figure 31.

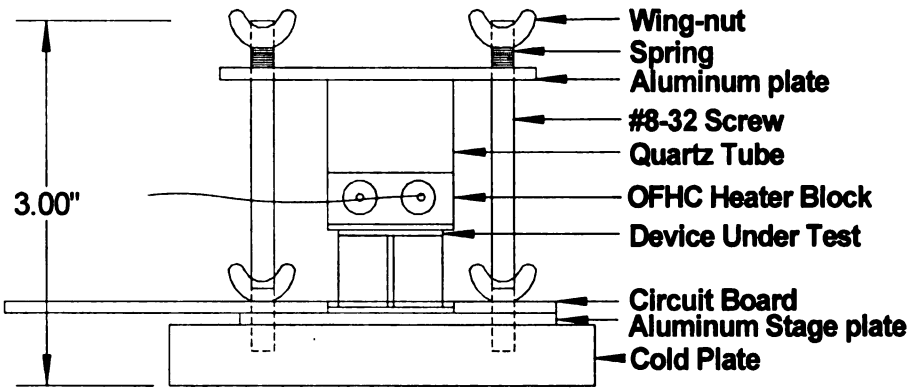

Figure 31: Spring-loaded assembly.

This cold plate assembly design works well, but has much room for improvement. One inconvenience in the design lies in the spring-loading of the device and stage to cold plate. The same screws are used for spring loading the device, gradient heater, and stage into place. During sample loading, the device, gradient heater or other wiring is often bumped and needs repair before testing begins. Therefore, another stage assembly was fabricated which uses the large cold plate, allows independent attachment of each section of the stage assembly,

and is slightly thicker. For this altered design, the device is spring loaded onto a 0.25 inch thick aluminum stage assembly with PCB, 0.125 inch thick where the device is mounted. This stage assembly then screws down to the cold plate that sits atop a large 10.5 inch diameter support plate that bolts to the main baseplate. This support plate was designed to utilize the real estate of the baseplate for testing larger devices (Appendix B).

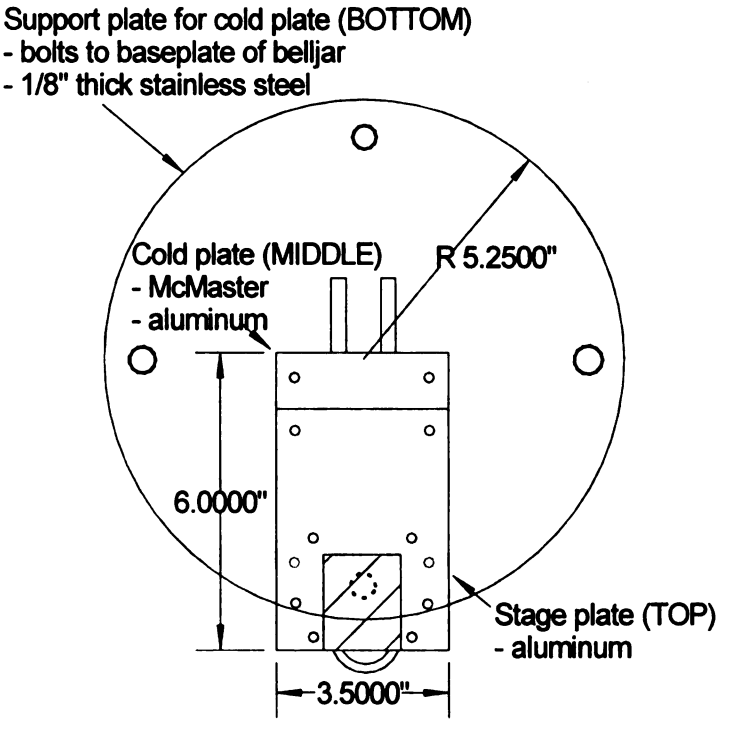

Figure 32: Large Device Cold Plate Assembly.

5.3.7 Cold Side Temperature Adjustment

It is sometimes necessary to operate power generation devices above a cold side temperature of 300°K for optimal performance. Therefore, a cold side heater was made to accomplish this, Figure 33. The heater is made using two

cartridge heaters are from McMaster[1] that are silver epoxied[2] into a 0.5 inch thick by 2 inch square OFHC block. The heaters are controlled with a Sorenson power supply[3] that can provide them with up to 25W each, 50W total in parallel.

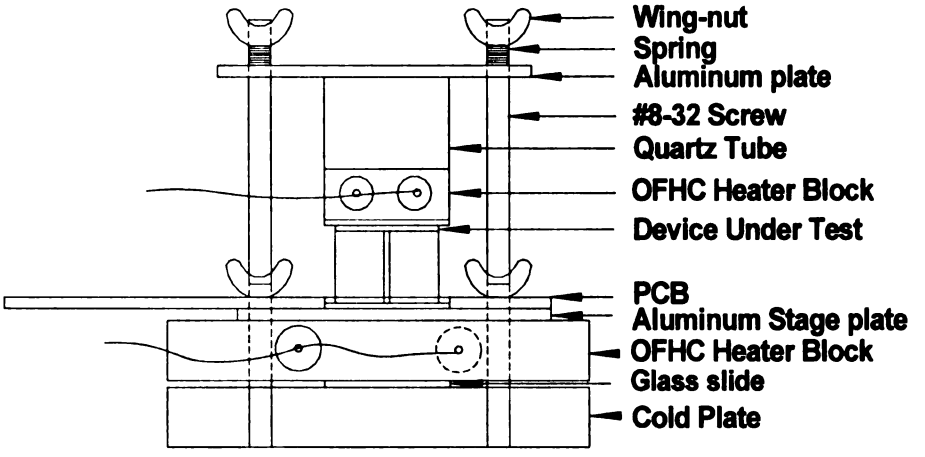

Figure 33: Cold plate stage with added heater.

The heat required to achieve the desired cold side temperature depends on the device characteristics and testing conditions. The cold side heater block was initially mounted to the cold plate, and the temperature controlled by adjusting power to the cold side heaters. A large amount of power was required to achieve temperatures above 350°K for some devices under certain testing conditions. Such high power caused electromagnetic interference with the data collection wiring, figures 34 and 35.

---

[1] McMaster Carr 0.25 inch diameter, 200 W, cartridge style heater

[2] Aremco silver filled epoxy, pyroduct 558

[3] Sorenson power supply model number: DCS60-18E

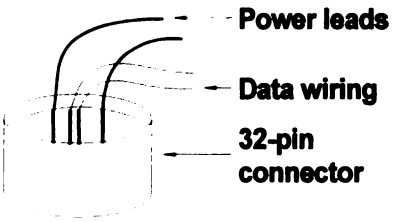

Figure 34: 32-pin EM interference with power and data wires.

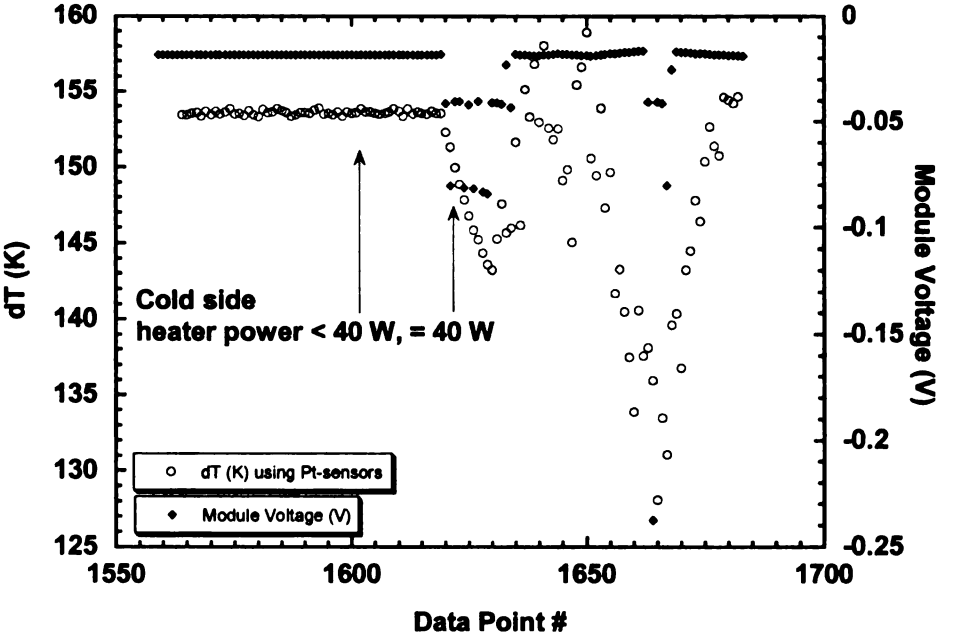

Figure 35: EM interference with cold side heater and data leads.

Two adjustments were made to the system design in order to correct this problem. First, the amount of power required to the cold side heaters was reduced by increasing the thermal resistance between cold plate and cold side heater. The thermal resistance was increased by simply placing a glass microscope slide between the heater and cold plate. Second, a 2.75 inch conflat

style electrical feedthrough[1] was added to the system to allow separation of the power supplied to the heaters and data collection wires.

5.3.8 Temperature Gradient Heaters

In order to test thermoelectric devices for power generation applications, a temperature gradient must be produced. The gradient needs to be uniform across the device and must often be sustained for different load testing conditions. As shown through the heat balance equation, $Q = \alpha TI - \frac{1}{2}I^2R + \mathrm{K}\Delta T$, changing the load current, I, affects the gradient, ΔT, across the device for some fixed heater power, Q. Therefore, the gradient heater must be able to provide enough heat uniformly for various load conditions. Depending on the size of the device tested, the size and type of heater may need to be adjusted. For example, if the heater surface area is much small than the device, the heat may not distribute evenly across the device; and, if the heater is too large, the heat radiated from the exposed surface area of the heater may induce undesired lateral temperature gradients on the device. Therefore, several heaters were investigated that varied in size, ability to supply high power at high temperatures under ambient and UHV conditions, and ability for use with laboratory available 50V/50A power supplies.

[1] Kurt J. Lesker company electrical feedthrough part number: FTT0181053

5.3.8.1 Temperature Gradient Heater, Large Devices

First, a single cartridge style heater[1] was embedded into a rectangular OFHC block with silver paint[2]. The OFHC heater block was sized to fit the cartridge style heater. The sample device for testing was a power generation device[3] whose cross sectional area was 1.2 in^2. This device was chosen because reference data was readily available. The heater block covered 50 percent of the total area of the device, figure 36.

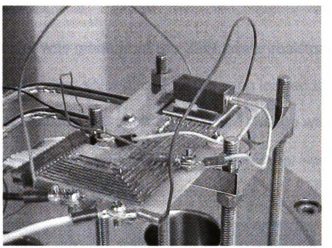

Figure 36: Early stage design under test.

The open circuit voltage was recorded under a 20° gradient with cold side at 300°K, and the Seebeck measured was 300μV/K per couple, a 21 percent difference from the expected 380μV/K [43]. The voltage collected from the device appeared clean from the 2182 nanovoltmeter as no spikes or random noise were observed, and the measurement repeated well. Next suspected was

[1] Omega Engineering 0.25 inch diameter cartridge style heater

[2] Ted Pella company silver paint

[3] Tellurex power generation device, model CZ1-1.0-127-1.27

that the gradient was not being measured correctly, however the thermocouples appeared to be adhered securely to the device under test, and the voltage to temperature conversion look up table for the thermocouple seemed correct. Next, it was presumed that the heat was not uniformly spread out across the device through the alumina plate to the device pellets. So, a 0.0156 inch thick piece of OFHC, the same size of the device, was silver painted between the copper block and device to spread out the heat, as shown in figure 36. This improved the agreement, but not by much, only to 310μV/K.

Next, a gradient heater was made from two 25W power resistors with aluminum housing connected in series, silver painted and spring loaded to the top of the device, figure 37. Results did not show a significant change with and without spring loading, but the devices under test are usually spring loaded to ensure an even thermal contact from run to run.

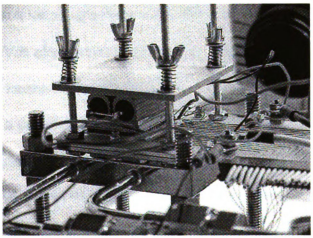

Figure 37: Series heaters for uniform dT.

The 25W resistors were chosen to deliver enough power to the device to generate temperature gradients as given in the reference data, near 150°K. To achieve 150°K, the amount of power is proportional to the thermal conductance of the device, neglecting losses. Based on thermal conductivity data for Bi_2Te_3 [27], measured pellet dimensions and the number of pellets, the thermal conductance was found to be 341mW/K. Therefore, the amount of heat required was found to be near 51W, and two resistors would achieve this if supplied the appropriate power. The resistors were also chosen for their size, which nearly covered the device surface by greater than 95 percent. Finally, the resistors were an appropriate load for the given power supply when connected in series or parallel. With these resistors as the heater, a small 10° gradient was established and voltage measured from the device which yielded a corresponding Seebeck of 354μV/K, less than a 3 percent difference from the expected 365μV/K. Although operated beyond the recommended temperature limits, the heaters were used to create a larger gradient, near 100°, but the measured Seebeck decreased to 320μV/K after an hour of testing. The test was stopped, device and heaters inspected, heater resistors gave the correct resistance, but no flaws were obvious; however, a smell of burnt electronics was noticed. The heaters were used once more, and an infrared camera was used to measure the temperature gradient in comparison with the thermocouples. Although the results in absolute temperature between thermocouples and camera did not agree, for reasons discussed in section 6, the camera discovered that one of the heaters (left) was hotter than the other (right), figure 38.

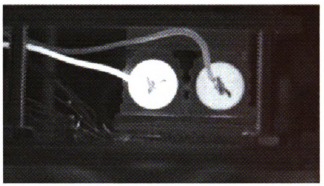

Figure 38: IR view of burnt aluminum housed style heater.

In fact, the heaters were taken out and inspected again, and one was found to have cracked and come loose from its aluminum housing, inhibiting heat transfer, and thereby appearing hotter on the infrared image. The heaters were no longer used, and replaced in later designs with ones that could deliver high power at high temperatures. Nevertheless, the importance of uniform heat transfer was made clear for accurate Seebeck measurements.

Another OFHC block was made which allowed two cartridge style heaters[1] to be embedded in parallel, figure 39. These heaters are wire wound resistors in stainless steel sheaths good to greater than 600°C (873°K), designed for 120V and were specified for good to 100W power ratings. The heaters are silver painted into the OFHC for a good thermal contact. The OFHC is then spring loaded to the top of the device under test. A 22mm O.D. quartz tube was used to separate the spring loaded aluminum plate and OFHC heater to reduce thermal losses. With a small 20° gradient, cold side at 310°K, the Seebeck measured 322μV/K, a 15% difference from the expected 380μV/K.

[1] McMaster Carr 0.25 inch diameter, 100W, cartridge style heaters

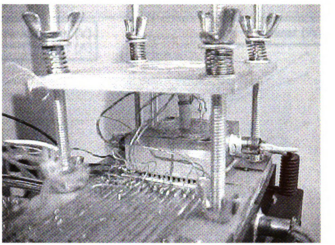

Figure 39: Parallel heaters in OFHC for large size devices.

The heaters work well, but were too high of resistance, and limit the power supply voltage to deliver them only 71W when connected electrically in parallel for combined reduced resistance. Although these heaters are rated for higher temperatures, they can not achieve the high temperatures desired, above 500°K, under atmospheric conditions, with the system power supply used. Under UHV, the heaters are sufficient to produce the high power at high temperatures, however when placed in the OFHC block, are too large for the majority of devices tested. Therefore, a substrate style heater[1] was purchased which can supply high temperatures at high power and is an appropriate load for the system power supply[2].

[1] TB-1175 model substrate heater from Heat Wave Labs
[2] Sorensen DCS60-18E power supply

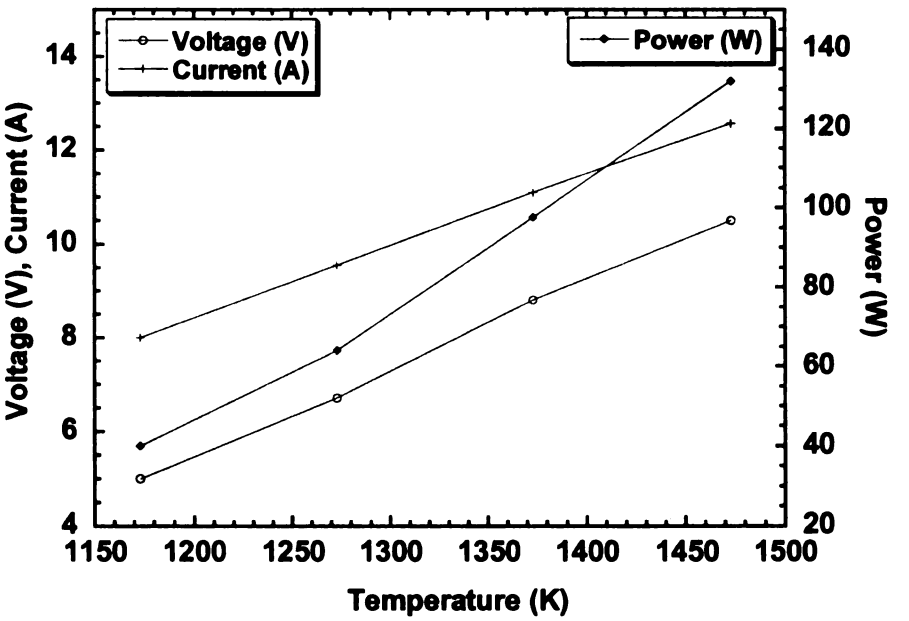

Figure 40: TB-175 characteristics.

The heater size is appropriate for testing smaller devices of 0.5in^2, and can be placed into an OFHC block to distribute heat evenly for larger devices. The heater is 0.75 inch diameter, made of a tungsten filament embedded in an alumina potting, with surrounding molybdenum shielding to reduce power lost due to radiation. This heater has yet to be used in the system.

5.3.8.2 Temperature Gradient Heaters, Small Devices

For small single couple devices, thin film platinum resistive temperature sensors[1] were first used as gradient heaters. Gradients up to 550°K have been established across 8mm high devices made from the LAST material [41]. The heater is made of two resistors connecter in series, and both are silver painted to

[1] Pt-500 platinum thin film sensor from Omega Engineering

the devices under test. The devices tested were made of metallized alumina plates silver paintd to the LAST material pellets.

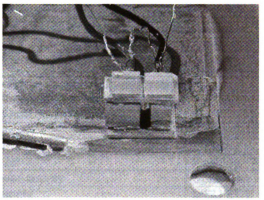

Figure 41: Small devices under test.

The heaters work well, and have supplied enough power to achieve hot side temperatures near 900°K under open circuit and UHV conditions. The Pt-103 resistors are made as a thin film device, and a protective coating covers the resistive material. However, the coating on the heater tends to burn at higher temperatures, near 900°K. The heaters were used repeatedly by adhering them with silver paint from device to device. While preparing the devices for testing, adhering heater to device, silver paint tended to creep from the heater to device pellets creating an undesirable conductive path to the pellets. Therefore, the Pt-103 sensors satisfied the gradient heater requirements for small devices, but could not be used for repeated testing. Although a thin film device, the Pt-103 sensors are too expensive to purchase for each device tested. The substrate style heater discussed in the previous section for testing larger devices is also appropriate for testing small devices.

5.4 DTS Hardware Costs

The following table gives the approximate cost of the system components.

Table 4: DTS cost, approximate.

Quantity	Item	Supplier	Cost ($)
1	18 inch stainless steel vacuum sub-assembly (cart, chamber, hoist, chiller, vacuum system, vacuum gauges and controller)	KJL	26,164
4	2182 Nanovoltmeter	Keithley	8,800
1	2002 Multimeter	Keithley	2,500
1	2400 Sourcemeter	Keithley	2,000
1	DCS60-18E power supply	Sorenson	2,000
1	EMS II power supply	MSU ECE shop	1,000
1	DAC	Measurement Supply and Computing	100
1	PC	MSU ECE shop	400
1	Sapphire viewport	KJL	1,000
1	IR camera (optional)	Indigo Systems	50,000
1	Water feedthrough	KJL	120
1	4-rod power feedthrough	KJL	262
1	32-pin feedthrough	KJL	367
1	8-pin power feedthrough	KJL	112
3	Conflat plate nut and silver plated bolt sets	KJL	250
1	Assortment of power resistors	Huntington Electric	75
1	Small cold plate	MSU Phys Mach shop	120
1	Large cold plate	McMaster Carr	30
2	Aluminum stages	MSU Phys Mach shop	40
3	OFHC heater blocks	MSU Phys Mach shop	120
1	TB-175 substrate heater	Heat Wave Labs	600
1	PCB	MSU ECE shop	40
1	Cold plate flex connectors	KJL	156
1	Cold plate VCO fittings	KJL	30
1	GPIB interface PCI card	National Instruments	445
1	Chiller damper	Custom	100
7	GPIB cables	MSU ECE shop	140
4	Cartridge style heaters	McMaster	100
1	Cartridge style heaters	Omega Engineering	30
1	Nickel plating	Adam's Plating	40
1	TAV vent valve	BOC Edwards	270
1	Conflat and QF-25 bellow, clamps, o-rings	Varian Inc.	300
		Total w/o camera	***47,823***

5.5 DTS Software

The DTS is not fully automated, so some operations require user feedback during the test. Data collection of device voltage, temperatures and power

supplied are fully automated, but the changing load conditions and temperature control are manually adjusted. The measurement equipment is controlled through a PC with LabView® National Instruments Software, version 7.0. LabView® was chosen because it is compatible with the other MSU measurement systems from which several programs and simple subroutines were readily available [45]. The system is intended to measure the properties of devices described in section 5.6. The flowchart for how the system operates is provided below, figure 42.

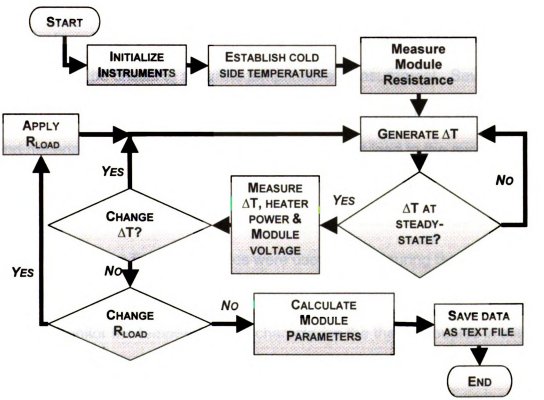

Figure 42: DTS Software flowchart.

The DTS LabView® programs are located on the DTS computer with the system, ***C:\Program Files\National Instruments\LabVIEW 7.0\user.lib***, and the library is named ***DTS programs.vi***. The main program to operate the system is named

DTS Main program.vi. Operating instructions for the DTS can be found in Appendix H.

5.6 DTS Device Measurements

The DTS measures device Seebeck, resistance, efficiency and power out for varying load and gradient conditions. These parameters are functions of temperature, and most of a temperature gradient. Therefore, careful consideration must be placed on measuring the gradient. The placement of the temperature sensors and materials used to make the testing stage apparatus was found to be critical to accurate temperature measurement. Several measurements have been performed until the proper placement was identified and materials used. Several of the experiments that lead to the success of the most accurate sensor placement are listed in (Appendix D).

Single-ended type T thermocouples were used for measuring temperatures 290-500°K, and type E for ranges of 300-900°K. Pt-100 platinum sensors were also used to monitor the temperatures to characterize the thermocouples in initial system development.

5.6.1 Device Seebeck Measurements

One of the most important properties of a good thermoelectric device is its overall Seebeck coefficient. Therefore, accurate Seebeck measurements are critical for assessing device performance. As discussed for measurements on bulk materials in section 3.3.2, the relationship between voltage and temperature is linear through the thermopower. Unlike measurements made on bulk materials where single ended thermocouples are used to measure the gradient and voltage produced at the same local point on the sample, the device Seebeck coefficient is found from the device open circuit voltage, and separate thermocouples are fixed to the hot and cold side of the device to measure the temperature gradient. The device voltage and temperature sensors are not in the same location, so they do not track each other in time. Thus, it is important to allow the device to achieve steady-state conditions before data collection, or else measurement errors can occur [46]. The time required to reach steady-state varies depending on testing conditions and device characteristics. When the voltage and temperature gradient do not track each other in time, a non-linear slope change result can occur, figure 43.

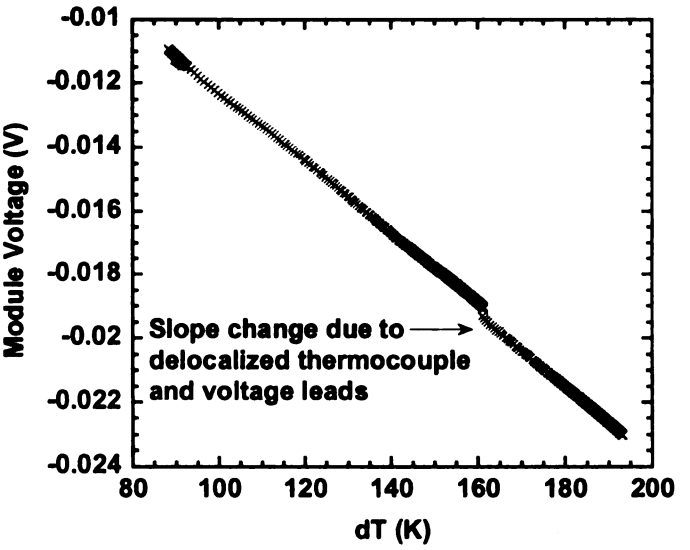

Figure 43: Nonlinear effects of time delay for dVdT on Seebeck results.

The resulting effects on the Seebeck coefficient are provided in figure 44.

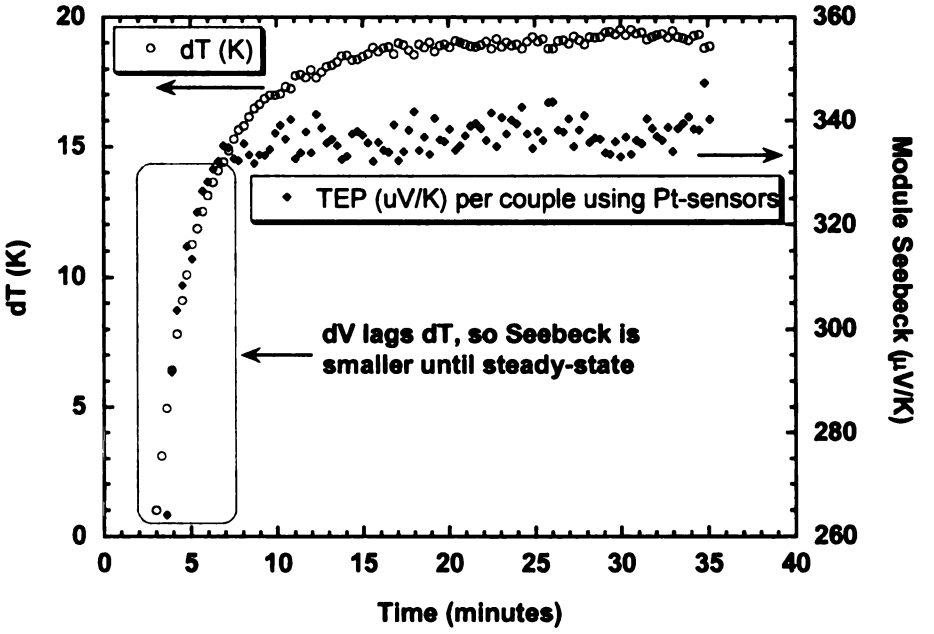

Figure 44: Seebeck results, steady-state versus non-steady-state.

The Seebeck coefficient for non-steady-state conditions is shown as the first 15 minutes of data collection, and steady-state conditions are shown thereafter.

The data collected is a little noisy because the system chamber was open and under atmospheric conditions, and tends to decrease substantially for tests done under vacuum.

In order to verify the system measures device Seebeck coefficient accurately, a standard reference device was needed; however, no such standard was found readily available. Nevertheless, Seebeck coefficients for a variety of thermocouples are well characterized and were therefore used as a reference [7]. In particular, a device made of type K thermocouples was used as a reference for characterizing the percent error in measurement of the Seebeck coefficients.

Three type K thermocouples were connected electrically in series, and thermally in parallel to make a thermoelectric device, figure 45. The device was used as a reference for characterizing system errors in Seebeck measurements. Any number of thermocouples could have been used for this test, but three were chosen to increase the voltage magnitude detected to that of other devices typically tested, and more than three would have served the same purpose but been more time consuming to assemble. The thermocouple wire is 10 mil diameter from the Omega Engineering Company[1]. The thermocouple junctions were made by spark welding, and then thermally anchored to two metallized

[1] Omega Engineering type K thermocouple wire part numbers: SPCH-010-50 and SPAL-010-50

alumina plates with alumina filled epoxy[1], spaced 2mm apart. A quartz tube was used to support the top plate, and is bonded to the quartz tube with the epoxy as well. A slit along the quartz tube length was made to allow manipulation of the wires so as not to cause any shorts. The starting and ending thermocouple leads are soldered to the bottom cold metallized alumina plate. Two 3mil teflon coated copper leads were soldered with the thermocouple leads to monitor the voltage.

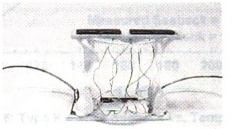

Figure 45: Type K thermocouple device.

The Seebeck coefficient for the device was found at various temperature gradients up to 220°K, as well as varying the cold side temperature from 295-340°K. The results agree well with expected reference [7], and are shown in figure 46.

[1] Aremco ceramabond 668

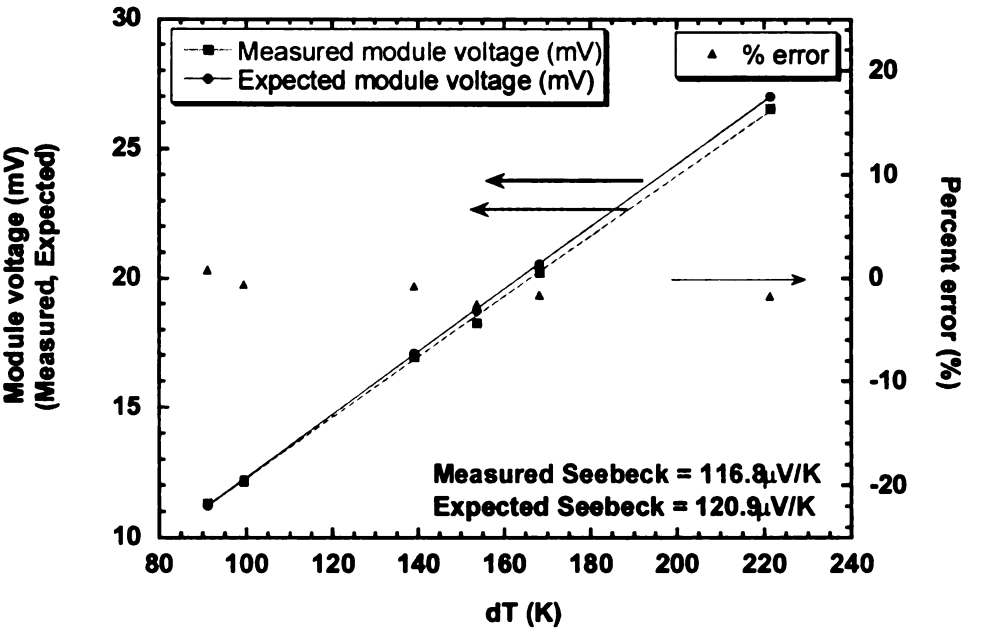

Figure 46: Type K device Seebeck vs. Temperature.

Since there are three couples that make this device, dividing the slope by 3 gives the corresponding Seebeck value for the thermocouple, near 40μV/K [7]. A three percent error in Seebeck measurements was on a type K thermocouple device.

5.6.2 Device Resistance Measurements

A second important device parameter is its overall resistance at various temperatures. The temperature dependent resistivity and dimensions of the materials used to make a thermoelectric device are usually known within some tolerance. However, parasitic electrical contact resistance plays a crucial role in device efficiency and is usually quite different than the material efficiency.

A standard four probe method is used to measure the device resistance, as done for electrical conductivity discussed in section 3.3.1. In order to verify the system

measures device resistance accurately, a standard reference device was needed; however, no such standard was found readily available. Therefore, a commercial device, with temperature dependent data provided, was used as a reference for calibration of resistance measurements from 300-400°K [43]. Results are provided in figure 47.

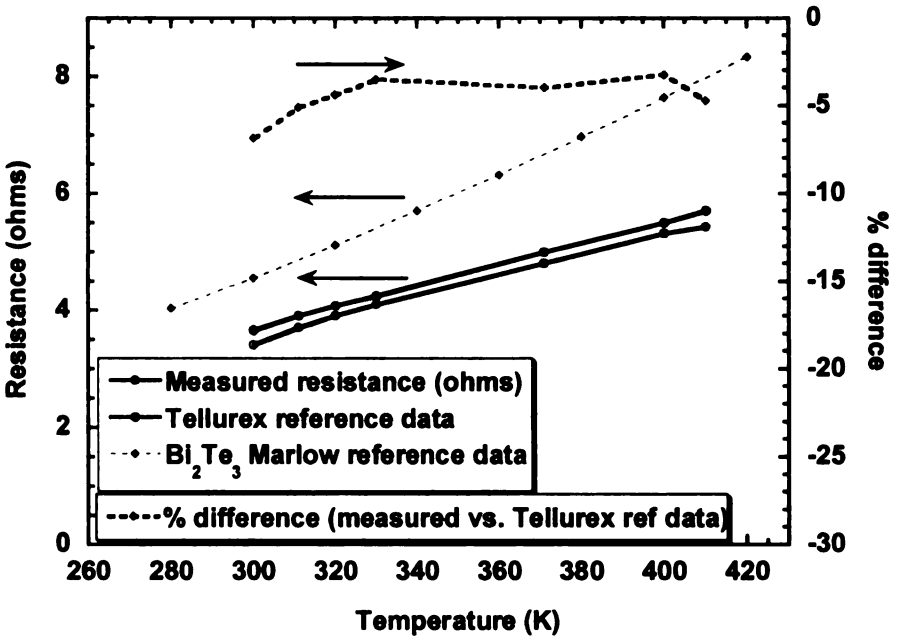

Figure 47: Tellurex device resistance versus temperature (300-400°K).

The device resistance was measured lower than the reference data by 5-10 percent. This percent difference may be due to manufacturing tolerances, as no two devices are made exactly the same[1]. Approaching the results as a result of manufacturing differences, this indicated the conductivity of the materials used in making this particular device is higher, or that the temperature was measured incorrectly. If the resistance is lower and conductivity is higher for the pellets of the device tested, then the device Seebeck should be lower. The device

[1] Per phone conversation with Tellurex employees.

Seebeck was measured lower, but could also have been a result of measuring temperature incorrectly. A second Pt-100 temperature sensor was used to verify the measurement of the average temperature measured by the first sensor, and both were in good agreement. Although the device tested was not a first choice for reference, it did indicate that the system measures device resistance within 10 percent. A second system measured the AC resistance of the exact same device at room temperature, and found good agreement, within 1 percent, with measurements taken by this system [42].

5.6.3 Device Figure of Merit Measurement Analysis

As shown in section, 4.3, the figure of merit, ZT, is directly related to the device conversion efficiency. Therefore, knowing ZT for a device can be one of the most important measurements performed by this system. The figure of merit for thermoelectric materials is commonly found by calculation of the three measured parameters discussed in section 3.3, however this requires careful consideration to the losses accounted for in accurate measurements of thermal conductivity. To avoid this measurement, the figure of merit measured for thermoelectric couples has been found using a variety of methods, some of which do not require measurement of thermal conductivity [47,48]. The method chosen uses a modified open-short circuit test [47], similar to the technique discovered by Al-Obaidi and Goldsmid (herein referred to as method 1) [48]. Method 1 determines the figure of merit through a ratio of open and short circuit condition thermal conductance under small temperature gradient conditions. When a small

temperature gradient is applied across a device under open circuit conditions, heat transport occurs by thermal conduction, $Q_{Open} = K\Delta T$. If the device is short circuited, an additional Peltier heat contributes to the conduction giving a total heat flow of $Q_{Short} = K\Delta T + S_{AB}IT$. For short circuit conditions, $S_{AB}\Delta T = IR_{Module}$, so $S_{AB}IT = S_{AB}\left(\frac{S_{AB}\Delta T}{R_{Module}}\right)T$. If the temperature gradient is held constant for open and short circuit measurements and Joule effects are neglected, the total heat flow under short circuit conditions may be rewritten in terms thermal conductance to yield the figure of merit.

$$ZT = \frac{K_{Short}}{K_{Open}} - 1 \tag{37}$$

Method 1 gives a quick approximate result for the figure of merit, but has several limitations. First, method 1 is used for obtaining the figure of merit under small temperature gradients. Most thermoelectric devices are used under high temperature gradients, so they must also be tested under high gradients. Second, method 1 neglects Joule and Thomson heating effects which are inherent with current flow in thermoelectric materials. Third, method 1 requires short circuit conditions, an impractical testing condition for thermoelectric devices with low resistances. For these reasons, method 1 was adapted by Min and Rowe to allow for testing under varied load conditions (herein referred to as method 2). Method 2 extends the use of method 1 by determining the figure of merit for non-short circuit conditions including Joule effects due to Peltier current. Starting with the heat flow at the device hot side,

$$Q_{Load} = \alpha_{Load} T_{Hot} I - \frac{1}{2} I^2 R_{Module} + \mathrm{K}\Delta T_{Load} \tag{38}$$

given open circuit conditions,

$$Q_{Open} = \mathrm{K}\Delta T_{Open} \text{ and } V_{Open} = \alpha_{Open} \Delta T_{Open} \tag{39}$$

and load circuit conditions from Kirchoff's laws,

$$\alpha_{Load} \Delta T_{Load} = (R_{Load} + R_{Module}) I = R_{Total} I \tag{40}$$

the figure of merit is determined.

$$ZT_{Ave} = \frac{\frac{\Delta T_{Open}}{\Delta T_{Load}} - 1}{\left[\left(\frac{R_{Module}}{R_{Total}}\right)\left(\frac{2T_{Hot}}{T_{Hot} + T_{Cold}}\right) - \left(\frac{T_{Hot} - T_{Cold}}{T_{Hot} + T_{Cold}}\right)\left(\frac{R_{Module}}{R_{Total}}\right)^2\right]} \tag{41}$$

Analysis for this approach is shown in Appendix E. The figure of merit can also be found for a fixed temperature gradient and varied heat source.

$$ZT_{Ave} = \frac{\frac{Q_{Load}}{Q_{Open}} - 1}{\left[\left(\frac{2T_{Hot}}{T_{Hot} + T_{Cold}}\right)\left(\frac{R_{Module}}{R_{Total}}\right) - \frac{1}{2}\left(\frac{T_{Hot} - T_{Cold}}{T_{Hot} + T_{Cold}}\right)\left(\frac{R_{Module}}{R_{Total}}\right)^2\right]} \tag{42}$$

Analysis for this approach is shown in Appendix F. Here, subscripts "Load" indicate effects under load conditions, and "Open" refers to effects when the device is open circuited. The device resistance, R_{Module}, is given at the average temperature under load conditions. Therefore, the device resistance is found at temperatures equivalent to the load circuit conditions, but with no load attached. Min and Rowe give their analysis for steady-state conditions, and neglect heat losses due to conduction, convection and radiation. Method 2 may be used for

testing under small temperature gradients, or when the material parameters are held constant with respect to some temperature. For testing under large gradients, the material parameters may not be approximated as constant, losses must be accounted for, and the analysis must be modified.

The losses must be accounted for since they are no longer considered equal or negligible for large gradient testing on large devices. With the heat supplied to the device hot side fixed for open and load circuit conditions, the temperature gradient across the device decreases for the loaded condition due to the additional Peltier effect. Therefore, conduction losses down measurement wires from the hot side, radiation and convection are all higher for the open circuit condition. The difference in losses between open and load circuit conditions is proportional to the difference in gradients. If the difference in temperature gradients is kept small, the change in losses may be neglected:

$$Q_{Open} = Q_{Load} + \Delta Q_{Losses} \Rightarrow Q_{Open} = Q_{Load}$$

Depending on testing conditions, losses for each condition should be calculated to verify if they can be neglected to simplify the analysis.

Method 2 was further improved by including the Thomson effects that are usually neglected for small temperature gradients (herein referred to as method 3). Larger commercial devices tested under large temperature gradients have shown that Thomson effects should not be ignored [32]. Depending on the device tested and the percent of measurement accuracy required, the Thomson effect

may or may not have a significant affect on the results. Method 3 further adapts the analysis to testing under large temperature gradients, but still holds the material parameters constant. The analysis for incorporating material temperature dependencies presents an opportunity for future work.

5.7 DTS Measurements of a Commercial Device

A commercially available power generation device from Tellurex Corporation, model CZ1-1.0-127-1.27, was tested under varied atmospheres, cold side temperatures, temperature gradients, and load conditions.

Figure 48: CZ1-1.0-127-1.27.

The results provided are for atmospheric conditions under a closed bell-jar, assumed 750 Torr. The device was previously tested under vacuum pressures from 10^{-3} to 10^{-6} Torr, but the expected Seebeck voltages did not agree well.

Table 5: Seebeck under pressure.

Pressure (Torr, Pa)	T-cold (K)	T-hot (K)	Seebeck measured (μV/K)	Seebeck expected (μV/K)	%diff
5×10-6, 6.66×10-4	311.8	334.4	314.6	380	17.2
7x10-1, 93.3	310.9	334.7	327	380	14
756, 1.01×10+5	311.6	334	345	380	9

Research on the pressure dependencies of some Bi_2Te_3 thermoelectric compounds may explain these results, but this has yet to be investigated further [49]. By comparisons with reference data provided, it was determined through various experiments that the devices were intended for use under atmospheric conditions.

For testing this device, the gradient heater was made from that described in section 5.3.8.1. The cold side stage used for testing this device is described in section 5.3.6. For testing under varied load conditions, the device was allow to reach near steady-state conditions for accurate data collection. Device size, gradient, ambient pressure, load, average temperature and several other conditions affect the steady-state time, so care must be taken when measuring devices under varied conditions. An example of steady-state testing is shown in figure 49 of raw data collected from the system on the Tellurex device while testing at a constant temperature gradient and varied load conditions.

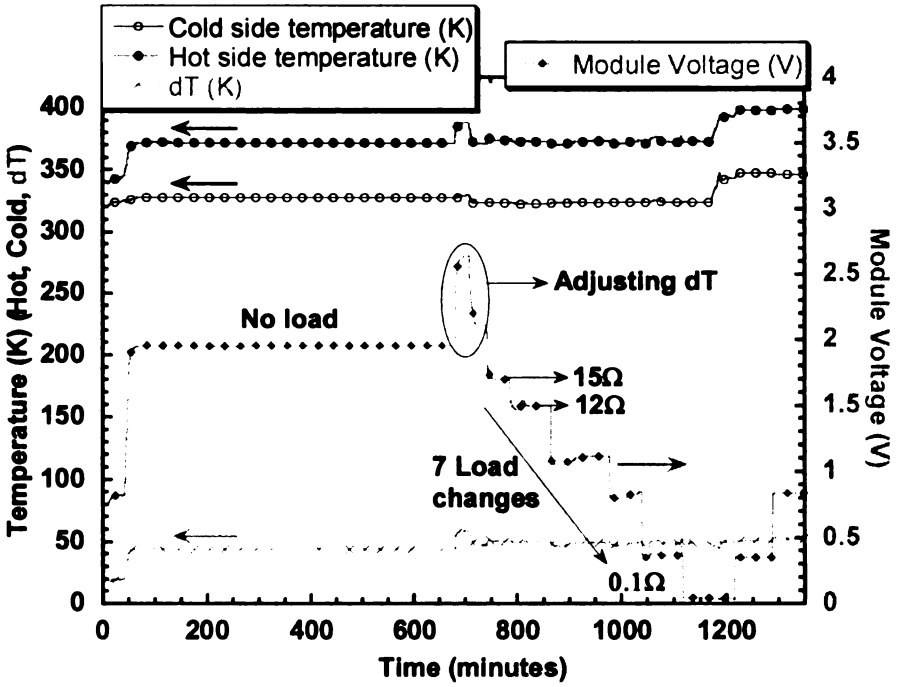

Figure 49: Raw data collection, temperature and voltage versus time.

The following load curves for the Tellurex device are provided as figures 50 through 55.

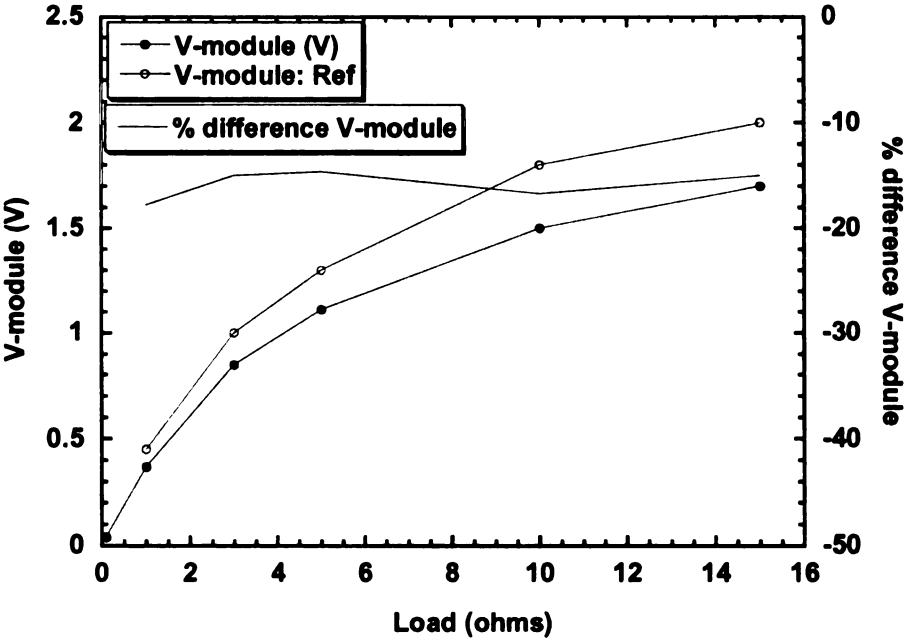

Figure 50: Tellurex load error curve, T-cold = 50°C, T-hot = 100°C.

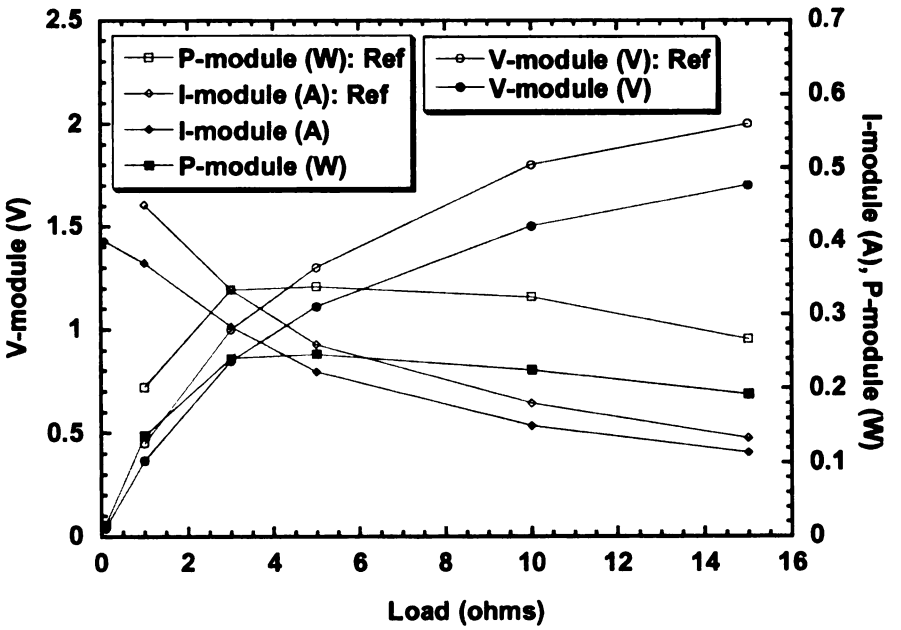

Figure 51: Tellurex load curve, T-cold = 50°C, T-hot = 100°C.

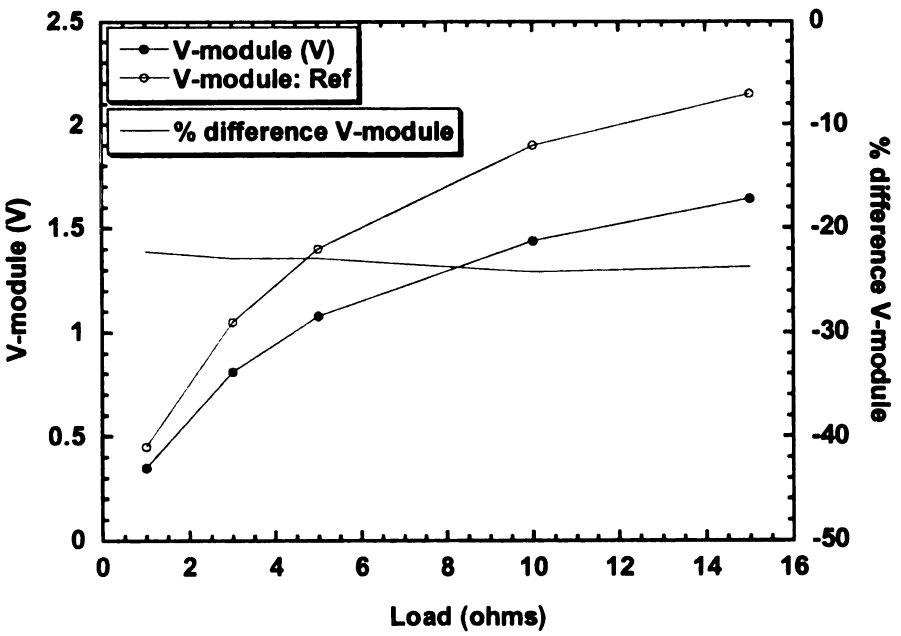

Figure 52: Tellurex load error curve, T-cold = 75°C, T-hot = 125°C.

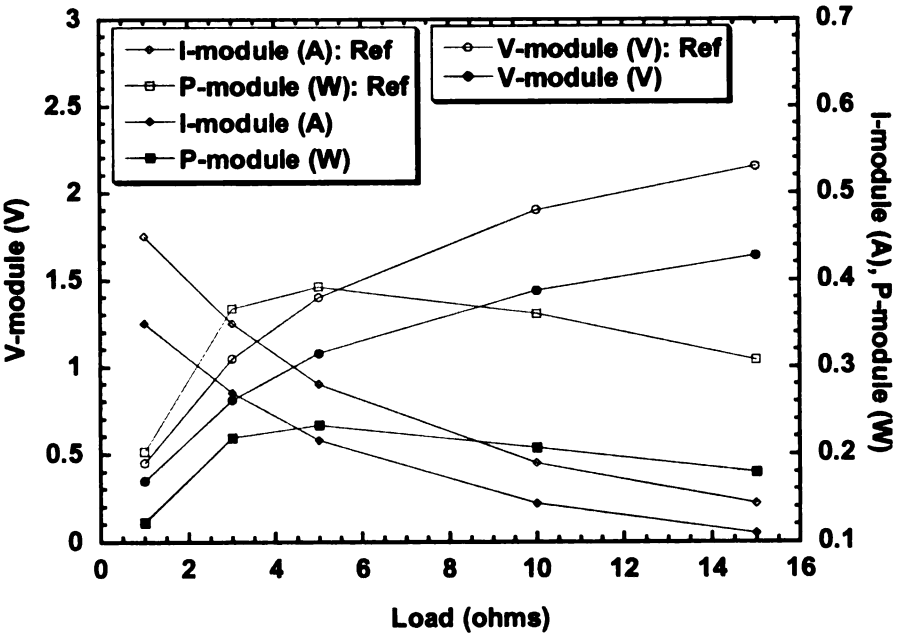

Figure 53: Tellurex load curve, T-cold = 75°C, T-hot = 125°C.

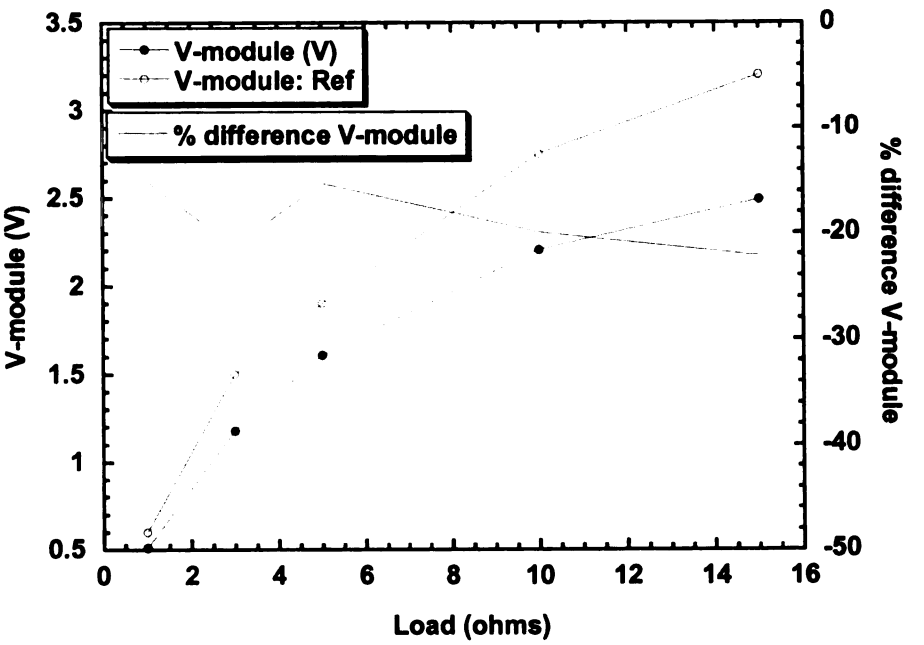

Figure 54: Tellurex load error curve, T-cold = 75°C, T-hot = 150°C.

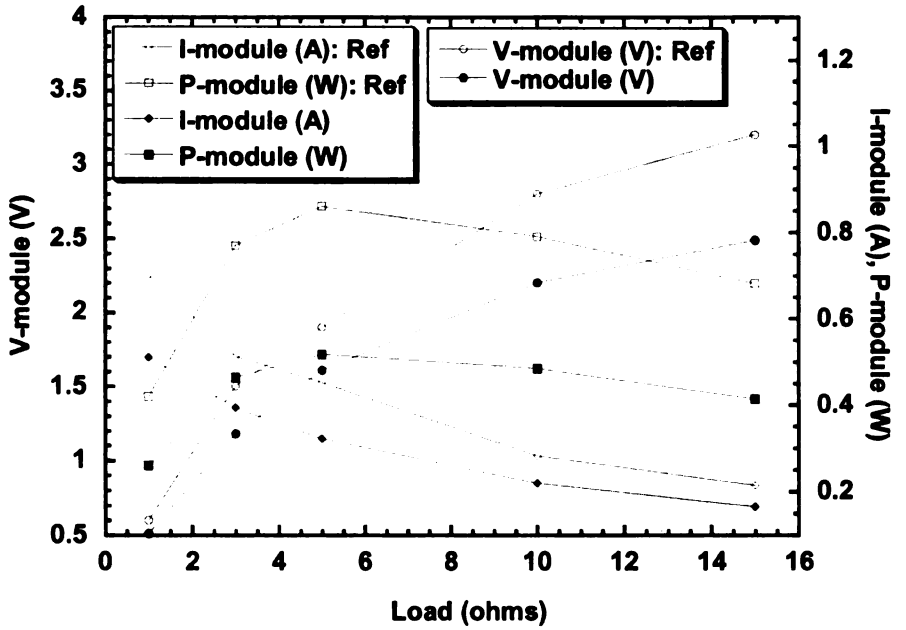

Figure 55: Tellurex load curve, T-cold = 75°C, T-hot = 150°C.

The Tellurex device has been tested under various load and temperature conditions. The percent errors in voltage and current measurements under load conditions ranged from 15-22 percent, and some of this error can be accounted for. First, this device has a tolerance of difference from device to device manufactured, and will therefore yield different results than the reference data. This would agree with the resistance measurements taken previously given in figure 47. Second, the reference data provided is in plot form, and was extracted to the best of the author's ability, but one should expect some error. Third, the deviations in open circuit voltage measurements merely transfer through for all load conditions.

As shown in figure 56, the figure of merit can be computed using the open-load circuit test with a fixed heat supply [47].

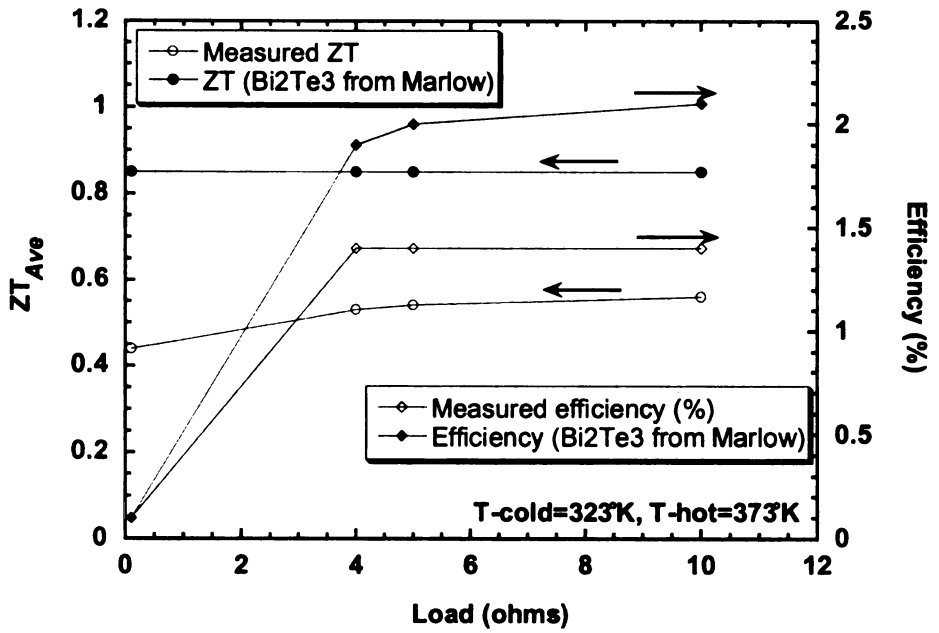

Figure 56: ZT_{Ave} and efficiency for Tellurex device, T-cold = 323°K, T-hot = 373°K.

The efficiency of figure 56 is calculated based on ideal effects because the contact resistance of the device is included in the measured device resistance, and the wiring resistance between device and load of 65mΩ is included in the load resistance. The figure of merit drops suddenly for a near short circuit condition, so one might want to investigate further.

Thermal losses due to conduction, convection, and radiation for open and load circuit conditions have been computed [45]. For the experimental setup provided, the difference in heat losses due to these three mechanisms was found to be near equal, and their effect negligible for this test. See Appendix G, for heat loss calculations.

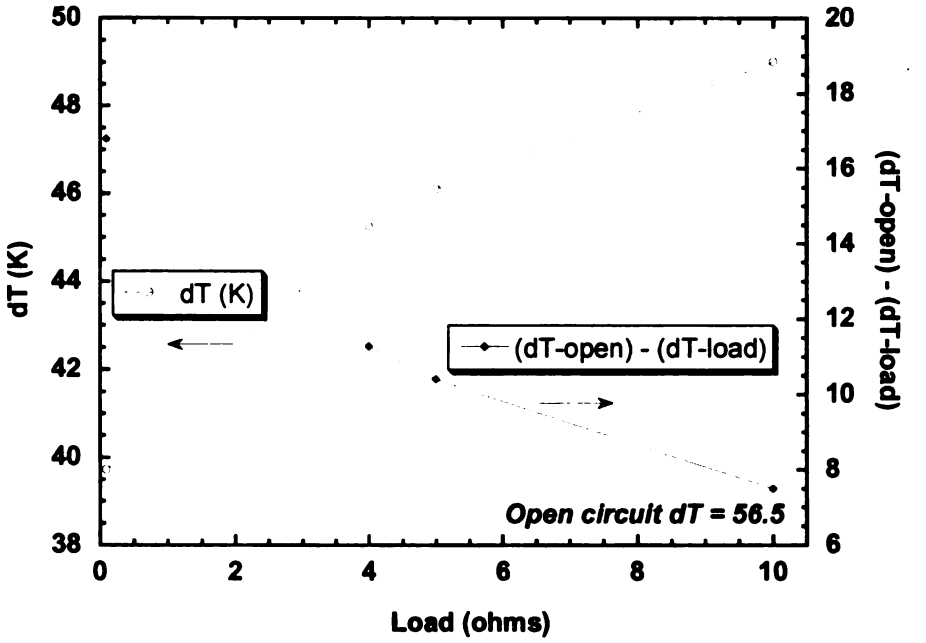

Figure 57: Tellurex device dT changes, T-cold = 50°C, T-hot near 100°C.

The Thomson heat generated is not accounted for in the analysis leading to the figure of merit. For the results presented, the effects of Thomson heating are compared, per couple, relative to the other load circuit effects to determine what inaccuracy this may cause on the figure of merit. A worst case scenario is considered under high electrical current outputs, and figure 51 is used for the 165mΩ load condition.

$$Q_{Load} = K(T)\Delta T + \alpha_{Hot}(T)T_{Hot}I - \frac{1}{2}I^2R_{Module} - \frac{1}{2}\tau\Delta TI$$

The right most term is the Thomson heat, found from Thomson coefficient as $\tau = T\frac{d\alpha}{dT}$, and is calculated from reference data obtained for the Seebeck voltage [43].

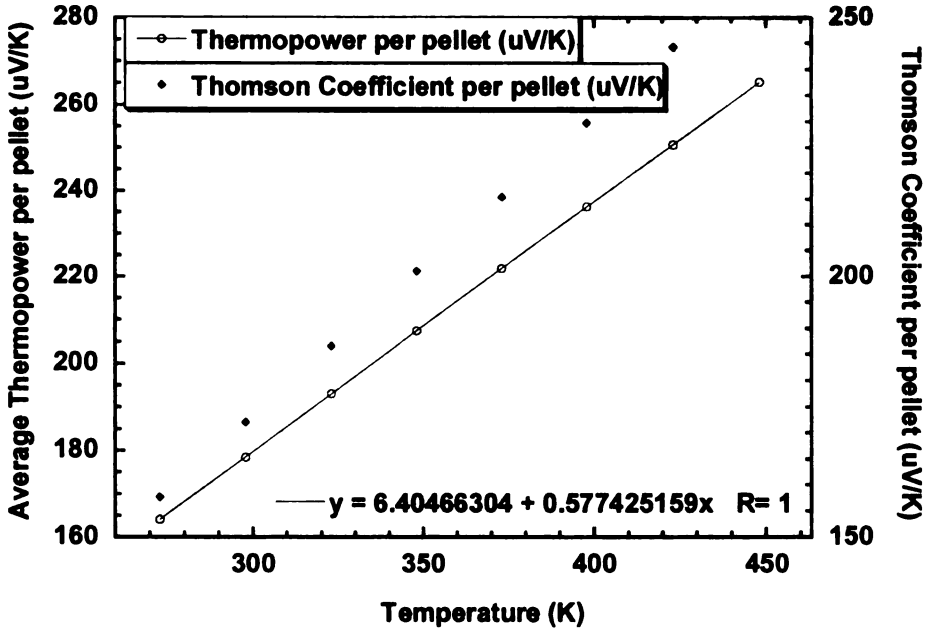

Figure 58: Thomson coefficient for Tellurex device.

For an average temperature of 75°C (348°K), $\tau = 200\frac{\mu V}{K}$. The Thomson heat is calculated for the 165mΩ load current of 1.4A as $T_Q = -\tau I \Delta T \cong 14mW$ per pellet (28mW per couple) is liberated since current flows with the gradient. The Thomson heating is not a junction effect like the Peltier, however only one half contributes to the hot side, acting as an additional 14mW "from" the hot side. The Peltier heat is found as $P_Q = S_{Hot} I T_{Hot} = 115mW$ per pellet (230mW per couple). The Joule heat per couple is calculated from the average device resistance value obtained from figure 47 as 4.4Ω divided into 127 couples. The Joule heat per couple is $J_Q = I^2 \frac{R}{127} = 68mW$, 34mW additional "from" the hot side.

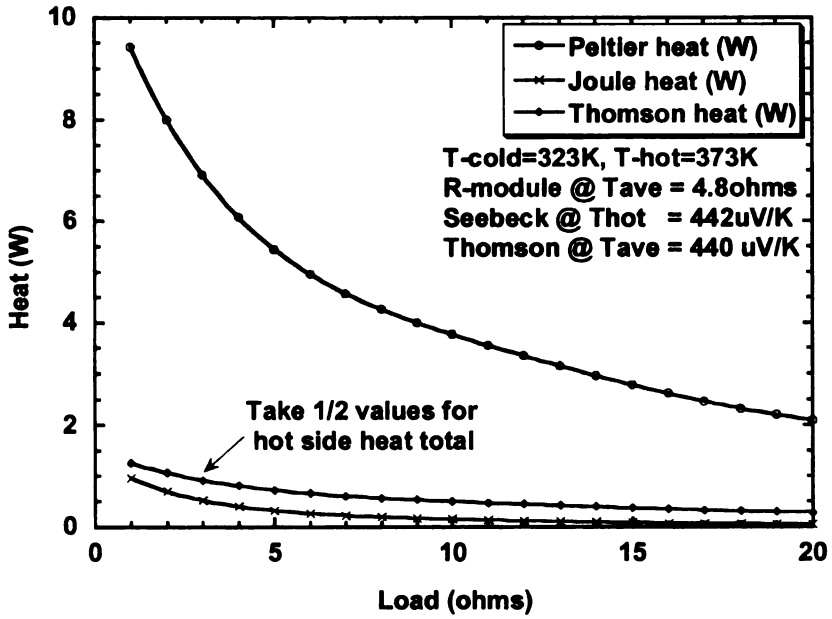

Figure 59: Thomson heat effects.

For the figure of merit analysis, the heat flow conditions for open and load circuit testing are assumed equal, thereby canceling the thermal conduction effect from both sides. Therefore, the Thomson effect contributes

$\frac{|T_Q|}{|T_Q|+|P_Q|+J_Q} = \frac{14mW}{278mW} = 5\%$ and is neglected for this analysis. This result may give insight to why the figure of merit is lower for the 165mΩ condition, and the incorporation of Thomson heating into the figure of merit analysis is left for future work.

The efficiency was also tested under higher temperature conditions, and the following results were obtained neglecting Thomson effects.

Table 6: ZT_{Ave} and efficiency for Tellurex device, T-cold = 75°C, T-hot = 150°C.

Load (Ω)[1]	ZT	Efficiency (%)
15	0.53	1.5
10	0.49	1.7

5.8 DTS Measurements of LAST Devices

Thermoelectric devices have been fabricated from the LAST materials and tested by the DTS measurement system. The LAST material thermoelectric properties have been measured at various temperatures, and the data has been used to determine the appropriate size of the thermoelements to fabricate a device to yield maximum efficiency [50, 51]. Various fabrication techniques with the LAST material and results of devices tested are discussed.

5.8.1 Calculated Performance

The size of the thermoelements used in fabricating a thermoelectric device can dramatically affect the device efficiency. In fact, the conversion efficiency decreases as leg length decreases because the ratio of electrical contact to material resistance increases, as well as an increase in the ratio of thermal conductivity of the material to the ceramic layers used [51,52].

[1] Wiring resistance adds 65mΩ to this value, and was done so for ZT and efficiency provided.

$$\eta = \frac{\eta_C}{\left(1+2\frac{\lambda L_c}{\lambda_c L_o}\right)^2\left[2-\frac{1}{2}\eta_C+\left(\frac{4}{ZT_{Hot}}\right)\left(\frac{1+\frac{2\rho_c}{\rho L_o}}{1+2\frac{\lambda L_c}{\lambda_c L_o}}\right)\right]} \tag{43}$$

Here $\eta_C, \lambda, \lambda_c, L_c, L_o, ZT_{Hot}, \rho_c, \rho$ are the Carnot efficiency, thermal conductivity of the thermoelement materials, thermal conductivity of the electrical and thermal contact materials, thickness of the ceramic layers, thickness of the thermoelement length, figure of merit at the hot side temperature, electrical contact resistivity, and thermoelement resistivity, respectively.

However, the device thermoelements can not be made too long or the rate of heat flow would decrease, as well as the power out.

$$P_{ElectricalOut} = \frac{\alpha^2 \Delta T_o A_o}{\left(2\rho L_o\right)\left(1+\frac{2\rho_c}{\rho L_o}\right)\left(1+\frac{2\lambda L_c}{\lambda_c L_o}\right)^2} \tag{44}$$

Here $\alpha, \Delta T_o, A_o$ are the Seebeck coefficient, temperature gradient and cross sectional area of the thermoelements, respectively. This shows there is a trade-off between device efficiency and the power produced when designing a device for optimal performance.

A thermoelectric material and device modeling program has been used to determine the dimensions of the thermoelements needed for maximum efficiency for the LAST materials [51]. Using the modeling program developed for LabView®, ***Efficiency vs. current density.vi***, and given temperature dependent

data for P and N type materials, the optimal thermoelement sizes were determined.

5.8.2 LAST Fabrication Methods and Results

A few fabrication methods have been investigated for use with the LAST material and are discussed; however as the summary of results table below shows, the best method may not have been discovered yet.

Table 7: Summary of LAST module results.

Contact method	% contact resistance	Expected ZT (T-ave=600K)	Expected efficiency	Measured ZT	Measured efficiency
Ag-paint	99	1.3	10	0.017	< 1
Ag-epoxy	99	-	-	-	-
Solder	40	-	-	-	-
Diffusion bond	15	0.4	4	0.020	< 1

5.8.2.1 LAST devices fabricated with silver paint

LAST devices were initially fabricated with a silver paint from the Ted Pella Company. There is a coefficient of thermal expansion (cte) mismatch between the thermoelement and contact materials, however the paint is able to withstand temperature cycling without any noticeable peeling or cracking up to 900°K. The silver paint is an excellent thermal and electrical conductor; however, the paint contributes a dominating contact resistance that substantially degrades device performance. When using silver paint, the contact resistance on one such device was found from data of table 10 in the following manner at room temperature.

Table 8: Data for computing contact resistance from silver paint.

Material	P-(LAST)	N-(Ag-Sn-Sb-Te)
Electrical conductivity (S/cm)	1,500	1,200
Length (cm)	0.80	0.80
Area (cm^2)	0.25	0.32
Resistance (mΩ)	2.13	2.08

The device resistance was measured as described in section 5.6.2,and measured near 2Ω, giving the percent contact resistance as,

$$\%R_{Contact} = \left(1 - \frac{R_{Thermoelements}}{R_{Overall}}\right) x100 = \left(1 - \frac{0.00421}{4}\right) x100 = 99.89\% \quad (45)$$

In order to lower the contact resistance, the silver painted devices were annealed at 400°C for 2 hours in a 54 sccm 95% Ar, 5% H atmosphere. After annealing, the device resistance decreased to 0.95Ω, but still yielded a contact resistance about 99.55%. One such device fabricated in this manner gave a figure of merit near 0.01 under a 200° gradient, and the result was confirmed by another temperature measurement system using the open-short thermal conductance method [54]. The expected figure of merit for the device was found from previous data taken on the individual thermoelements, Table 9, and by using $Z = \left[\frac{z_1^{1/2} \pm \gamma z_2^{1/2}}{1+\gamma}\right]^2$, where $\gamma = \left(\frac{\rho_1 \kappa_1}{\rho_2 \kappa_2}\right)^{1/2}$ [53]. The expected figure of merit for an average temperature of 400°K was calculated to be 0.48.

Table 9: Room temperature thermoelement data for calculating ZT.

Material	P-(LAST)	N-(Ag-Sn-Sb-Te)
Thermal Conductivity (W/m·K)	≈ 2	≈ 2
Figure of merit (400K)	0.21	0.25

When applying the silver paint, if too much was applied, some tended to spill over the edges of the thermoelement decreasing the effective length and increasing the overall contact area. However, if not enough silver paint is applied, some pores are formed in the contact when the drying occurs and alcohols evaporate. Furthermore, pores form while the paint dries and cause pores to form in the paint weakening the contact mechanically, thermally and electrically. As evidence of this, another silver paint fabricated device was repeatedly tested under various temperature gradients. The hot and cold side temperatures were ranged up to 900°K and 300°K, respectively. The device temperature gradient was cycled once a day for three days in UHV conditions. The system UHV conditions were measured daily, 1×10^{-5} Torr on the first day, 2×10^{-6} Torr the second day, and 5×10^{-7} Torr the third day before the testing chamber was released back to atmosphere. On the last day of testing, vacuum conditions were released from 5×10^{-7} Torr to 750 Torr over a 30 minute period. After each of the temperature cycles, the device resistance and Seebeck were measured, and decreased after each time of cycling.

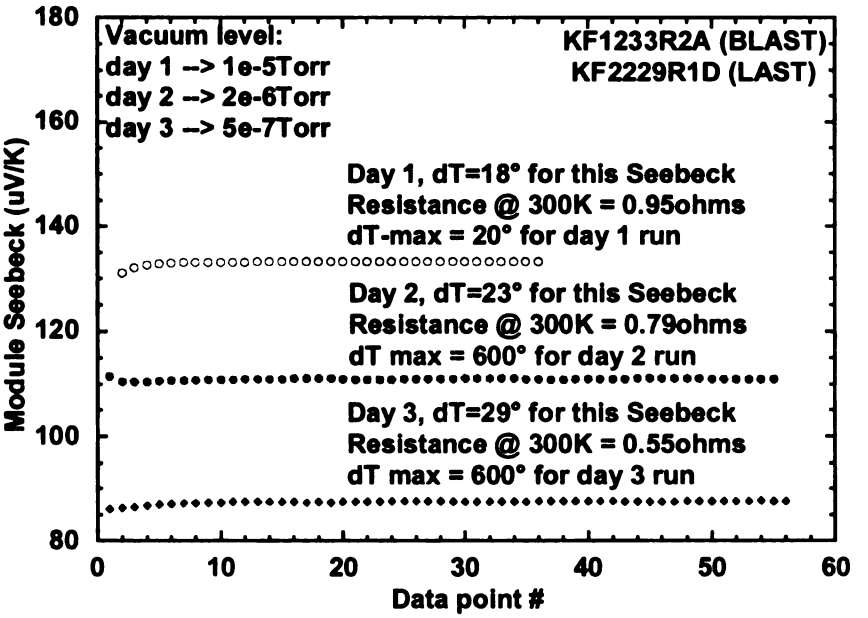

Figure 60: LAST module 3 day test.

Due to the decreasing device resistance and Seebeck, it was suspected that silver atoms from the paint moved into the thermoelements and contaminated the device, as with the affect of copper contacts to Bi_2Te_3 based devices [11]. Therefore, the system was released to atmospheric conditions. At atmosphere the device resistance increased unexpectedly to 1.2Ω. The device was disassembled and the electrical conductivity of the thermoelements were measured at room temperature by a separate system, but the thermoelements did not show any change in room temperature electrical conductivity from the initial measurements made prior to device fabrication. During disassembly, it was noticed that the top conducting plate removed easier than usual. It was therefore suspected that the device contacts were changing during the testing, such that as the device was cycled in temperature under UHV, any air pores formed in the silver painted contact when initially fabricated were able to escape.

As the pores decreased and density of the contact material increased, the contact resistance decreased.

The electrical and mechanical properties of silver painted contacts for thermoelectric device fabrication with the LAST materials does not seem appropriate. To improve upon this fabrication method, a silver filled epoxy[1] was purchased from Aremco for use in device fabrication. This epoxy was chosen because it was good to high temperatures, offered low electrical resistance, and is applicable with simple curing conditions.

5.8.2.2LAST devices fabricated with silver filled epoxy

A silver filled epoxy from Aremco was used to fabricate devices of the LAST materials. Dilute solutions of phosphoric acid to clean etch the surface, applied epoxy layer thickness, dilute version of the epoxy, and drying and baking times were varied for device fabrication. The silver filled epoxy followed the same contact resistance trend as the silver paint. The epoxy also began peeling at temperatures above 420°K, indicating a mismatch in coefficient of thermal expansion (cte); however, the epoxy has a room temperature cte of 17.3 in/in/°C and Pb-Te alloys are near 18in/in/°C [54]. It is not presently understood why the peeling occurs for some of the prepared samples but not others.

---

[1] Aremco silver filled epoxy pyroduct 597.

The silver epoxy fabricated devices formed a good mechanical contact, as the material broke before the bond during stress testing. However, the epoxy gave a dominating electrical contact resistance worse than that of the silver paint. The overall device resistance ranged from 40-1000Ω, depending on how the devices were prepared and cured, and gave a best case contact resistance of,

$$\%R_{Contact} = \left(1 - \frac{R_{Thermoelements}}{R_{Overall}}\right)x100 = \left(1 - \frac{0.006}{40}\right)x100 = 99.98\%$$

To reduce the contact resistance, gentle polishing and several acids[1] were experimented with to etch the thermoelement surfaces before applying the epoxy. Also, deionized water, acetone, and alcohols[2] were experimented with in removing the various acids etchants before applying the epoxy. The best results for low contact resistance were found by first etching the material with a dilute phosphoric acid, cleaning with DI water, and then following up with the manufacturers recommended epoxy curing procedure of a 2 hour room temperature dry, and 2 hour 200°F bake. While drying, some of the devices fabricated tended to have air pores that burst while baking. Therefore, the devices were dried and hot plate baked under spring loading, in atmospheric conditions under a hood. Spring loading was applied to make the contact as thin as possible for a low thermal resistance, as well as inhibit the epoxy from forming contact weakening pores as found with the silver painted devices. The force of spring loading was not measured directly, but estimated to be less than 1psi. The majority of thermoelements prepared with the dilute phosphoric acid and

[1] Phosphoric, comet bond flux, and Kester flux acids.

[2] Methanol and Isopropanol

cleaned with DI water gave average device resistances of 40-200Ω, but no consistency was found in the process toward obtaining 40Ω or lower each time. With hopes to reduce the contact resistance, devices were annealed on a hot plate under a hood at 500°F for an additional 2-8 hours under atmospheric conditions. After annealing, the contact resistance results did not improve and the epoxy peeling became worse for some of the contacts. These devices were not further tested under varied load and gradient conditions due to the high electrical contact resistance.

As with the silver paint in fabricating devices using the LAST materials, the silver epoxy does not seem a good choice for making electrical contacts. Others have reported that the size and structure of the silver particles in a paint or epoxy has shown to dramatically influence the contact resistance, and this may have been the case for the paint and epoxy chosen for these experiments [55]. Other paints and epoxies may lead to improved performance, and such experiments are opportunities for future work.

5.8.2.3 LAST devices fabricated with various solders

Different fluxes, solders and soldering temperatures[1] were experimented with for fabricating devices made of the LAST materials, and best results were obtained

[1] Comet bond flux, Kester flux, Zn-based and PbSn solders, and temperatures from 400-700°F

through use of a comet bond flux[1], Bi-Sn-Sb based solder[2] with soldering temperatures near 450°F. The soldered devices were not intended for testing at high temperature gradients, moreover for improving the contact resistance. A solder showing low contact resistance was considered a possible candidate for making cold side electrical contacts to the LAST materials. The completely soldered devices gave a lower overall resistance, ranging from 38-50mΩ, giving a contact resistance of near 40 percent depending on how the devices were cleaned and soldered. Some of the LAST specimens cracked due to thermal stress after using a soldering iron to apply the solder. To reduce the stress, a hot plate was used to slowly raise the thermoelements to near the solder melting point, and then a solder iron was used for additional heat to melt and apply the solder. The device resistance was measured, and contact resistance extracted based on the material properties. The contact resistance results gave good agreement with testing done using a transmission line method (TLM) experiment.

Varied load and gradient testing has not been performed on these devices due to the high contact resistance. Of the solders, fluxes and preparation methods demonstrated, none seemed to give a reasonable contact resistance to the LAST materials. The electrical characteristics of the Bi-Sn-Sb solder are proprietary, and there seems to be a lattice mismatch between the solder and LAST materials leading to the high contact resistance. To further lower the contact

---

[1] Comet bond flux is from Kapp Alloy and Wire

[2] Bi-Sn-Sb based solder is from Tellurex Corporation

resistance, different metals were electron beam and sputter deposited onto the LAST material as an intermediate step to the solder.

5.8.2.4 LAST devices fabricated with deposited contacts and solder

LAST based devices were fabricated with electron beam (ebeam) deposited and sputter deposited contacts using materials such as silver, gold, and tungsten. The deposited metals were to provide an intermediate step between solders, paints and epoxies. Tungsten was chosen because of the success it has given with PbTe fabricated devices [56]. Silver and gold were chosen as a combination of layers to offer high electrical conductivity from the silver, and a thin layer of gold for reduced oxidation effects.

The silver and gold were ebeam deposited onto plasma etched LAST materials. The plasma etching was made with an ebeam prior to deposition to remove any oxide layers. The LAST material was at room temperature during deposition, and deposition took place under sub 10^{-6} Torr atmospheric conditions. The materials seemed to deposit well, and gave interesting results when combined with the Bi-Sn-Sb solder to form a contact. For the silver and gold deposited contacts, the gold and or silver and gold seemed to ball up with the solder, figure 61.

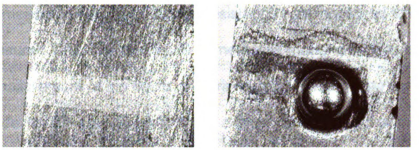

Figure 61: Soldered contacts.

Because of the dissolved intermediate deposited contact, no devices were fabricated with this method of materials.

Next, Tungsten was ebeam deposited onto a new pellet of the LAST material. Attempts to solder at various temperatures and with different fluxes were unsuccessful. The solder did not wet the surface well and balled onto the soldering iron tip. When trying to use a hot plate, the solder again balled up and did not spread evenly for a uniform contact. No devices were fabricated with this method of materials. Attempts of soldering with an intermediate metal contact were not unsuccessful because it initiated a more involved investigation of diffusion bonded contacts.

5.8.2.5 LAST devices fabricated by diffusion bonding

Devices have been successfully made by diffusion bonding contacts of nickel and antimony. Several other materials have been investigated, but this combination gives the best present results. The contact resistance was measured very small, giving only a 15 percent contact resistance as verified

through TLM measurements. The device resistance was measured to be 18mΩ, Seebeck measured 120μV/K, and figure of merit was found to be approximately 0.02. The measurement of the figure of merit requires steady-state conditions, however this device did not appear to reach a steady-state condition even after a two day period for each of the load and open circuit conditions. For the testing conditions applied to this device, calculations show that if the gradient is measured incorrectly by just 0.1°, ZT can vary by 0.05. In addition to testing the device using the open load circuit method, results for the device resistance and figure of merit were found to be in good agreement with an AC method using two lock-in amplifiers [42]. With the applied gradient, the expected ZT was found from literature to be near 0.3, but this is not guaranteed to yield the same results for the materials used in this device [41]. Temperature dependent data was not taken on the materials prior to device fabrication and testing, so a precise predicted figure of merit was not known.

The diffusion bonding methods for making contacts to the LAST material are showing much promise over the initial attempts with paints, epoxies, and solders. More devices are presently being fabricated with nickel-antimony diffusion bonded contacts, and their properties will then be measured with the use of the new device testing system.

6 Using an IR Camera for Device Testing

The temperature gradient applied across a thermoelectric device is one of the measurements required to characterize its figure of merit [47]. Most device gradients are measured by direct contact with the sample, by conduction of heat to the junction of a thermocouple, diode or platinum resistor sensor; however, each has limitations. The use of an infrared (IR) camera will be investigated as a non-contact measurement of temperature gradients used for calculating the figure of merit based on the open load circuit testing method.

6.1 Why Infrared

Direct contact measurements of the temperature gradient may involve thermocouples, diodes or platinum resistive sensors. Diodes and platinum resistive sensors are generally too large to measure small enough regions of interest on smaller objects such as thermoelectric pellets or couples. Thermocouples are also limited to a spatial resolution dictated by the size of the junction of materials used to make it or the material that bonds it to the surface for which it is placed upon. Furthermore, thermocouples conduct heat away from an object that can distort the temperature profile or cause other undesirable effects. Larger thermocouples are easier to prepare for sample testing, but suffer smaller spatial resolution of temperature and have more conductive losses. Decreasing the size of the thermocouple wires reduces both of these effects, but many difficulties arise in sample preparation because they are small to handle

and manipulate. Errors in temperature measurements vary depending on the size ratio of specimen under test and thermocouple contact. Also, the purity of the materials used to make the thermocouple can affect its performance, so materials are often sold as matched pairs based on their purity. Thermocouples are fairly inexpensive compared to other tools used for obtaining temperature gradients in thermoelectric testing, but do not offer as many features as more recent technologies.

IR cameras provide an alternate method of measuring temperature that alleviates many of the difficulties associated with direct contact measurements employing thermocouples. In addition to measuring temperature by conduction, temperature can be measured by the amount of electromagnetic radiation emitted from an object. IR cameras are tools used to measure electromagnetic radiation, and thus temperature without direct contact to the device under test. However as with thermocouples, measurements with IR cameras offer new challenges that must be overcome for obtaining accurate measurements.

6.2 How Infrared Cameras Measure Temperature

All objects continuously emit and absorb energy in the form of electromagnetic radiation. An object at thermal equilibrium with its surroundings emits and absorbs energy at equal rates, but an object hotter than its surroundings emits energy. For solid objects, the radiation is a function of the objects temperature and surface characteristics, and is commonly referred to as thermal radiation.

Objects that emit and absorb energy perfectly without any reflections are called blackbodies, and have an emissivity value of one. All other objects emit or absorb a fraction of the energy involved as governed by the temperature dependent emissivity value, $\varepsilon(T)$ of the object. The emissivity is also frequency dependent with a value typically given as a weighted average for the range of corresponding wavelengths, ε. The total amount of energy emitted from an objects surface may be calculated relative to a black body by use of the Stefan-Boltzmann law. This law states that the emitted energy, $R(T)$, is a function of temperature whose magnitude is proportional through a constant, σ_{SB} [5].

$$R(T) = \varepsilon\sigma_{SB}T^4 \frac{W}{m^2} \tag{46}$$

$$\sigma_{SB} = \frac{2\pi^5 k_B{}^4}{15h^3c^2} = 5.67x10^{-8} \frac{W}{K^4m^2} \tag{47}$$

Here σ_{SB}, k_B, h and c are the Stefan-Boltzmann constant, Boltzmann constant, Planck's constant and the speed of light, respectively. For objects at temperatures of 10-5000°K, the radiation predominantly occurs in the IR part of the spectrum of 0.2-500μm wavelengths, so IR detectors are commonly used to measure temperature. IR cameras have detectors made up of an array of IR sensors to monitor temperature, and each sensor of the array represents a pixel in an acquired thermal image.

Each material has a unique emissivity and therefore emits a different amount of thermal energy for a particular temperature. Since IR cameras rely on the

magnitude of thermal energy hitting a sensor to yield a corresponding temperature, two objects at the same temperature of different emissivity may be measured at different temperatures. Thermoelectric devices are made of several materials: thermoelectric material, electrical interconnects, solders, paints, and thermal conduction layers. The device emissivity can be normalized by coating the surfaces with a material that doesn't greatly affect the material properties such as electrical or thermal conductivities. The coating material must also be able to withstand high temperatures, from room temperature to 900K for our testing purposes. Therefore, a Rustoleum® flat black high temperature spray paint has been used for this purpose, and a few coats are applied on a narrow region of the device. It seems best to only apply a limited number of coatings, or else the luster increases and decreases the emissivity further from the desired black body effect. Now, the device is heated to a particular gradient also measured by thermocouples, and the camera emissivity is adjusted to correspond with the thermocouples. The thermocouple junctions are not directly visible with the IR camera in the present testing apparatus, so the surrounding areas of the thermocouples are viewed. The camera emissivity with use of the black spray paint gave best agreement with the thermocouples when set to 0.7.

6.3 *The Infrared Camera used at MSU for Thermoelectrics*

The IR camera[1] used in the Pulsed Laser Deposition and Transport Characterization Laboratory at MSU uses a cooled InSb detector array and is designed for use with 3-5μm wavelengths, corresponding to temperatures of approximately 273-1000°K. Due to the high measurement range, this camera is an ideal choice for testing thermoelectric devices for power generation applications. It was purchased with interchangeable 25mm and 50mm lenses, and has focal length adapters to allow precise viewing from several inches and beyond. The resolution varies depending on which lens and adapter are used. It also has intensity filters for measuring above 573°K. The camera is part of a system that includes a PC with Windows 2000 ® based environment and Thermagram ® software for a user friendly system. Further specifications are available from the manufacturer's website[2].

The camera is not directly positioned near the devices since they are enclosed in a vacuum environment, so a viewport window made of sapphire has been chosen. Quartz[3] transmits 0.18-2.5μm wavelengths, whereas sapphire will transmit > 90% of wavelengths in range of 1-5μm. The total transmission of radiation from sample, $\Psi_{Transmitted}$, to camera is, $\Psi_{Transmitted} = 0.9\Psi_{Emitted}$.

---

[1] Mid-range Merlin from Indigo Systems Company, a division of Flear International.

[2] http://www.indigosystems.com/product/merlin.html

[3] Quartz transmission from Goodfellow

6.4 Using the IR camera

Different lenses and focal length adapters are provided with the camera to maximize the magnification for a given field of view and distance to object. With the present testing conditions, there exists about 4.5 inches between device and IR camera, and this includes space between device to sapphire, and IR camera only 0.5 inches away from the closed bell-jar viewport.

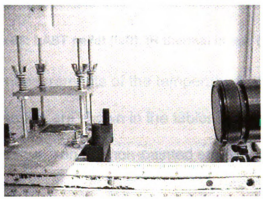

Figure 62: Closest camera to device distance is 11cm.

With present lenses, maximum magnification of 0.5 is obtained with the 50mm lens and 1 inch focal length adapter (referred to as an extender ring). An infrared image may not look good visually, but can still be very good thermally. However, devices tested appear quite clear, especially those made with the LAST material of larger sizes. The devices by Tellurex are difficult to obtain a clear image, but shows up thermally very well when each pixel temperature is profiled across a specified region of interest.

6.4.1 IR measurements on bulk materials

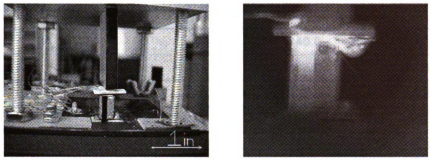

Figure 63: LAST pellet (left), IR thermal image (right).

Results of comparing measurements of the temperature gradient using thermocouples to IR camera are shown in the tables below. Best agreement with the thermocouples was found on the non-painted surface under atmospheric conditions.

Table 10: TC vs. IR dT comparison, no vacuum (750 Torr).

dT_1 (thermocouples)	dT_2 (IR camera, w/o paint)	dT_3 (IR camera, painted surface)	TC vs. IR w/o paint (%)	TC vs. IR w/ paint (%)
10.15	12	26.4	18.2	160.1
35	40	58	14.3	65.7
68	92	107	35.3	57.4

However, with reduced convection ($8x10^{-2}$ Torr) the result is just the opposite and better agreement was found with the thermocouples on the painted surface.

Table 11: dT comparison, $8x10^{-2}$ Torr vacuum.

dT_1 (thermocouples)	dT_2 (IR camera, w/o paint)	dT_3 (IR camera, painted surface)	TC vs. IR w/o paint (%)	TC vs. IR w/ paint (%)
4.5	2.7	4	40.0	11.1
16	10.4	14	35.0	12.5
34.2	11.2	29	67.3	15.2
57.2	42	48	26.6	16.1
87.3	60.9	71.3	30.2	18.3

More testing should be done to decrease the atmospheric pressure to see if results between thermocouple and IR improve further. Although the absolute temperatures do not agree between camera and thermocouples, the key feature of the IR camera is that it measures several points along the gradient as opposed to just two from the thermocouple. A temperature profile versus pellet length is provided in figure 64. For this plot, there exist 105 data points collected across the 7mm high pellet, corresponding to a resolution of 21pixels/mm (0.095°/pixel). This is not necessarily the defined resolution for the camera, but is for the configuration used for this measurement. This configuration of 1inch focal length adapter and 50mm lens was chosen to yield the highest magnification for an object 4.5 inches away from the detector.

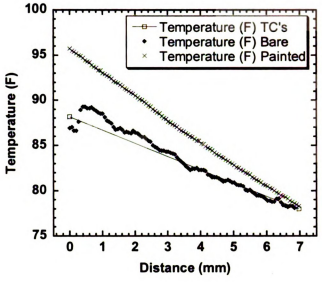

Figure 64: N16 dT profile.

6.4.2 IR Measurements on a Commercial Device

IR measurements have also been used on the large Tellurex power generation device. Figure 65 shows the device tested under the assembly of figure 39.

Figure 65: Tellurex device.

The IR measurements are compared to that as taken with thermocouples previously and show good agreement. Using the infrared camera with an average device temperature of 310°K, the figure of merit was measured as ZT =

0.65. The thermocouples were used in a different test with average temperature of 340°K and gave ZT = 0.55. For the Bi_2Te_3 based Tellurex device, the temperature dependent figure of merit follows a parabolic curve for the temperature range tested. This may explain why the figure of merit is higher for the lower temperature test measured with the IR camera than the one measured with the thermocouples at higher temperatures.

6.4.3 IR Measurements on a LAST Device

The IR camera has been used to test thermoelectric devices made from the LAST material as well. Results are for an early fabricated silver painted device are shown at steady-state conditions, and no black spray paint was used to normalize the material emissivity differences. Notice how the thermal image of figure 66 (*right*) has a odd thermal distribution from light (hot) to dark (cold) areas in a non-linear fashion.

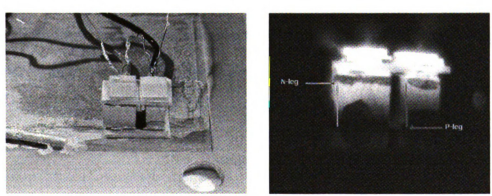

Figure 66: LAST made device.

This uneven thermal image temperature distribution is due to changes in emissivity between the materials used. Thermocouples were used to measure

the temperature gradient as well, and did not show any unordinary behavior such as this. If the thermal profile were real, and emissivities all matched, then the device ends would be cooler than the middle section, not possible for the steady-state condition. The figure of merit was not determined from use of the IR camera in its early uses, so no ZT data is provided here. This device was used to show the capability of testing with an IR camera. Further devices made from diffusion bonding methods described earlier will soon be tested using the IR camera.

The IR camera has shown use for testing bulk materials, commercial devices, and devices made from the new LAST materials. The technique needs to be investigated further for use under varied vacuum conditions. The IR camera has obtained good agreement with the use of thermocouples, and provides the temperature profile in addition to the gradient by acquiring several points along the length of the sample. This data may also be useful for providing additional insight with thermal modeling techniques that divide the thermoelectric device thermoelements into a finite number of small sections.

7 Conclusions

A new measurement system has been developed for testing thermoelectric devices based on new materials for power generation applications. The process of developing the device testing system (DTS), it's features and capabilities have been discussed. This system allows measurement of several device properties that previous systems in the MSU lab could not accommodate. This system is unique because it allows for testing of larger devices in addition to bulk samples and single couples that commercial systems, such as Z-Meters, are designed for. The capability of non-contact measurements using an IR camera has also been proposed. The system measurement tolerances have been given by testing of reference materials. Device resistance and Seebeck versus temperature, device performance under varied load and gradient conditions, figure of merit and efficiency have all been measured by this system. Several device fabrication methods for the new LAST material have been shown, as well as their results. The results of fabricating devices of the LAST material are helping to provide insight for additional device improvements. Some of the system limitations have been presented and provide opportunities for extending its capabilities through future work.

8 Future Work

The main topic ideas for future work are present below with brief descriptions. Several of these ideas have been presented throughout the paper, and are just reiterated in summary here.

8.1 Autonomous operation

In order to control the temperature gradient across the device, a temperature feedback system would need to be incorporated. This could be satisfied through use of a temperature controller, such as those available through Lakeshore Cryogenic industries[1] of through additional system programming.

The load changing can be automated with a switchbox of low contact switch resistance. With such modifications to the system, near autonomous operation may be achieved.

8.2 Software

The software used presently works, but may be modified with more autonomous features.

[1] Lakeshore model 330 series temperature controllers.

8.3 *Analysis*

The calculations for heat losses and their affects on high gradient changes should be considered. Also, non-linear temperature gradients and their affect on the Joule and Thomson effects at large gradients should be derived for the analysis leading to the figure of merit.

8.4 *Sample Stage*

A new sample stage should be developed to test samples at higher temperatures that present conditions, limited by the melting of PCB used with GE varnish and soldered leads. New bonding materials to fix heater to device should be investigated, matching coefficient of thermal expansion. This new sample stage may also be designed to test bulk samples.

8.5 *Larger devices*

A larger sample stage, higher cooling capacity chiller, and larger heater is required for testing devices required for the 1kW generator. The system can presently can test devices up to 1.5in^2.

8.6 *Hardware*

- An automated vent valve with Nitrogen backfill for clean venting should be installed on the Turbo pump for more efficient venting.

- RS-232 should be utilized on the vacuum gauge controller for vacuum dependent testing on materials and devices. This could also be used to control the flow of a backfill gas.
- A new DAC controller for PC to old EMSII analog controlled power supply is needed since original one malfunctioned. The same DAC should not be purchased as it seemed to cause fluctuations in the power supply voltage.
- An infrared camera mounting stage should be designed and attached to the bell-jar housing, as any vibration caused by the system or user would be in unison while viewing.

APPENDIX A

On a microscopic scale, semi-conductors are of crystalline form, for which the atoms are not randomly placed to make up the material, but bonded with some periodic pattern. Consider a semi-conductor material subjected to energy in the form of heat. The atoms are chemically bonded to each other fixing their center of mass, so they can not move very far unless more energy is given to break their bond with neighboring atoms. Suppose just enough energy is applied to elastically displace the atoms from their original positions in the lattice, hence no bonds are broken. The atoms will begin to vibrate around their center of mass as a function of the energy induced, and the effect of one atom's movement onto another carries on until the energy is distributed and damped by each interaction of neighboring atoms. Each atom has a distinct associated mass. If two atoms, one small and one large, are subjected to some fixed energy, the smaller atom will displace more than the larger because the larger can not change it's momentum as easily. This is analogous to striking a billiard ball with a cue stick, compared to applying the same energy with a cue stick to a bowling ball. The energy that disrupted atoms from their natural positions can be quantized and represented as a particle called a phonon [57].

APPENDIX B

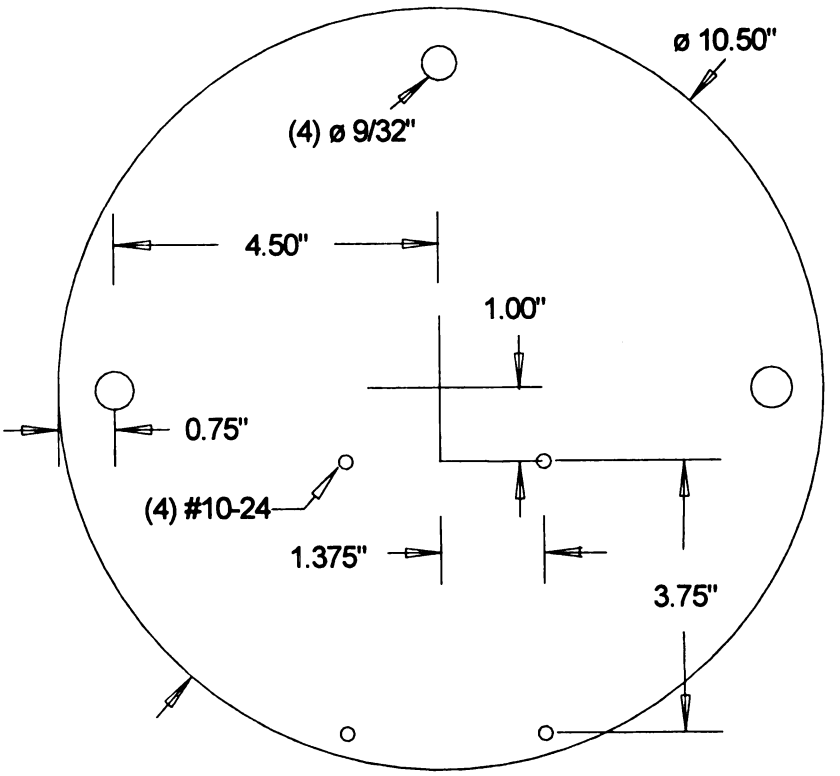

Figure 67: Cold plate support plate.

The stage is made of 0.25 inch thick aluminum, ground and polished upon completion. All holes are #8-32 unless otherwise specified, and the red inner holes are counterbore only as affirmed in the side view. All dimensions are symmetric unless otherwise specified, and the 1/16 inch diameter hole was placed along the horizontal at 1.75 inch vertical.

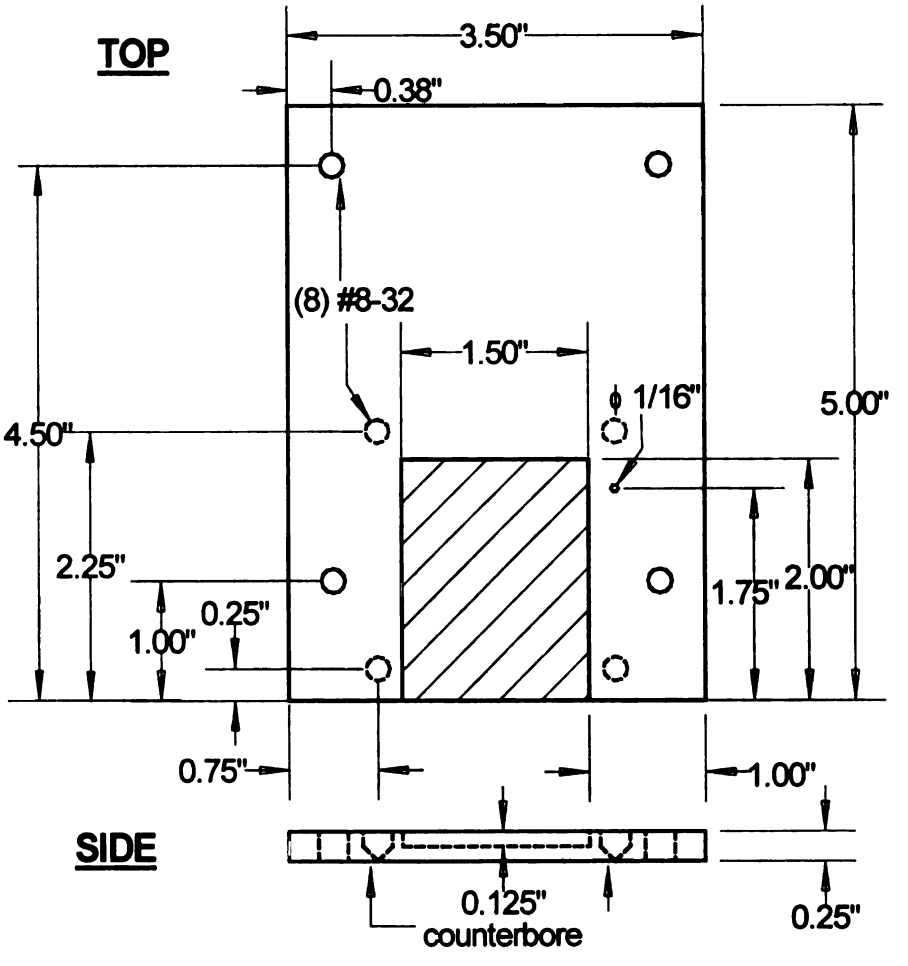

Figure 68: Large stage assembly aluminum stage.

The cold plate is as shown in Figure 28: DTS large cold plate.

APPENDIX C

The following figure is the wiring diagram for the device testing system, which includes wiring to 32-pin military connector and power feedthrough ports on the baseplate from the PCB and heaters. The gradient heater and load are wired directly, so no PCB pin is designated for these.

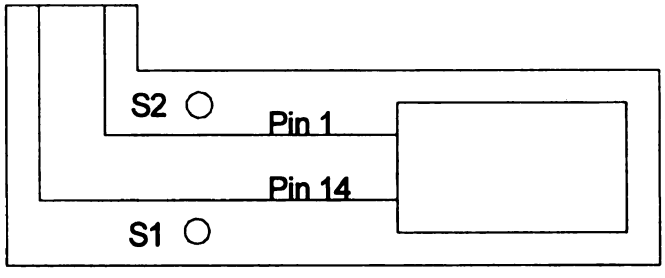

PCB Pin	32-Pin Mil	Use	Meter
1	A	Thermocouple + (cold)	2182 #1 (+)
2	B	Thermocouple - (cold)	2182 #1 (-)
3	C	Thermocouple + (hot)	2182 #2 (+)
4	D	Thermocouple - (hot)	2182 #2 (-)
5	E	Module/Load V +	2182 #4 (+)
6	F	Module/Load V -	2182 #4 (-)
7	G	Pt-100 I + (hot)	2400 (rear)
8	H	Pt-100 I - (hot)	2400 (rear)
9	J	Pt-100 I + (cold)	2002 HI (front)
10	K	Pt-100 I - (cold)	2002 LO (front)
11	L	Pt-100 V + (cold)	2002 SENSE HI (red)
12	M	Pt-100 V - (cold)	2002 SENSE LO (blk)
13	N	Pt-100 V + (hot)	2182 #3 (+)
14	P	Pt-100 V - (hot)	2182 #3 (-)
	V	Heater I + (cold)	DCS60-18E (+)
	f	Heater I - (cold)	DCS60-18E (-)

PCB Wide Traces	Power Feedthru	
1	1	Load Attachment
2	2	Load Attachment
	3	Heater I + (hot)
	4	Heater I - (hot)

Figure 69: PCB wiring Diagram.

APPENDIX D

1. Differential thermocouples: not accurate because of reasons stated earlier in the thermocouple section of this document.
2. Single-ended type E, 1mil bare
    a. Placed under the heater atop of the device: forces heater to not be in good thermal contact with the device, and I shorted by the Ag-paint holding the heater in place.
    b. Placed on side of alumina: no noticeable difference as opposed to atop of heater. However, must be adhered to each device, not convenient for device loading and unloading.
3. Single-ended type T, 10mil coated and leads twisted together
    a. GE varnished to stage next to device: measuring too cold compared to actual temperature across device. So placed atop of alumina on device bottom plate.
    b. GE varnished between device electrical leads, more accurate. Placed a Pt-100 sensor next to the TC to monitor and compare. This Pt-100 is used as a reference for the cold side thermocouples, which if the device and reference temperature of the electrical leads on circuit board are the same temperature, should read near zero if no gradient exists.
    c. Placed inside alumina tube and silver epoxied into the heater block, and verified the temperature by placing a Pt-100 sensor atop of the heater block. The Pt-100 and TC agreed within 10%, but this was

still not accurate enough. Next the Pt-100 was placed inside the heater with silver epoxy 4mm away from it, in a 3/8 inch deep hole in the heater block that is 0.5 inches thick.

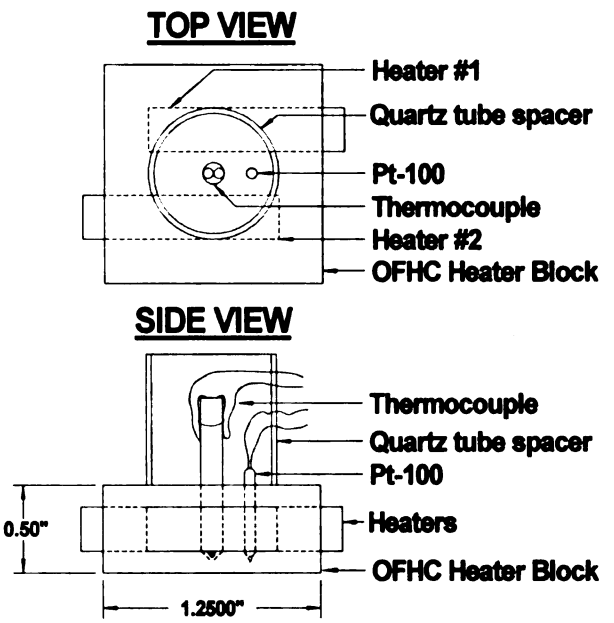

Figure 70: Temperature sensor trial.

4. An infrared camera was used to verify both sensors, but is not taken as absolute rather the gradient, only for comparison. The gradient was in best agreement at an emissivity setting of 0.8, and agreed within 10% of the platinum sensors.
5. The bottom Pt-100 was mounted on the aluminum stage bottom in an alumina filled epoxy, which was milled out to allow wiring and sensor to be embedded without affecting the smooth thermal interface: best agreement between sensors and thermocouples.
    a. The cold side Pt-100 was using the curve on the 2002, and the hot side was found from a 4-wire measurement and linearly fit data

from Omega, but the linear curve gave 3° inaccuracy so was regenerated as a polyfit with one tenth of a degree accuracy.

APPENDIX E

Equating the heat supplied for open and load testing conditions gives,

$$\Delta T_{Open} = \frac{\left[\alpha_{Load} T_{Hot} I - \frac{1}{2} I^2 R_{Module} + \mathrm{K}\Delta T_{Load}\right]}{\mathrm{K}}$$

Substituting for the load circuit current,

$$\Delta T_{Open} = \frac{\left[\alpha_{Load} T_{Hot}\left(\frac{\alpha_{Load}\Delta T_{Load}}{R_{Total}}\right) - \frac{1}{2}\left(\frac{\alpha_{Load}\Delta T_{Load}}{R_{Total}}\right)^2 R_{Module} + \mathrm{K}\Delta T_{Load}\right]}{\mathrm{K}}$$

Factoring out a ΔT_{Load} to the other side, and moving K into the numerator,

$$\frac{\Delta T_{Open}}{\Delta T_{Load}} = \alpha_{Load} T_{Hot}\left(\frac{\alpha_{Load}}{(R_{Total})\mathrm{K}}\right) - \frac{1}{2}\Delta T_{Load}\left(\frac{\alpha_{Load}}{R_{Total}}\right)^2 \frac{R_{Module}}{\mathrm{K}} + 1$$

Factor out the $\frac{\alpha_{Load}{}^2}{(R_{Total})\mathrm{K}}$ and multiply numerator and denominator by $\frac{R_{Module}}{R_{Module}}$

and rewrite to obtain,

$$\frac{\Delta T_{Open}}{\Delta T_{Load}} = \left(\frac{\alpha_{Load}{}^2}{R_{Module}\mathrm{K}}\right)\left(\frac{R_{Module}}{R_{Total}}\right)\left[T_{Hot} - \frac{1}{2}\Delta T_{Load}\left(\frac{R_{Module}}{R_{Total}}\right)\right]$$

Substitute for the figure of merit and factoring the equation,

$$\frac{\Delta T_{Open}}{\Delta T_{Load}} = Z\left[\left(\frac{T_{Hot} R_{Module}}{R_{Total}}\right) - \frac{1}{2}\Delta T_{Load}\left(\frac{R_{Module}}{R_{Total}}\right)^2\right] + 1$$

Multiply the numerator and denominator by $T_{Ave} = \frac{T_{Hot} + T_{Cold}}{2}$, and replace ΔT_{Load} with $T_{Hot} - T_{Cold}$,

$$\frac{\Delta T_{Open}}{\Delta T_{Load}} = ZT_{Ave}\left[\left(\frac{R_{Module}}{R_{Total}}\right)\left(\frac{2T_{Hot}}{T_{Hot}+T_{Cold}}\right)-\left(\frac{T_{Hot}-T_{Cold}}{T_{Hot}+T_{Cold}}\right)\left(\frac{R_{Module}}{R_{Total}}\right)^2\right]+1$$

APPENDIX F

For the following analysis, ideal conditions of zero losses are assumed. Again, starting from the heat balance equation,

$$Q_{Load} = \alpha_{Load} T_{Hot} I - \frac{1}{2} I^2 R_{Module} + \mathrm{K}\Delta T_{Load}$$

open circuit conditions,

$$Q_{Open} = \mathrm{K}\Delta T_{Open}$$

$$V_{Open} = \alpha_{Open} \Delta T_{Open}$$

and load circuit conditions from Kirchoff's laws,

$$\alpha_{Load} \Delta T_{Load} = (R_{Load} + R_{Module}) I = R_{Total} I$$

the formula for ZT is obtained by the following method. First, the open and load circuit conditions are coupled into a single equation.

$$\frac{Q_{Load}}{Q_{Open}} = \frac{\alpha_{Load} T_{Hot} I - \frac{1}{2} I^2 R_{Module} + \mathrm{K}\Delta T_{Load}}{\mathrm{K}\Delta T_{Open}}$$

Substituting for the device current,

$$\frac{Q_{Load}}{Q_{Open}} = \frac{\alpha_{Load} T_{Hot} \left(\frac{\alpha_{Load} \Delta T_{Load}}{(R_{Total})} \right) - \frac{1}{2} \left(\frac{\alpha_{Load} \Delta T_{Load}}{(R_{Total})} \right)^2 R_{Module} + \mathrm{K}\Delta T_{Load}}{\mathrm{K}\Delta T_{Open}}$$

and maintaining a constant temperature gradient allows $\Delta T_{Open} = \Delta T_{Load} = \Delta T = T_{Hot} - T_{Cold}$. Also, thermal conductance of the device does not change significantly in open circuit conditions compared to load conditions, as it is a material property only dependent on temperature.

$$\frac{Q_{Load}}{Q_{Open}} = \frac{\left(\frac{\alpha_{Load}{}^2 T_{Hot}}{(R_{Total})}\right) - \frac{1}{2}(T_{Hot} - T_{Cold})\left(\frac{\alpha_{Load}}{(R_{Total})}\right)^2 R_{Module}}{\mathrm{K}} + 1$$

Next, multiply by $\frac{R_{Module}}{R_{Module}}$ and moving K into the numerator to get

$$\frac{Q_{Load}}{Q_{Open}} = \left(\frac{\alpha_{Load}{}^2 T_{Hot}}{R_{Module}K}\right)\left(\frac{R_{Module}}{R_{Total}}\right) - \frac{1}{2}(T_{Hot} - T_{Cold})\left(\frac{\alpha_{Load}{}^2}{R_{Module}K)}\right)\left(\frac{R_{Module}}{R_{Total}}\right)^2 + 1$$

Using the relationship for the figure of merit, $Z = \frac{\alpha_{Load}{}^2}{R_{Module}K}$, and multiplying the

first term by $\frac{2(T_{Hot} + T_{Cold})}{2(T_{Hot} + T_{Cold})}$, and using $T_{Ave} = \frac{T_{Hot} + T_{Cold}}{2}$,

$$\frac{Q_{Load}}{Q_{Open}} = ZT_{Ave}\left[\left(\frac{2T_{Hot}}{T_{Hot} + T_{Cold}}\right)\left(\frac{R_{Module}}{R_{Total}}\right) - \frac{1}{2}\left(\frac{T_{Hot} - T_{Cold}}{T_{Hot} + T_{Cold}}\right)\left(\frac{R_{Module}}{R_{Total}}\right)^2\right] + 1$$

Finally, rewriting in terms of ZT_{Ave},

$$ZT_{Ave} = \frac{\frac{Q_{Load}}{Q_{Open}} - 1}{\left[\left(\frac{2T_{Hot}}{T_{Hot} + T_{Cold}}\right)\left(\frac{R_{Module}}{R_{Total}}\right) - \frac{1}{2}\left(\frac{T_{Hot} - T_{Cold}}{T_{Hot} + T_{Cold}}\right)\left(\frac{R_{Module}}{R_{Total}}\right)^2\right]}$$

APP

Calc

des

Cal
in t

No

---

k =

l =

a =

K

Q

sa

et

S

APPENDIX G

Calculations for heat losses contributed from testing of the Tellurex device described in section 5.7 are provided below.

Calculations for heat losses in thermoelectric device testing
in the DTS system with a Tellurex device.

Notations

---

k = thermal conductivity
l = length
a = cross sectional area
K = thermal conductance
Q = heat
sa = surface area
em = emissivity

Subscripts

---

q = quartz
c = copper
co = constantan
ch = chromel
w = wiring
tc = thermocouple
p = pellets (device)
t = total
cn = conduction
cv = convection
r = radiation

Conduction Loss Calculations

--> Thermal conductivity, k, data for near room temperature, from Goodfellow
--> Quartz heat insulator:

$kq := 1.46\frac{W}{m \cdot K}$

$lq := 2.54cm$

$$aq := \pi\left(22\frac{mm}{2}\right)^2 - \pi\cdot\left(20\frac{mm}{2}\right)^2$$

$$Kq := kq\cdot\frac{aq}{lq}$$

--> Copper wiring from heater:

$$kc := 401\frac{W}{m\cdot K}$$

$$lc := 25.4cm$$

$$ac := \pi\cdot(1mm)^2$$

$$Kc := 2\cdot kc\cdot\frac{ac}{lc}$$

--> Thermocouple wiring:

$$kch := 19\frac{W}{m\cdot K}$$

$$lch := 25.4cm$$

$$ach := \pi\cdot\left(\frac{.0508cm}{2}\right)^2$$

$$Kch := kch\cdot\frac{ach}{lch}$$

$$kco := 19.5\frac{W}{m\cdot K}$$

$$lco := 25.4cm$$

$$aco := \pi\cdot\left(\frac{.0508cm}{2}\right)^2$$

$$Kco := kco\cdot\frac{aco}{lco}$$

For open circuit conditions:

$$Th := 423K$$

$$Tc := 330K$$

$$dT := Th - Tc$$

--> quartz losses

$$Qq := Kq\cdot dT$$

$$Qq = 0.353W$$

--> copper losses

$$Qc := Kc\cdot dT$$

$$Qc = 0.923W$$

--> thermocouple losses

$$Qtc := (Kch + Kco)\cdot dT$$

$$Qtc = 2.857\times 10^{-3}W$$

--> conduction total loses

$$Qcnt := Qq + Qc + Qtc$$

$$Qcnt = 1.278W$$

For 0.165 ohm load circuit conditions:

$Th := 403K$

$Tc := 330K$

$dT := Th - Tc$

$Qq := Kq \cdot dT$

$Qc := Kc \cdot dT$

$Qtc := (Kch + Kco) \cdot dT$

$Qt := Qq + Qc + Qtc$

$Qt = 1.003W$

Convection Loss Calculations

--> Device pellets, 4 sides of each as 1x1.5mm:

$sap := (127) \cdot (4) \cdot (1mm) \cdot (1.5mm)$

$sah := (1) \cdot (4 \cdot 1.2in \cdot 0.5in + 1.2in \cdot 1.2in)$

$saw := (2)\pi \cdot (0.02in) \cdot lch$

$saq := \pi \cdot 22mm \cdot 1in$

--> Note: 1 mm of mercury is 1 Torr

$sat := saq + saw + sah + sap$

$sat = 58.057cm^2$

--> Convection total losses, assuming argon atmosphere

--> hconv = an approximate convection transfer coefficient for atmospheric conditions found from:

$$hconv := 10\frac{W}{m^2 \cdot K}$$

For open circuit conditions:

$Qformula := hconv \cdot (373K - 323K)$

$Qcvt := Qformula \cdot sat$

$Qcvt = 2.903W$

For 0.165 ohm load circuit conditions:

$Qformula := hconv \cdot (357K - 323K)$

$Qcvt := Qformula \cdot sat$

$Qcvt = 1.974W$

Radiation Losses

--> Stefan Boltzmann constant, sbc

$sbc := 5.67 \cdot 10^{-8} \frac{W}{K^4 \cdot m^2}$

--> emissivity of copper, emc

emc := 0.0

--> emissivity of Bismuth Telluride, guess as close to graphite, 0.98

emp := 0.9

--> outer surface area of the pellets, osap

osap := (60)·(1)·1mm·1.5mm

For open circuit conditions:

Tc2 := 323K

Th2 := 373K

--> radiation losses for the copper

$Qrc := \left[sbc \cdot \frac{emc}{(2 - emc)} \right] \cdot \left(Th2^4 - Tc2^4 \right) \cdot sah$

--> radiation losses for the outside pellets, with only outside face exposed

$Qrp := \left[sbc \cdot \frac{emp}{(2 - emp)} \right] \cdot \left(Th2^4 - Tc2^4 \right) \cdot osap$

Qrt := Qrc + Qrp

Qrt = 0.06W

For 0.165 ohm load circuit conditions:

Tc3 := 323K

Th3 := 357K

--> radiation losses for the copper

$Qrc := \left[sbc \cdot \frac{emc}{(2 - emc)} \right] \cdot \left(Th2^4 - Tc2^4 \right) \cdot sah$

--> radiation losses for the outside pellets, with only outside face exposed

$Qrp := \left[sbc \cdot \frac{emp}{(2 - emp)} \right] \cdot \left(Th2^4 - Tc2^4 \right) \cdot osap$

Qrt := Qrc + Qrp

Qrt = 0.06W

Qrt = 0.06W

APPENDIX H

STARTING THE SYSTEM

1. Prepare a device for testing (*see device mounting instructions*)
2. With a vented system chamber at atmospheric conditions, open the bell-jar with the yellow hoist operating switch, located in the left instrument panel of the system cart.
3. Insert the device testing stage, and screw it into place, either with the provided #8-32 screws or spring loaded assembly. Add thermal grease between stage and cold plate heater as necessary.
4. Solder the device load leads to the 12 AWG feedthrough wiring.
5. Attach the edge card connector to the device testing stage PCB.
6. Alligator connect the dT heater leads to the feedthrough lead wiring (larger devices only).
7. Ensure all wiring is in place properly and nothing inhibits the bell-jar from sealing to the baseplate.
8. Close the system chamber with the hoist operating switch. The bell-jar sealing O-ring should press evenly on the baseplate, and the baseplate to be-jar spacing is near 1/16 of an inch.
9. Ensure the Turbo pump manual vent valve is closed, a black plastic screw located on the pump housing side toward the front of the system.
10. Turn ON the rough pump.
11. Turn ON the switch for the Turbo pump and turbo cooling fan, located on the front panel of the right side instrument bay of the system cart.

12. The BA gauge turns ON when the first set point is reached.
13. Monitor vacuum until desired, then turn OFF using the switch on the vacuum gauge controller.
14. Turn ON the chiller, and adjust the flow rate using the bypass valve located between the chiller supply and return lines of the chiller, observe the pressure gauges on the chiller and chiller vibration damper located just next to the chiller. This bypass needs to be adjusted manually for the desired device cold side testing temperature.
15. Using LabView®, open the ***DTS Main.vi*** in the ***DTS programs*** library, and set the desired testing conditions and fill in entries for the device information.
16. Adjust the gradient and cold side heater power on the fly during testing, and pause data collection for changing the loads.

STOPPING THE SYSTEM

17. Stop the ***DTS Main.vi*** by pressing the STOP button in the program. Stopping the VI using the main LabView® menu will not reset the instruments properly, and may cause problems for starting a future run.
18. Turn OFF the turbo switch, leave the fan running however.
19. Turn OFF the chiller.
20. When vacuum has returned to 10^{-3} – 10^{-2} Torr ranges, turn OFF the turbo fan and rough pump.
21. Vent the system chamber by unscrewing the manual vent valve on the turbo pump housing.
22. Wait until the system bell-jar to baseplate spacing is back to 1/16 of an inch, and the air hissing sound has stopped from the vent valve.
23. Open the bell-jar chamber using the hoist switch.
24. Unsolder load leads, detach edge card connector, remove the stage mounting screws and remove the sample testing stage from the system.
25. Close the bell-jar and keep closed when the system is not in use.

REFERENCES

[1] Harman and Honig, *Thermoelectric and Thermomagnetic Effects and Applications*, McGraw-Hill, Lincoln Laboratory Publications, 1967.

[2] http://www.commercial.carrier.com, April 10, 2005.

[3] Gary L. Bennett, "Space Applications", Chap. 41, *CRC Handbook of Thermoelectrics edited by D. M. Rowe*, CRC Press LLC, New York, pg. 503, 1995.

[4] Section H, *CRC Handbook of Thermoelectrics edited by D. M. Rowe*, CRC Press LLC, New York, 1995.

[5] C. L. Foiles, *Encyclopedia of Physics*, VCH Publishers, Inc., New York, pg. 1263, 1991.

[6] Heikes, R. R., Ure, R. W., *Thermoelectricity: Science and Engineering*, Interscience Publishers, New York – London, 1961.

[7] http://srdata.nist.gov/its90/download/download.html, April 1, 2005.

[8] http://www.me.pdx.edu/~gerry/epub/pdf/thermocouple.pdf, February 3, 2004.

[9] A T type thermocouple consists of copper and constantan wires, K type is chromel and alumel, E type consists of platinum and chromel, S type is platinum/10% rhodium and platinum, and J type is iron and constantan.

[10] Gao Min and David M. Rowe, "Peltier Devices as Generators", Chap. 38 in *CRC Handbook of Thermoelectrics edited by D. M. Rowe*, CRC Press LLC, New York, pg. 482, 1995.

[11] H. J. Goldsmid, *Electronic Refrigeration*, Plenum, New York, 1964.

[12] Mahan, G. D., "Figure of Merit for thermoelectrics", *J. of App. Phys.*, Vol. 65, pg. 1578-1583, 1989.

[13] Mahan, G. D. and Sofo, J. O., "The best thermoelectric", *Proc. from the Nat. Acad. of Sci. U. S. A., App. Phys. Sci.*, Vol. 93, pg. 7436-7439, 1996.

[14] Z. H. Dughaish, "Lead telluride as a thermoelectric material for thermoelectric power generation", *Physica B*, Vol. 322, pg. 205-223, 2002.

[15] Slack and Hussain, "The maximum possible conversion efficiency of silicon-germanium thermoelectric generators", *J. of App. Phys.*, Vol. 70, pg. 2695, 1991.

[16] Tim Hogan, Sim Loo, Fu Guo, Jarrod Short, "Measurement Techniques for Thermoelectric Materials and Modules", *Mat. Res. Soc. Sym. Proc.*, Vol. 793, pg. 405-411, 2004.

[17] Jarrod Short, Sim Loo, Sangeeta Lal, Kuei Fang Hsu, Eric Quarez, Mercouri G. Kanatzidis, Timothy P. Hogan, "Hall Effect Measurements on New Thermoelectric Materials", *Mat. Res. Soc. Sym. Proc.*, Vol. 793, pg. 323-332, 2004.

[18] Geoff D. Staneft, Paul D. Asimow and Thierry Caillat, "Synthesis and thermoelectric properties of $Ce(Ru_{0.67}Rh_{0.33})_4Sb_{12}$", *Mat. Res. Soc. Conf. Proc.*, Vol. 793, 2004.

[19] S. Seal, S.C. Kuiry, P. Georgieva, and A. Agarwal, "Manufacturing Nanocomposite Parts: Present Status and Future Challenges", *Mat. Res. Soc. Bull.*, pg. 16-21, January 2004.

[20 S. Bhattacharya, Terry M. Tritt, Y. Xia, V. Ponnambalam, S. J. Poon, and N. Thadhani, "Grain structure effects on the lattice thermal conductivity of Ti-based half-Heusler alloys", *App. Phys. Lett.*, Vol. 81, No. 1, 2002.

[21] L. D. Hicks and M. S. Dresselhaus, "Effect of quantum-well structures on the thermoelectric figure of merit", *Phys. Rev. B*, Vol. 47, No. 19, pg. 727-731, 1993.

[22] T. C. Harman, P. J. Taylor, M. P. Walsh, B. E. LaForge, "Quantum Dot Superlattice Thermoelectric Materials and Devices", *Science*, Vol. 297, No. 27, 2002.

[23] R. Venkatasubramanian et al., "MOCVD of Bi_2Te_3, Sb_2Te_3 and their superlattice structures for thin-film thermoelectric applications", *J. of Crystal Growth*, Vol. 170, pg. 817-821, 1997.

[24] R. Venkatasubramanian et al., "Thin-film thermoelectric devices with high room-temperature figures of merit", *Nature*, Vol. 413, pg. 597-602, 2001.

[25] Streetman and Banerjee, *Solid State Electronic Devices, 5th ed.*, Prentice Hall, NJ, 2000.

[26] R. Venkatasubramanian et al., "Thin-film thermoelectric devices with high room-temperature figures of merit", *Nature*, Vol. 413, pg. 597-602, 2001.

[27] C. M. Bhandari, "Minimizing the Thermal Conductivity", Chap. 38 in *CRC Handbook of Thermoelectrics edited by D. M. Rowe*, CRC Press LLC, New York, pg. 56, 1995.

[28] H.J. Goldsmid and J.W. Sharp, "Estimation of the Thermal Band Gap of a Semiconductor from Seebeck Measurements", *J. of Elec. Mat.*, Vol. 28, No. 7, 1999.

[29] I. A. Nishida, "Measurement of Electrical Properties", Chap. 15 in *CRC Handbook of Thermoelectrics edited by D. M. Rowe*, CRC Press LLC, New York, pg. 158-180, 1995.

[30] O. Maldonado, "Pulse method for simultaneous measurement of electric thermopower and heat conductivity at low temperatures", *Cryogenics*, Vol. 32, No. 10, 1992.

[31] Cobble, Milan H., "Calculations of Generator Performance", Chap. 39 in *CRC Handbook of Thermoelectrics edited by D. M. Rowe*, CRC Press LLC, New York, pg. 489-501, 1995.

[32] Gao Min, D M Rowe, and K Kontostavlakis, "Thermoelectric figure-of-merit under large temperature differences", *J. of Phys. D*, Vol. 37, pg. 1301-1304, 2004.

[33] Hugh H. Woodbury, Lionel M. Levinson, and Robert S. Lewandowski, "Z-Meters", Chap. 17 in *CRC Handbook of Thermoelectrics edited by D. M. Rowe*, CRC Press LLC, New York, pg. 181, 1995.

[34] T. C. Harman, "Special Techniques for Measurement of Thermoelectric Properties", *Letters to the Editor, Amer. Inst. of Phys.*, pg. 1373, 1958.

[35] Hideo Iwasaki, Mikio Koyano, and Hidenobu Hori, "Evaluation of the figure of Merit of Thermoelectric Materials by Harman Method", *J. of App. Phys.*, Vol. 41, pg. 6606-6609, 2002.

[36] Hideo Iwasaki, Shin-ya Yokoyama, Tomoharu Tsukui, Mikio Koyano, Hidenobu Hori, and Seijirou Sano, "Evaluation of the figure of Merit of Thermoelectric Modules by Harman Method", *J. of App. Phys.*, Vol. 42, pg. 3707-3708, 2003.

[37] Edward J. Kroliczek and M. Nelson Ross, "Design and Operation of Couple Testers", *IEEE Conf. Proc.*, 1960.

[38] Larry Selwitz and Gerhard Stapfer, "The Development and Use of an Integrated Thermoelectric Life and Performance Testing System", *IEEE Conf. Proc.*, 1960.

[39] Ikushi Yoshida and Isamu Yunoki, "Automatic Measuring System of Thermoelectric Properties with a Desk-top Computer", *Proc. of the Sixth Int. Conf. on Thermoelectric Energy Conversion*, pg. 39-42, 1986.

[40] Van Wynsberghe, R., "Rapid simultaneous measurement of thermoelectric material properties", *Proc. of the Sixth Int. Conf. on Thermoelectric Energy Conversion*, pg. 28-34, 1986.

[41] Kuei Fang Hsu et al., "Cubic AgPb(m)SbTe(2+m) Bulk Thermoelectric Materials with High Figure of Merit", *Science*, Vol. 303, 2004.

[42] Adam Downey and Timothy P. Hogan, "Circuit model of a thermoelectric module for AC electrical measurements", *Int. Conf. on Thermoelectrics Proc.*, 2005.

[43] http://www.tellurex.com/12most.html July 12, 2004.

[44] http://www.apiezon.com/greasetable.htm February 10, 2005.

[45] T. Hogan, N. Ghelani, S. Loo, S. Sportouch, S.-J. Kim, D.-Y. Chung, M. G. Kanatzidis, *Proc. from the Int. Conf. on Thermoelectrics*, pg. 671-674, 1999.

[46] C. Wood, D. Zoltan, and G. Stapfer, "Measurement of Seebeck coefficient using a light pulse", *Rev. of Sci. Inst., Amer. Inst. of Phys.*, Vol. 56, No. 5, pg. 719-722, 1985.

[47] Gao Min and D M Rowe, "A novel principle allowing rapid and accurate measurement of a dimensionless thermoelectric figure of merit", *J. of Meas. of Sci. and Tech.*, Vol. 12, pg. 1261–1262, 2001.

[48] T. A. Al-Obaidi and H. J. Goldsmid, "Determination of the Thermoelectric Figure of Merit from Thermal Conductivity Measurements", *Energy Conversion*, Vol. 9, pg. 131-132, 1969.

[49] T. J. Scheidemantel and J. V. Badding, *Chemistry, Physics, and Materials Science of Thermoelectric Materials*, pg. 203-218, Kluwer Academic/ Plenum Publishers, New York, 2003.

[50] Sim Loo, Jarrod Short, Kuei Fang Hsu, Mercouri Kanatzidis, Tim Hogan, "High Temperature Measurement System Design for Thermoelectric Materials In Power Generation Application", *Mat. Res. Soc. Sym. Proc.*, Vol. 793, pg. 375-383, 2004.

[51] T. Hogan and Tom Shih, "Modeling and Characterization of Power Generation Modules Based on Bulk Materials", *CRC Handbook on Thermoelectrics,* 2005.

[52] Gao Min and David M. Rowe, "Peltier Devices as Generators", Chap. 38 in *CRC Handbook of Thermoelectrics edited by D. M. Rowe*, CRC Press LLC, New York, pg. 485, 1995.

[53] Heikes, R. R., Ure, R. W., *Thermoelectricity: Science and Engineering*, Interscience Publishers, New York – London, pg. 512-513, 1961.

[54] Sim Loo, "Transport Characterization of New High Temperature Quaternary Thermoelectric Materials And Devices", Ph.D. thesis, Michigan State University, 2003.

[55] Atsushi Suzuki, Yasuhiro Hasegawa, Yoshiaki Ishikawa, Takashi Komine, Hiroyuki Morita, and Hajime Shirai , "Investigation of physical and electric properties of silver paints as a binder for thermoelectric materials", *Rev. of Sci. Inst.*, Vol. 76, 2005.

[56] H. E. Bates and Martin Weinstein, " The Preparation and Properties of Segmented Lead Telluride-Silicon-Germanium Thermoelements", *IEEE Thermoelectrics Conf. Proc. (Fourth)*, 1966.

[57] C. Kittel, Chap. 4, *Introduction to Solid State Physics*, Seventh ed., John Wiley and Sons, Inc., 1996.